Technical University of Crete
School of Electrical and Computer Engineering
Electronics Laboratory

Development of MID-IR Hyperspectral Imaging System Based on Quantum Cascade Laser

by

Reppas Panagiotis

Diploma Thesis

A thesis submitted in partial fulfillment of the requirements for the diploma of Electrical and Computer Engineering

Thesis Commitee

Balas Costas, Professor, Supervisor
Xekoukoulotakis Nikolaos, Professor
Kortsalioudakis Nathanail, Ph.D.

Chania, March 2018

Abstract

Infrared hyper-spectral imaging is a non-contact, non-destructive detection technology that integrates conventional imaging and spectroscopy to get both spatial and spectral information of a target. This technique has in recent times become a powerful tool for scientific and industrial analysis in many different fields. Its applications range from security, through chemistry and biomedical applications. Infrared hyper-spectral images represent observations of a scene at many different wavelengths and most importantly associate each pixel in the image with a full spectral vector or spectral signature. The work presented in this thesis deals with the design and development of a mid-infrared hyper-spectral imaging system based on a quantum cascade laser. The implementation employs a sensitive camera, a coherent light source, a light expander, and software specially designed for the purposes of this system and exploits the full potential of the hardware. In order to acquire the spectrum of a surface, the light source illuminates a surface with light beams of different wavelength; consequently the sensor acquires optical information captured at different wavelengths at a time. After completing the acquisition process of the spectral cube the spectrum of each pixel can be generated and displayed as a diagram. Each substance absorbs different wavelengths and as a result its absorption diagram can be used in order to identify the substances of which the targeted surface is composed. The features described above make this device suitable for demanding spectral imaging applications, such as microscopic images and non-destructive analysis.

Acknowledgements

It is a great opportunity to bestow my heartful regards to all people who have been either directly or indirectly involved in the fulllment of this diploma dissertation.

First and foremost, I would like to express my sincerest gratitude to my professor and supervisor, Professor Constantinos Balas, for giving me the opportunity to deal with such an interesting topic. Not only did he help me completing my studies, but also motivated me to work more eciently and professionally by conducting a lot of extra research, being familiar with experimental devices and gaining valuable knowledge.

Besides my supervisor, I would like to thank the rest of my thesis commitee: Prof. Xekoukoulotakis Nikolaos and Dr. Nathanail Kortsalioudakis, for their insightful comments and encouragement, but also for the hard question which incented me to widen my research from various perspectives.

My sincere thanks also goes to the whole team of the *Optoelectronics and Imaging Diagnostics Lab*, Tsapras Athanasios (PhD Candidate), Rossos Christos (PhD Candidate), Kastrinakis Marios (M.sc), Papathanasiou Athanasios (M.sc Candidate), Gkouzionis Ioannis (M.sc Candidate) and Vardoulakis Emmanouil (M.sc Candidate) for their numerous brainstorming discussions, and selfless advice.

Furthermore I would like to thank my best friends Antonis , Filippos , Trifonas , Themos , Panos , Giorgos and Alexandros for the countless support in whatever decision I made and of course because they were by my side whenever I needed it.

Finally, I must express my very profound gratitude to my beloved parents, Mihalis and Ivelina for providing me with unfailing support and continuous encouragement throughout my years of study and through the process of researching and writing this thesis. This accomplishment would not have been possible without them.

Contents

List of Figures

Chapter 1

Introduction

1.1 Introduction

Spectral Imaging is a technique which combines spectroscopy and imaging. Both fields are well developed and used intensively in many fi

elds including life sciences. However, the combination of these two is not trivial, mainly because it requires creating a three-dimensional (3D) data set that contains many images of the same object, where each one of them is measured at a different wavelength.

Mid-Infrared Spectral Imaging exploits the vibrations of the molecules in order to extract information about their nature. Each substance absorbs different wavelengths and as a result its absorption diagram can be used in order to identify it.

The task assigned to this thesis does require the development of a Mid-Infrared Imaging system based on a Quantum Cascade Laser. The implementation employs a sensitive thermal camera, a coherent light source, a light expander, and software specially designed for the purposes of this system and exploits the full potential of the hardware. In order to acquire a spectrum, the light source illuminates a surface with light beams of different wavelength; consequently the sensor acquires optical information captured at different wavelengths at a time. After completing the acquisition process of the spectral cube the spectrum of each pixel can be generated and displayed as a diagram.

1.2 Thesis Outline

Chapter 2 provides a theoretical backround about imaging and spectroscopy.

Chapter 3 presents infrared vibrational spectroscopy, which is the analysis of infrared light interacting with a molecule. The main use of this technique is in organic and inorganic chemistry is to determine functional groups in molecules.

Chapter 4 presents a technique called FTIR spectroscopy, which is used to obtain an infrared spectrum of absorption or emission of a solid, liquid or gas .

Chapter 5 presents an overview of thermal cameras and quantum cascade lasers physics.

Chapter 6 presents a comparisson between QCL-based spectrometers and FTIR-based spectrometers.

Chapter 7 presents the set-up of the system. It describes the software developed, the additional set-up and all the experiments conducted.

Chapter 8 is the conclution and possible future work of this implementation.

Chapter 2

Theoretical Background

It is important to outline the bedrocks of this work in order to render readers familiar with the basic concepts and developed methods. However, followers who feel confident, as far as their knowledge is concerned on these scientific domains, may sidestep this section of introduction and continue with the following chapters.

For explaining the characteristics of spectral imaging, it is better to start with an introduction of its two elements; imaging and spectroscopy.

2.1 Imaging

Imaging is the visual representation or reproduction of an object. At this time, digital imaging is the most advanced and applicable method where data are recorded using a digital camera, such as a charged coupled device (CCD).

The amount of information that can be extracted from an image is determined by the quality of it. Image quality is determined by the following parameters:

- **Spatial resolution** determines the closest distinguishable features in an object. It depends mainly on the wavelength (λ), the numerical aperture (NA) of the objective lens, the magnification, and the pixel size of the array-detector, usually a CCD camera. The last two play an important role because they determine the sampling frequency which must be sufficiently high to achieve full resolution. Spatial resolution also depends on the signal quality.
- Lowest detectable signal depends on the **quantum efficiency** of the detector (the higher the better), the **noise level** of the system (the lower the better), the **NA** (numerical aperture) of the optics (the higher the better), and the **quality** of the optics.

- **Dynamic range** of the acquired data determines the number of different intensity levels that can be detected in an image. It depends on the maximal possible number of electrons at each pixel and on the lowest detectable signal (basically it is the ratio of these two values). If, however, the measured signal is low, so that the CCD well associated with a pixel is only partially filled, the dynamic range will be limited accordingly. As an example, if a CCD well if fulfilled to only 10% of its maximum capacity, the dynamic range will be reduced to 10% of its nominal value.
- **Field of view (FOV)** determines the maximal area that can be imaged.
- Other parameters include the exposure time range (usually determined by the detector) and the binning of the CCD pixels to gain sensitivity.

2.2 Spectroscopy

Spectroscopy is the field of study concerning the interaction between matter and radiated energy. Historically, it referred to the dispersion of visible light according to its wavelength. Later on, the concept was greatly expanded to comprise any interaction with radiative energy as a function of its wavelength or frequency. As a result, the definition of spectroscopy was expanded to an alternative field, that one of frequency. A further extension added energy (E) as a variable, due to the equation E = h*v. Spectroscopic data is often represented by a spectrum, meaning the plot of the response in proportion of wavelength or frequency. Spectroscopy is strictly associated with the measurement of radiation intensity with reference to the wavelength or frequency. This sort of measurements can be conducted by experimental spectroscopic devices such as spectrometers, spectrophotometers, spectrographs or spectral analyzers.

2.2.1 Electromagnetic Spectrum

The electromagnetic spectrum, Figure 2.1, is the complete range of wavelengths of electromagnetic radiation, beginning with the longest radio waves (including those in audio range) and extending through visible light (a very small part of the spectrum) all the way to the extremely short gamma rays that are a product of radioactive atoms. Nearly all types of electromagnetic radiation can be used for spectroscopy, to study and characterize matter.

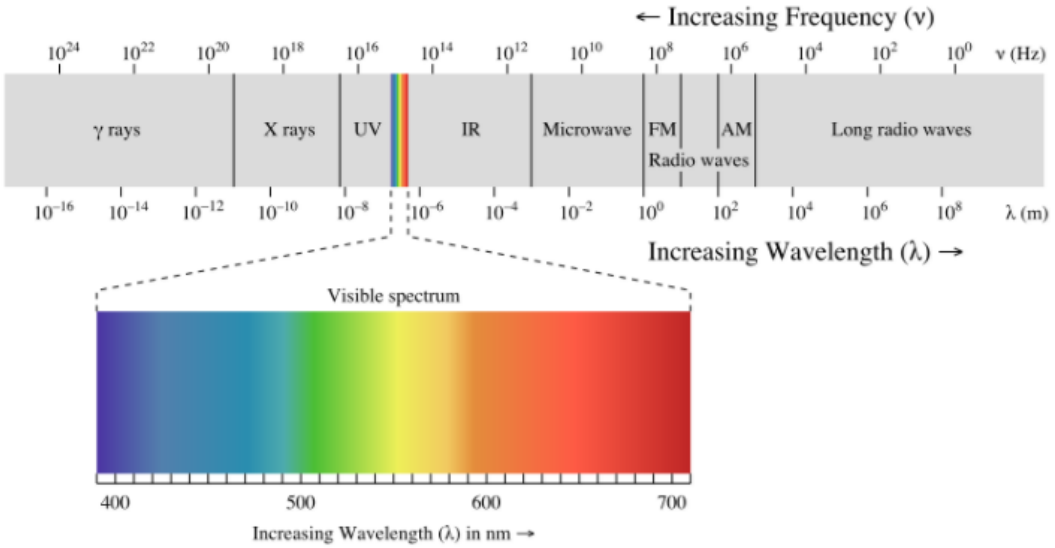

Figure 2.1: *Electromagnetic Spectrum*

The types of radiation are generally grouped by the kinds of chemical and physical effects they can produce on matter. For example, in a magnetic field, exposure to the low-energy radio frequency radiation only reorients nuclei, while exposure to the slightly higher-energy microwave region changes electron spin states of molecules with unpaired electrons. Microwave radiation can also change the rotational energy of molecules; this effect is used to heat food quickly in a microwave oven. In the middle regions of the electromagnetic spectrum, absorption of IR radiation causes changes in the vibrational energy of molecules. Visible (Vis) and ultraviolet (UV) radiations alter the electron energies of loosely held outer electrons of atoms and molecules. Higher-energy X-rays can cause electron transitions between inner electron levels, and gamma radiation produces changes within atomic nuclei. As all compounds absorb radiation in multiple regions of the spectrum, the information on molecular activity in each region provides complementary data for material characterization. The following overview of the relationship of radiant energy to its effects on matter has a focus on IR absorption theory.

2.2.1.1 Range of the Spectrum

Electromagnetic waves are typically described by any of the following three physical properties: the frequency f, wavelengthλ, or photon energy E. Wavelength is inversely proportional to the wave frequency, so gamma rays have very short wavelengths that are fractions of the size of atoms, whereas wavelength on the opposite end of the spectrum can be of thousand kilometers. Photon energy is directly proportional to the wave frequency, so gamma ray photons have the

highest energy (around a billion electron volts), while radio wave photons have very low energy (approximately a femtoelectronvolt). These relations are illustrated by the following equations:

$$f = \frac{c}{\lambda}, or f = \frac{E}{h}, or E = \frac{hc}{\lambda}$$

The behavior of EM radiation depends on its wavelength. When EM radiation interacts with single atoms and molecules, its behavior also depends on the amount of energy per quantum (Photon) it carries.

2.2.1.2 Infrared Radiation

Infrared radiation, or simply infrared or IR, is electromagnetic radiation (EMR) with longer wavelengths than those of visible light, and is therefore invisible, although it is sometimes loosely called infrared light. It extends from the nominal red edge of the visible spectrum at 700 nanometers (frequency 430 THz), to 1000 nanometers (300 GHz). Most of the thermal radiation emitted by objects near room temperature is infrared.

The infrared spectrum, Figure 2.2, is separated into four different regions:

- Near Infrared (NIR), 700 1000 nm.
- Sort Wave Infrared (SWIR), 1000 2.500 nm.
- Mid Wave Infrared (MWIR), 3000 5000 nm.
- Long Wave Infrared (LWIR), 7000 14000 nm.

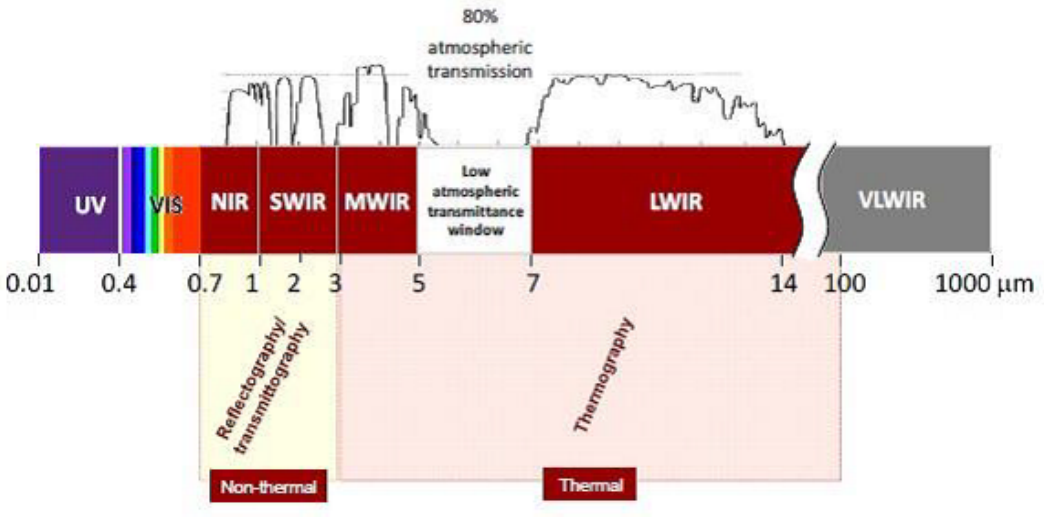

Figure 2.2: *Infrared Region of the Spectrum*

2.3 Spectroscopy

Spectrometry constitutes the technique that is being used so as to assess the concentration or amount of a specific chemical compound. It is a common practice to combine spectrometry along with spectroscopy, mentioned above, in physical and analytical chemistry for the identification of substances through the spectrum either emitted from or absorbed by them. In addition, they contribute to the field of astronomy and remote sensing as well.

2.4 Spectral Imaging (SI)

Spectral imaging is a combination of spectroscopy and photography in which a complete spectrum or partial spectral information (such as the Doppler shift or Zeeman splitting of a spectral line) is acquired at each position of an image plane. Spectral imaging allows extraction of additional information the human eye fails to capture with its receptors for red, green and blue. Applications related to astronomy, solar physics, analysis of plasmas in nuclear fusion experiments, planetology, and Earth remote sensing are sparked by the benefits of spectral imaging.

Various distinctions among techniques are applied, based on criteria including spectral range, spectral resolution, number of bands, width and contiguousness of bands, and application. The terms include Multi-Spectral Imaging, Hyper-Spectral Imaging, full spectral imaging, imaging spectroscopy or chemical imaging.

Important new developments in the field of Biomedical Optical Imaging (OI) allow for unprecedented visualization of tissue microstructure and enable quantitative mapping of disease-specific endogenous and exogenous substances [2]. Spectral imaging (SI) is one of the most promising OI modalities.

A spectral imager provides spectral information at each pixel of an image sensor array. The SI Systems acquire a three-dimensional (3D) data set of spectral and spatial information, known as spectral cube. The spectral cube can be considered as a stack of images, each of them acquired at a different wavelength. Combined spatial and spectral information offers great potential for the non-destructive/invasive investigation of a variety of studied samples.

Spectroscopy finds application in analytical chemistry since a long time. Different spectroscopy types and modalities exist, depending on the optical property that it is intended to be measured, namely, absorption, spontaneous emission (fluorescence, phosphorescence), scattering (Rayleigh elastic, Raman inelastic) spectroscopy, etc. As the light travels into the sample, photons are experiencing absorption, which may result in fluorescence emission and multiple scattering due to the local variation of the index of refraction. Spectrometers measure the intensity of the light emerging from the sample as a function of the wavelength. The collected light passes

through a light-dispersing element (grating), which spatially splits the light wavelengths onto the surface of an optical sensor array, interfaced with a computer for recording and processing the spectrum. Sample illumination can be provided by either a broadband (e.g., white light) or a narrow-band light source. In the first case, the measured spectra provide information for the absorption and scattering characteristics of the tissue. In the second case, the measured spectra probe the fluorescence characteristics of the sample. Particularly, in steady-state fluorescence spectroscopy, a narrow-band light source is used for fluorescence excitation, such as lasers, LEDs, or filtered light sources, emitting typically in the blue-ultraviolet band. A sensitive optical sensor is used for collecting the emission spectra [3].

The collected emission spectra can provide diagnostic information for the composition of the sample. This makes spectroscopy an indispensable tool for non-destructive analysis and for the development of novel, non-invasive diagnostic approaches. Particularly, in biomedical sciences, the diagnostic potential of tissue spectroscopy is based on the assumption that the absorption, fluorescence, and scattering characteristics of the tissue change during the progress of the disease. Over the last 20 years, spectroscopy has been extensively investigated as a tool for identifying various pathologic conditions on the basis of their spectral signatures. It had been demonstrated that spectroscopy can successfully probe intrinsic or extrinsic chromophores and fluorophores, the concentration of which changes during the development of the disease. In its conventional configuration, spectroscopy uses single-point probes that cannot easily sample large areas or small areas at high spatial resolution (SR). It is obvious that this configuration is clearly suboptimal when solid and highly heterogeneous materials, such as the biological tissues, are examined. In these cases, the collected spectrum is the result of the integration of the light emitted from a great number of area points. This has the effect of mixing together signals originating from both pathologic and healthy areas, which makes the spectral signature-based identification problematic. Looking at the same problem from another perspective, point spectroscopies are considered as inefficient in cases where the mapping of some characteristics, spectrally identifiable property, is of the utmost importance.

Spectroscopy probes optical signals with high spectral resolution but with poor spatial resolution (SR). The vastly improved computational power together with the recent technological developments in tunable optical filter and imaging sensor technologies have become the catalysts for merging together imaging and spectroscopy. Both areas, imaging and spectroscopy, continue to be affected by technological innovations that enable faster acquisition of superior - quality data. SI has the unique feature of combining the advantages of both imaging and spectroscopy (high spatial and spectral resolution) in a single instrument. In SI, light intensity is recorded as a function of both wavelength and location. In the image domain, the data set includes a full image at each individual wavelength. In the spectroscopy domain, a fully resolved spectrum at each individual pixel can be recorded. These devices can measure the spectral content of light energy at every point in an image. Multiple images of the same scene at different wavelengths

are acquired for obtaining the spectra. As an example, an SI device integrating an imaging sensor with 1000x1000 pixels provides 1 million individual spectra. A spectrum containing 100 data points results from an equal number of spectral images. Assuming that the intensity in each pixel is sampled at 8 bits, then the size of the resulting spectral cube equals to 100 Mbytes. Due to the huge size of the collected data sets, SI data processing, analysis, and storage require fast computers and huge mass memory devices. Several mathematical approaches are used for spectral classification and image segmentation on the basis of the acquired spectral characteristics. The spectra are classified using spectral similarity measures, and the resulting different spectral classes are recognized as color-coded image clusters. SI can be easily adapted to a variety of OI instruments such as camera lenses, telescopes, microscopes, endoscopes, etc. For this reason, applications of SI span from earth observation including ground and atmosphere (remote sensing) to general medicine and molecular biology [2].

2.4.1 Spectral Reflectance

It has already been mentioned how materials print a spectral signature on the light they reflect. In order to get this signature, a parameter called spectral reflectance is of interest. It represents the ratio between reflected and incident light, as a function of wavelength. This dependence is due to the fact that light is scattered or absorbed to different degrees at certain wavelengths, and it exists for almost every material.

There are several physical processes involved that determine the nature of the reflected light, and thus, the spectral signature of the material. Firstly, almost every object shows some degree of specular reflection, which means that some of the light rebounds directly on the surface of the material, as on a mirror. In this case, the spectrum of the reflected light remains the same as that of the incident light. There is no signature printed. Secondly, part of the light diffuses into the material where some is absorbed and some is randomly scattered, which is known as diffuse reflection. Finally, fluorescence, which is the emission of light by a substance that has absorbed light or other electromagnetic radiation, may also take place. In this case, a photon at shorter wavelength is absorbed and a photon at longer wavelength is emitted consequentially.

A white-colored material, for example, does not absorb any wavelength while a multi-colored material will absorb some wavelengths and diffusely reflect others. These reflected wavelengths are responsible for the color of the material. In a way, they shape the nature of the incident light to create what we perceive as color. This effect can be thought from the continuous spectrum point of view: it explains why matter prints a signature on the incident light depending on how different spectral components of light are absorbed or reflected.

2.4.2 Spectral Cubes

The information that is primarily collected by spectral imagers and then appropriately processed based on the kind of application running, is stored in 3D data structures for further analysis. This sort of data structures are known as Spectral Cubes (SC). A spectral cube consists of the three dimensional projection of a great number of consecutive and registered sets of hyper-spectral or multi-spectral images. Being more specific, the first two dimensions respond to spatial dimensions, for account of pixel coordinates and the third one refers to spectral dimension, meaning a specific wavelength of the electromagnetic spectrum. A glance at Figure 2.4 can offer profound perception of how a spectral cube does look like.

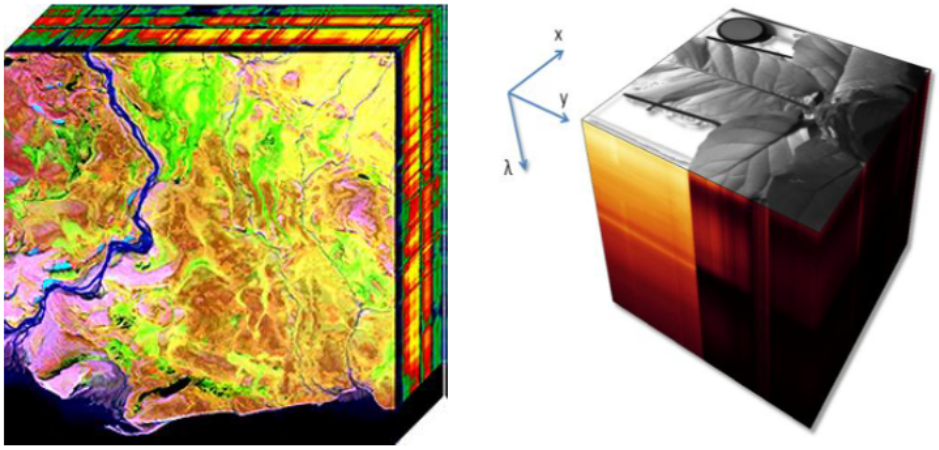

Figure 2.3: *Hyper-spectral cubes*

Simply put, an imaging spectrometer acquires the spectrum of each pixel in a two-dimensional spatial scene. As shown in the figure below, the easiest way to think of such a scheme is as band sequential imaging, in which multiple images of the same scene at different wavelengths are acquired. A key point is that the spectra be sampled densely enough to reassemble a spectrum (commensurate with the need for analysis). There are many technological means to obtain these data. The images are typically stacked in a computer, from the lowest wavelength to the highest, to create an image cube of the data set. The spectrum of a selected pixel is obtained by skewering it in its third dimension, wavelength, as the inset in Figure 2.4 shows.

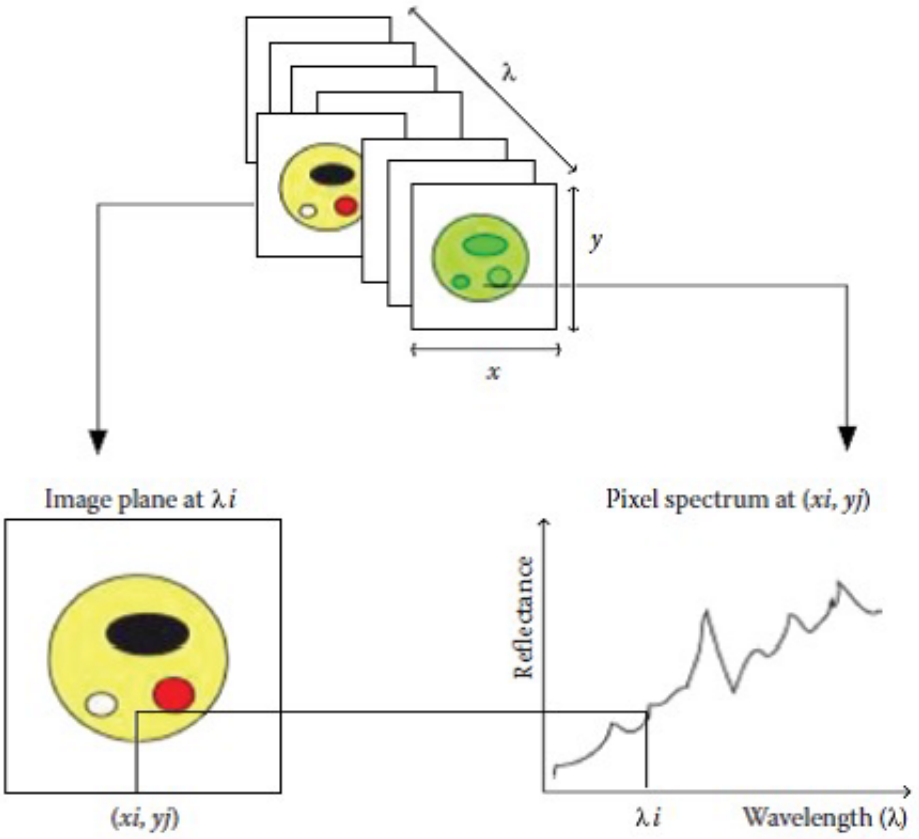

Figure 2.4: *Schematic representation of a hypercube showing the relationship between spatial and spectral dimensions.*

As an example, the hyper-spectral cube of a fish fillet acquired using reflectance mode is illustrated in Figure 2.5. The raw hyper-spectral cube consists of a series of contiguous sub-images one behind each other at different wavelengths Figure 2.5.a. Each sub-image provides the spatial distribution of the spectral intensity at a certain wavelength. That means a hyper-spectral image described as I(x; y; λ) can be viewed either as a separate spatial image I(x; y) at each individual wavelength (λ), or as a spectrum I(λ) at each individual pixel (x; y). From the first viewpoint, any spatial image within the spectral range of the system can be picked up from the hyper-spectral cube at a certain wavelength within the wavelength sensitivity Figure 2.5.b. The gray scale image shows the different spectral intensity of the imaged object at a certain wavelength due to the distribution of its corresponding chemical components. For example, an image within the hypercube at a single waveband centered at 980 nm with bandwidth of 5 nm Figure 2.5.b can relatively show the information of moisture distribution in the fish fillet, which is difficult to be observed in RGB image Figure 2.5.c. From the second viewpoint, the resulting spectrum of a certain position within the specimen can be considered as its own unique spectral fingerprint of this pixel to characterize the composition of that particular pixel Figure 2.5.d.

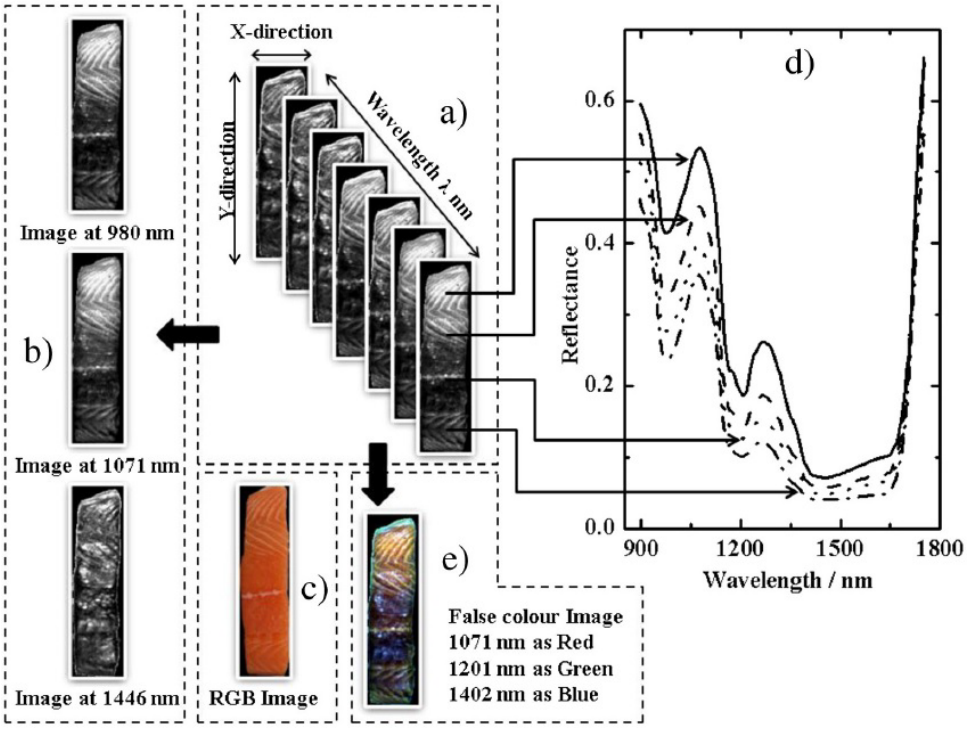

Figure 2.5: *Schematic diagram of hyper-spectral image (hyper-spectral cube) for a piece of fish fillet*

2.4.2.1 Acquisition of hyper-spectral images

There are four approaches to acquire 3-D hyper-spectral image cubes (I(x, y,)), which are point scanning, line scanning, area scanning, and the single shot method, as illustrated in the upper half of Figure 2.7. In the point scanning method (also known as the whiskbroom method), a single point is scanned at one pixel to provide the spectrum of this point 2.7.a), and other points are scanned by moving either the detector or the sample along two spatial dimensions (x and y). Its obtained hyper-spectral cube is stored in the band-interleaved-by-pixel (BIP) format. For an image stored in BIP format, the first pixel for all bands is in sequential order, followed by the second pixel for all bands, followed by the third pixel for all bands, etc., interleaved up to the number of pixels. This format is optimal for accessing the spectral information of each pixel. The disadvantages of whiskbroom are very time-consuming for positioning the sample and need advanced repositioning hardware to ensure repeatability.

The second approach illustrated in Figure 2.7.b is called as line scanning method or pushbroom method, which records a whole line of an image as well as spectral information simultaneously corresponding to each spatial pixel in the line. A complete hyper-spectral cube can be obtained

as the line is scanned along the direction of x dimension (Figure 2.7.b), and the obtained cube is stored in the format of band-interleaved-by-line (BIL). BIL format is a scheme for storing the pixel values of an image in a file band for each line, or row, of the image. Because of its characteristics of continuous scanning in one direction, line scanning is particularly suitable in conveyor belt systems that are commonly used in food process lines. Therefore, line scanning is the most popular method of acquiring hyper-spectral images for food quality and safety inspection. The disadvantage of the pushbroom technique is that the exposure time can be set at only one value for all wavelengths. Such exposure time has to be short enough to avoid saturation of spectrum at any wavelength, resulting in underexposure of other spectral bands and low accuracy of their spectral measurement.

The first two methods are spatial scanning methods, while the area or plane scanning (also known as band sequential method or wavelength scanning) is a spectral scanning method as illustrated in Figure 2.7.c. This approach keeps the image field of view fixed and acquires a 2-D monochrome image (x, y) with full spatial information at a single wavelength at a time. Such scanning repeats over the whole wavelength range, results in a stack of single band images stored in the band sequential (BSQ) format. As a simple format, BSQ encodes each line of the image at the first band is followed immediately by the next line in the same spectral band, followed by the second band for all lines, followed by the third band for all lines, etc., interleaved up to the number of bands. This format provides an easy access of spatial (x; y) access of at a single spectral band. As the detector is exposed to only a single wavelength each time, a suitable exposure time can be set for each wavelength. In addition, the area scanning does not need to move either sample or detector and is suitable for the applications where the object should be stationary for a while, such as excitation-emission in fluorescence imaging. A disadvantage of area scanning is that it is not suitable for a moving sample or the inspection of real-time delivery.

Last but not least, the single shot method records both spatial and spectral information using a large area detector with one exposure to capture the images (Figure 2.7.d), making it very attractive when fast hyper-spectral imaging is required. However, it is still in the early stage of development and has limited resolutions for spatial dimension and narrow ranges for spectral dimension.

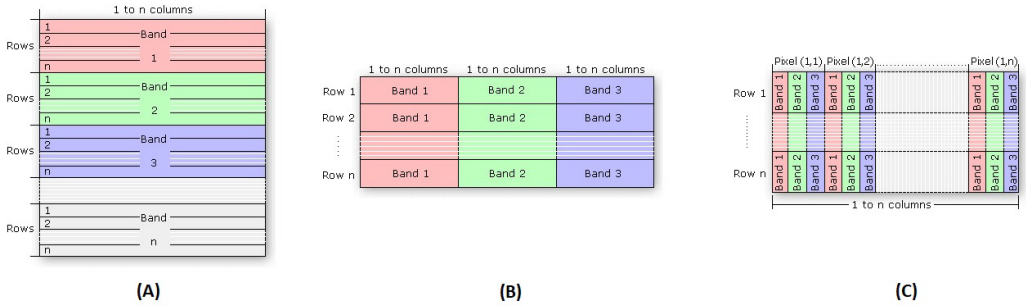

Figure 2.6: *The file layout of the: (A) BSQ, (B) BIL, and (C) BIP interleav*

2.4.2.2 Acquisition of hyper-spectral images

There are three common sensing modes for hyper-spectral imaging, namely reflectance, transmittance, and interactance as illustrated in lower half of Figure 2.7. Positions of light source and the optical detector (camera, spectrograph, and lens) are different for each acquisition mode. In reflectance mode, the detector captures the reflected light from the illuminated sample in a specific conformation to avoid specular reflection (Figure 2.7.e). External quality features are typically detected using reflectance mode, such as size, shape, color, surface texture and external defects. In transmittance mode, the detector is located in the opposite side of the light source (Figure 2.7.f), and captures the transmitted light through the sample which carries more valuable internal information but is often very weak. Transmittance mode is usually used to determine internal component concentration and detect internal defects of relative transparent materials. However, transmittance mode has a low signal level from light attenuation and is affected by the thickness of sample. In interactance mode, both light source and the detector are located in the same side of sample and parallel to each other (Figure 2.7.g). On the basis of such setup, the interactance mode can detect deeper information into the sample and has less surface effects compared to reflectance mode. Meanwhile, the interactance mode reduces the influence of thickness, which is a practical advantage over transmission. It should be noted that a special setup is required in the transmittance mode to seal light in order to prevent specular reflection directly entering the detector.

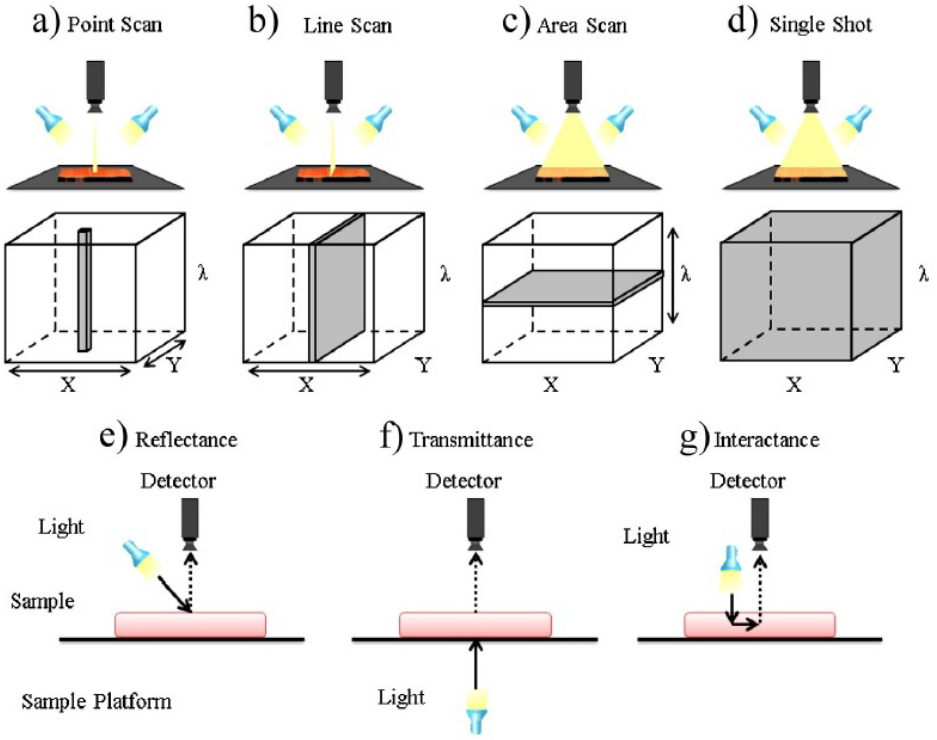

Figure 2.7: *Acquisition approaches of hyper-spectral images and image sensing modes*

2.4.3 Multi-Spectral Imaging

Multi-Spectral Imaging (MI) is responsible for capturing image data at specific frequencies across the electromagnetic spectrum. The wavelengths may be separated by filters or by the use of instruments that are sensitive to particular wavelengths, including light from frequencies beyond the visible light range, such as infrared. MI images are the main type of images acquired by remote sensing (RS) radiometers. Dividing the spectrum into many bands, MI is the opposite of panchromatic, which records only the total intensity of radiation falling on each pixel. Spectral Imaging with more numerous bands, finer spectral resolution or wider spectral coverage may be called Hyper-Spectral or Ultra-Spectral.

2.4.4 Hyper-Spectral Imaging

Hyper-Spectral Imaging (HI) is a technology widely used for remote imaging, so as to extract a maximum of information out of images captured under strongly varying imaging conditions. It provides options for three-dimensional data generation with high spectral resolution across the full electromagnetic spectrum of frequencies, beyond the visible. This visual extension beyond the scope of human eye renders HI a powerful analytical tool, which has been extensively used

in a wide variety of fields including agriculture, medicine, artistic [4], satellite imaging [5], astronomy, surveillance [6], [7], chemical imaging, physics and environment [5].

2.4.5 Multi-Spectral vs. Hyper-Spectral Imaging

The distinction between Hyper-Spectral and Multi-Spectral Imaging pertains to the number of narrow bands or the type of measurement. Multi-Spectral Imaging deals with several images at discrete and somewhat narrow bands. Being discrete and somewhat narrow is what distinguishes MI in the visible from color photography. A MI sensor may have many bands covering the spectrum from the visible to the long wave infrared. MI images do not produce the spectrum of an object. On the other hand, Hyper-Spectral deals with imaging narrow spectral bands over a continuous spectral range, and produce the spectra of all pixels in the scene. So, a sensor with only 20 bands can also be HI when it covers the range from 500 to 700 nm with 20 bands each 10 nm wide. Figure 2.8 helps us understand at the differences pinpointed above.

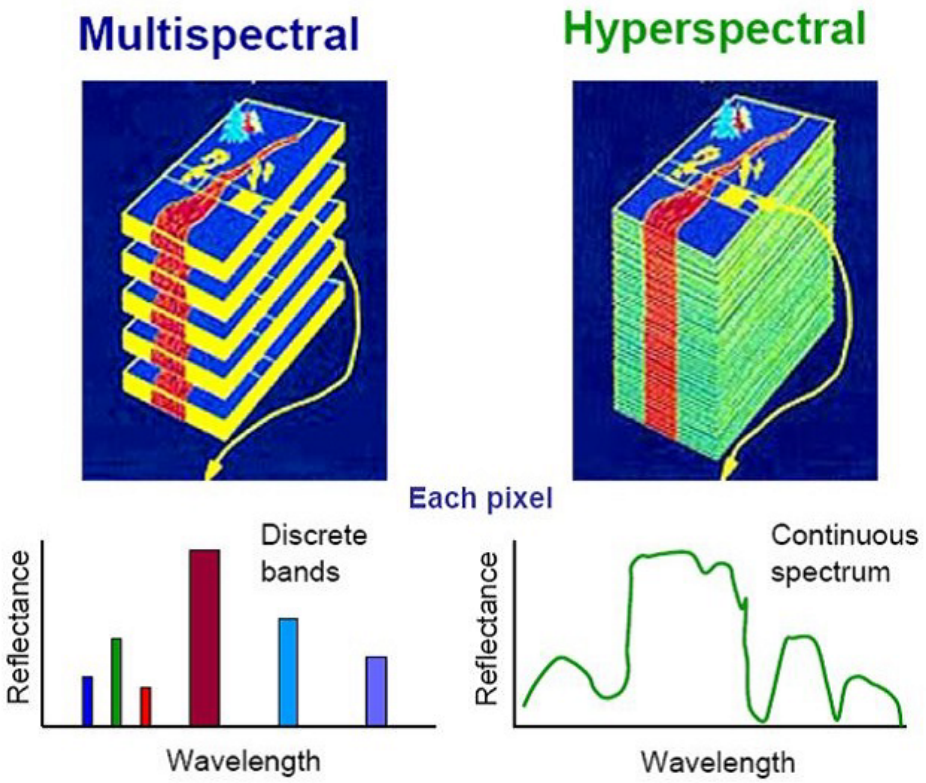

Figure 2.8: *Acquisition approaches of hyper-spectral images and image sensing modes*

2.5 Hyper-Spectral Imaging Applications

As it has already been mentioned, there are numerous applications emerging from the spectral analysis that is being provided by hyper-spectral imaging. For nearly a decade, this technology was primarily used for purposes like surveillance, reconnaissance, environmental and geological studies. However, the application of hyper-spectral imaging in the biomedical area has been negligible due to high-instrumentation costs and problems arising from the clinical use of hyper-spectral sensors. With recent achievements in sensor technology and increasing affordability of high performance spectral imagers, hyper-spectral imaging systems constitute one of the most important key areas in medical imaging. The early diagnosis of cancer, one of the thorniest medical problems, is now possible, since the evolution of hyper-spectral sensors allows the scanning of a patient's body to identify precancerous lesions or to provide critical spectral data through endoscopic procedures. The extension and improvement of hyper-spectral imaging in biomedical and clinical diagnosis is within the grasp of researchers [10]. The advantages of this technology regarding diagnostic health care applications include a high resolution imaging of tissues either at macroscopic or cellular levels and the capability to generate highly accurate spectral information related to the patient, tissue sample, or any other disease condition. In particular, the vast investment of hyper-spectral imaging in medicine lies on the generation of wavelength-specific criteria for disease conditions on spectral features. As a consequence, an ideal technology for high-throughput patient screening and non-invasive diagnosis is begotten.

Due to their unparalleled ability to reveal abnormal spectral signatures, hyper-spectral medical instruments hold great potential for non-invasive diagnosis of cancer, retinal abnormalities and assessment of wound conditions, for instance diabetes. A portable hyper-spectral imager could also aid the analysis of human body fluids, such as blood, urine, saliva, semen and determine blood oxygenation levels of tissues, which could be of prime importance during surgeries. Yet importantly, it could perform diagnosis for dental diseases. It is a great advantage for a patient the fact that not only does an early diagnosis of an ailment can take place, but also an appropriate treatment may be applied at the same time [2].

Hyper-spectral signatures when combined with targeting algorithms would in essence offer unique diagnostic information. There is an increasing level of interest on the part of health care providers to investigate possible ways of reducing health care costs by providing timely treatments for many types of disease conditions. Hyper-Spectral scanning imaging is expected to contribute a lot in this pursuit [3].

2.6 Measures of Spectral Similarity

Considering the spectral nature of this research work, it is essential to be able to compare the estimated spectra with the reference spectra, in order to probe the efficiency of the system. The spatial information is perceived as a group of n-dimensional vectors in the processing procedure, where n responds to the total number of different spectra being measured. As a consequence, a wide variety of statistic measures can be applied in order to measure the degree of similarity between the achieved and expected results. The metrics, which has been used for the needs of this implementation, are the following.

2.6.1 Euclidean Distance

In mathematics, the Euclidean Distance or Euclidean Norm is the ordinary distance between two points that one would measure with a ruler. In Cartesian coordinates, if p = $(p_1, p_2, ..., p_n)$ and q = $(q_1, q_2, ..., q_n)$ are two points in Euclidean n-space, then the distance from p to q or from q to p is given by the formula:

$$d(p,q) = d(q,p) = \sqrt{(q_1 - p_1)^2 + (q_2 - p_2)^2 + ... + (q_n - p_n)^2}$$

$$\sqrt{\sum_{i=1}^{n} (q_n - p_n)^2}$$

2.6.2 Root Mean Squared Error (RMSE)

Mean Squared Error (MSE) is one of many ways to quantify the difference between values implied by an estimator and the true values of the quantity being estimated. MSE measures the average of the squares of errors. The error is the amount by which the value implied by the estimator differs from the quantity that is being estimated. Taking the square root of MSE yields the Root Mean Squared Error (RMSE) or Root Mean Squared Deviation (RMSD), which has the same units as the quantity being estimated. If p = $(p_1, p_2, ..., p_n)$ and q = $(q_1, q_2, ..., q_n)$ are two vectors, then the RMSE between them is given by the formula:

$$RMSE(p,q) = \sqrt{\frac{\sum_{i=1}^{n} (q_n - p_n)^2}{n}}$$

2.6.3 Root Mean Squared Error (RMSE)

Another metric for the evaluation of the results of spectral reconstruction algorithms is the Goodness-of-Fit Coefficient (GFC). GFC is a metric developed in [11] to test reconstructed daylight spectra. The GFC is based on the inequality of Schwartz and it is calculated by:

$$GFC = \frac{\sum_{i=1}^{N} q_i p_i}{\sqrt{\sum_{i=1}^{N} q_i^2}\sqrt{\sum_{i=1}^{N} p_i^2}}$$

This metric is interesting because its value is bounded to the interval [0, 1] and it provides an easy interpretation. From [11], if GFC is greater than 0.999 the spectral match is considered as good and if GFC is greater than 0.9999 the match is considered as excellent.

Chapter 3

Mid-Infrared Spectroscopy

One of the most common and widely used spectroscopic techniques is infrared (IR) spectroscopy. An instrument called infrared spectrometer acquires the infrared spectrum, which is most commonly depicted as a graph of wavelength n the horizontal axis, and infrared light absorbance (or transmittance) on the vertical one.

Traditionally, the measurement unit that is used to describe infrared radiation frequency is the reciprocal centimeter (cm^{-1}), or wavenumber, which symbolizes the number of wave cycles in one centimeter. It is preferred more than the Hz because the numbers are more manageable.

$$W = \frac{1}{\lambda}$$

Where W is the wavenumber in cm^{-1}. And is the wavelength in cm.

3.1 Vibrational Spectroscopy

By the end of the 1930s, scientists managed to expand Bohr's theories to model multielectron atoms and molecules. The creation of detailed models that accounted for the placement of electrons in orbitals provided key links in understanding elemental bonding, molecular structures, and chemical reactions; this new knowledge resulted to a greater understanding of molecular spectroscopy.

Each photon according to its wavelength corresponds to a specific molecular transition or motion: electronic, translational, rotational or vibrational. In electronic motion, the electrons change energy levels or directions of spin. In translational motion, the entire molecule shifts to a new position and in rotational motion, the molecule rotates around its center of mass. In order for

individual atoms in a molecule to move to new positions relative to one another while at the same time the molecule doesnt move, vibrational energy is required.

The energy levels can be rated in the following order: electronic ¿ vibrational ¿ rotational. Each of these transitions differs by an order of magnitude. Rotational transitions occur at lower energies (longer wavelengths) and this energy is insufficient and cannot cause vibrational (infra-red) and electronic (ultraviolet) transition because higher energy levels are required.

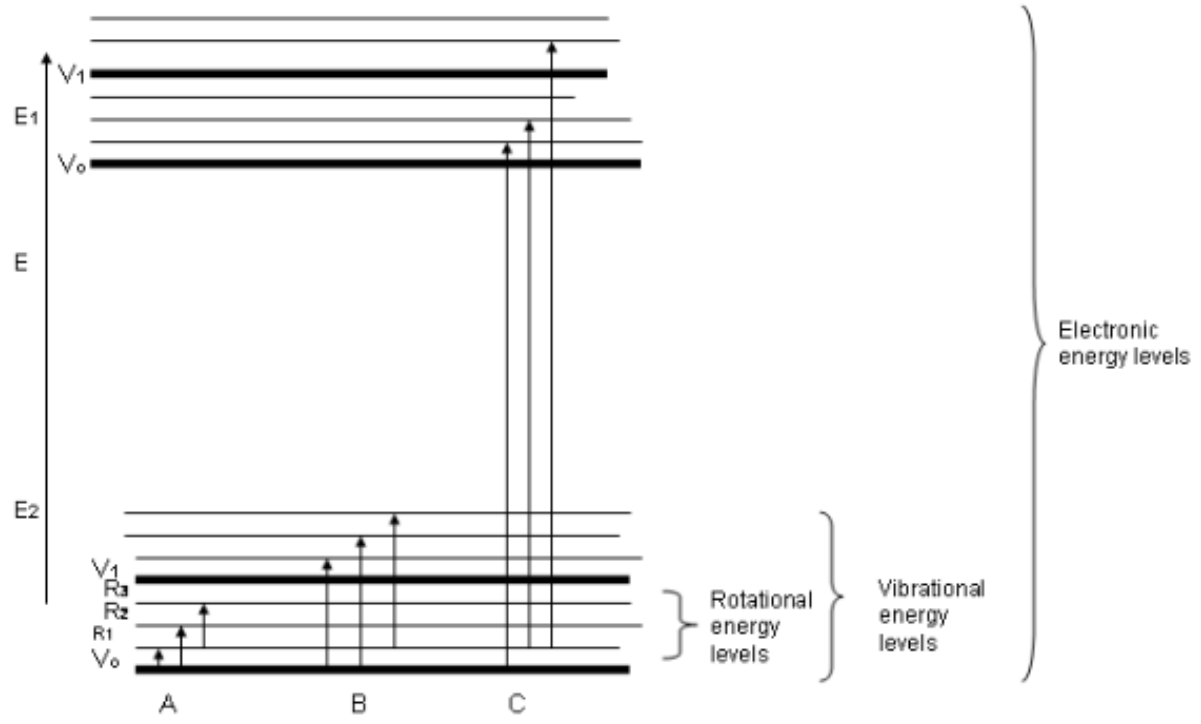

Figure 3.1: *Energy Levels that determine an atoms state*

Electrons within an atom arent affected by IR radiation because the energy is too low. However, IR radiation corresponds to the required energy for translational, rotational and vibrational energy transitions. If the fact that, a molecule's movements are unique to its structure is taken into account, it is obvious that the measurement of these transitions make IR a powerful tool for compound characterization. The aid of high resolution instruments is necessary to detect the primary transitions in the IR region. Those transitions are vibrational and are very weak to be detected with conventional methods.

A way to detect IR absorption is to study the net change in dipole moment in a molecule during vibration. In other words, if there is a change in the magnitude of the charge or the distance between the two centers of charge then we can assume that the dipole moment has changed. During molecular vibration, there is a fluctuation in its dipole moment and as a result an electric

field associated with radiation is generated. Absorption takes place when radiation frequency coincides with the frequency of the molecules natural vibration and this alters the amplitude of the molecular vibration. This also occurs when the rotation of asymmetric molecules around their centers results in a dipole moment change, which permits interaction with the radiation field.

3.2 Degrees of Freedom

In a molecule, the atoms are constrained by molecular bonds to move together in certain specified ways, called degrees of freedom. Given a known molecular structure, molecular transitions can be predicted due to its constraints. If this molecule is placed in the center of a three-dimensional Cartesian coordinate system (x, y, and z) and each atom is designated by its coordinates in space, it can be deduced that a molecule with N (any number) atoms will possess up to 3N coordinates. Those coordinates are the potential transitions that the molecule can go through, or in other words its degrees of freedom. For example, given a molecule with 6 atoms, the degrees of freedom are 18.

The 3N degrees of freedom can be assigned to the translational, rotational, and vibrational motions of the molecule. Three of those degrees of freedom represent the molecules center of mass movement on the x, y or z axis. When it comes to non-linear molecules, three additional degrees of freedom represent the spinning around each one of the x, y or z axis. On the contrary, linear molecules have one less rotational degree of freedom, because two rotational directions are practically the same. As a result the amount of translational and rotational degrees of freedom is 6 (5 for linear molecules) and it can be deduced that a molecules remaining, 3N - 6, possible motions are its vibrational degrees of freedom (3N - 5 in the case of linear molecules). The importance of this number as far as infrared spectroscopy is concerned can easily be understood since vibrational transitions are the strongest and most important in IR spectroscopy.

The sentence above can be illustrated with an example; a nonlinear molecule with 3 atoms has 3 fundamental vibrations, as shown in the Figure below. All vibrational motions of the atoms can be described completely in terms of these 3N - 6 fundamental vibrations, which are called the normal modes of vibration for the molecule. Stretching, torsional, and bending modes are the vibrations most commonly seen and those that will be studied in the following chapters. The term stretching is used to describe the increase or decrease of the length of the bonds between the atoms. Skeletal or torsional vibration is the twisting of the backbone of the molecule. Lastly, a change in the bond angles of the atoms relative to one another or to the rest of the molecule is called bending vibration. This type vibration can be further classified as scissoring, rocking, wagging, and twisting. Vibrations are also characterized by their symmetry and can either be symmetric or asymmetric [12].

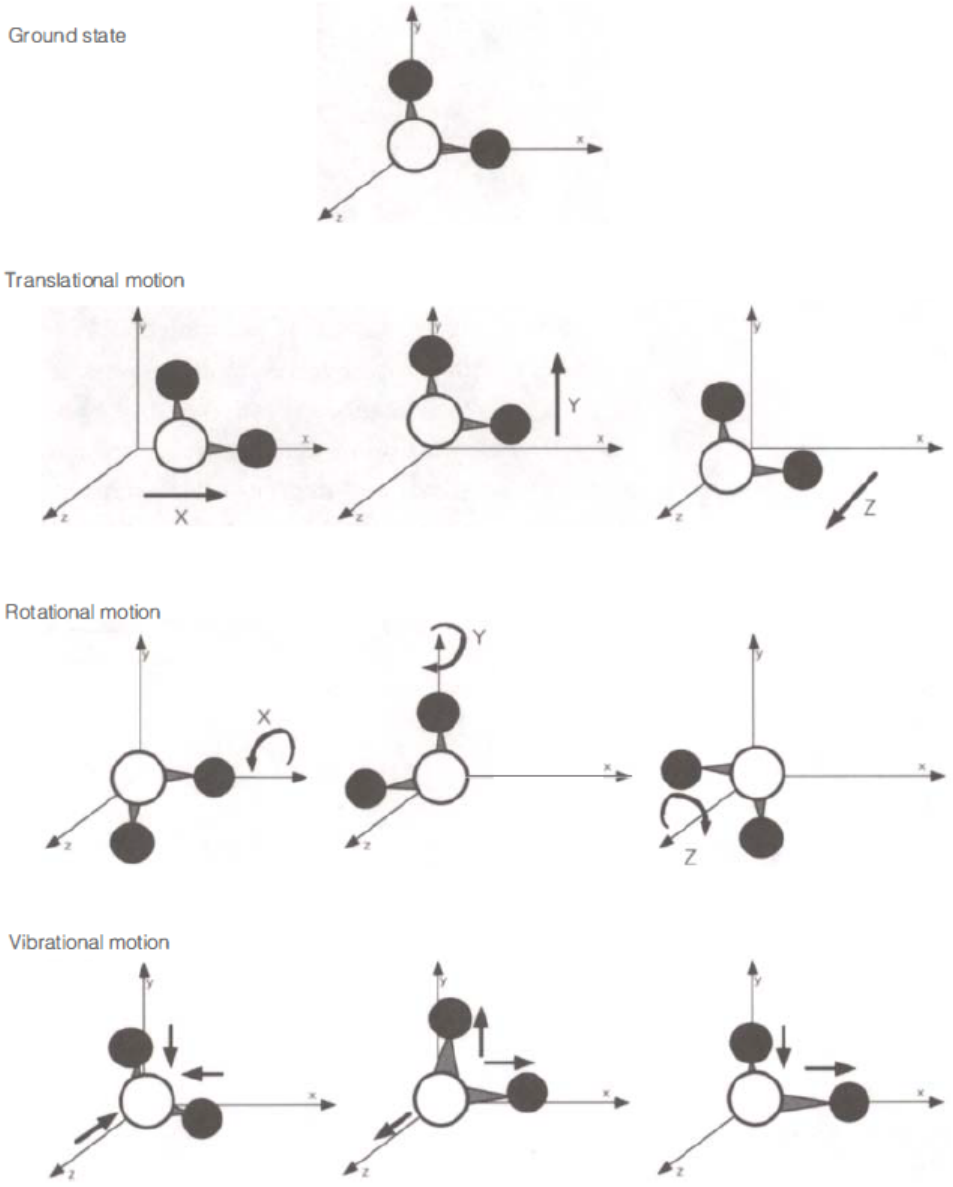

Figure 3.2: *A molecule's degrees of freedom*

3.3 Molecular Vibrations

Covalent bonds do not connect atoms by rigid links. On the contrary, the reason why atoms are held together is because both nuclei are attracted to the same pair of electrons. This causes the nuclei to vibrate around this position in a direction that can be backwards and forwards, towards and away from each other. We define as a molecular vibration the periodic motion of the atoms

in a molecule, while at the same time the molecule as a hole retains a constant translational and rotational motion. The frequency of the periodic motion is known as a vibration frequency, and the typical frequencies of molecular vibrations range from less than 10^{13} to approximately 10^{14} Hz, corresponding to wavenumbers of approximately 300 to 3000 (cm^{-1}. Bonds are constantly vibrating, but if light of the exactly right amount of energy is shined on a bond, it kicks it into a higher state of vibration. The amount of energy required depends on the kind of the bond, so different bonds will absorb light of different frequency (and hence energy) in the infra-red band of the spectrum.

When a molecule absorbs a quantum of energy, E, corresponding to the vibration's frequency, f, according to the relation E = h (where h is Planck's constant). A fundamental vibration is excited when one such quantum of energy is absorbed by the molecule in its ground state. When two quanta are absorbed the first overtone is excited, and so on to higher overtones.

To a first approximation, the motion in a normal vibration can be described as a kind of simple harmonic motion. In this approximation, the vibrational energy is a quadratic function (parabola) with respect to the atomic displacements and the first overtone has twice the frequency of the fundamental. In reality, vibrations are inharmonic and the first overtone has a frequency that is slightly lower than twice that of the fundamental, thus excitation of the higher overtones involves progressively less and less additional energy.

3.3.1 Vibration Coordinates

The coordinate of a normal vibration is a combination of changes in the positions of atoms in the molecule. When the vibration is excited the coordinate changes with a frequency f, the frequency of the vibration.

Internal coordinates are of the following types:

- **Stretching :** a change in the length of a bond.
  - Symmetric
  - Asymmetric
- **Bending**
  - Scissoring : a change in angle between groups of atoms.
  - Rocking : a change in angle between groups of atoms.
  - Wagging : a change in angle between the planes of a group of atoms.
  - Twisting : a change in the angle between the planes of two groups of atoms.

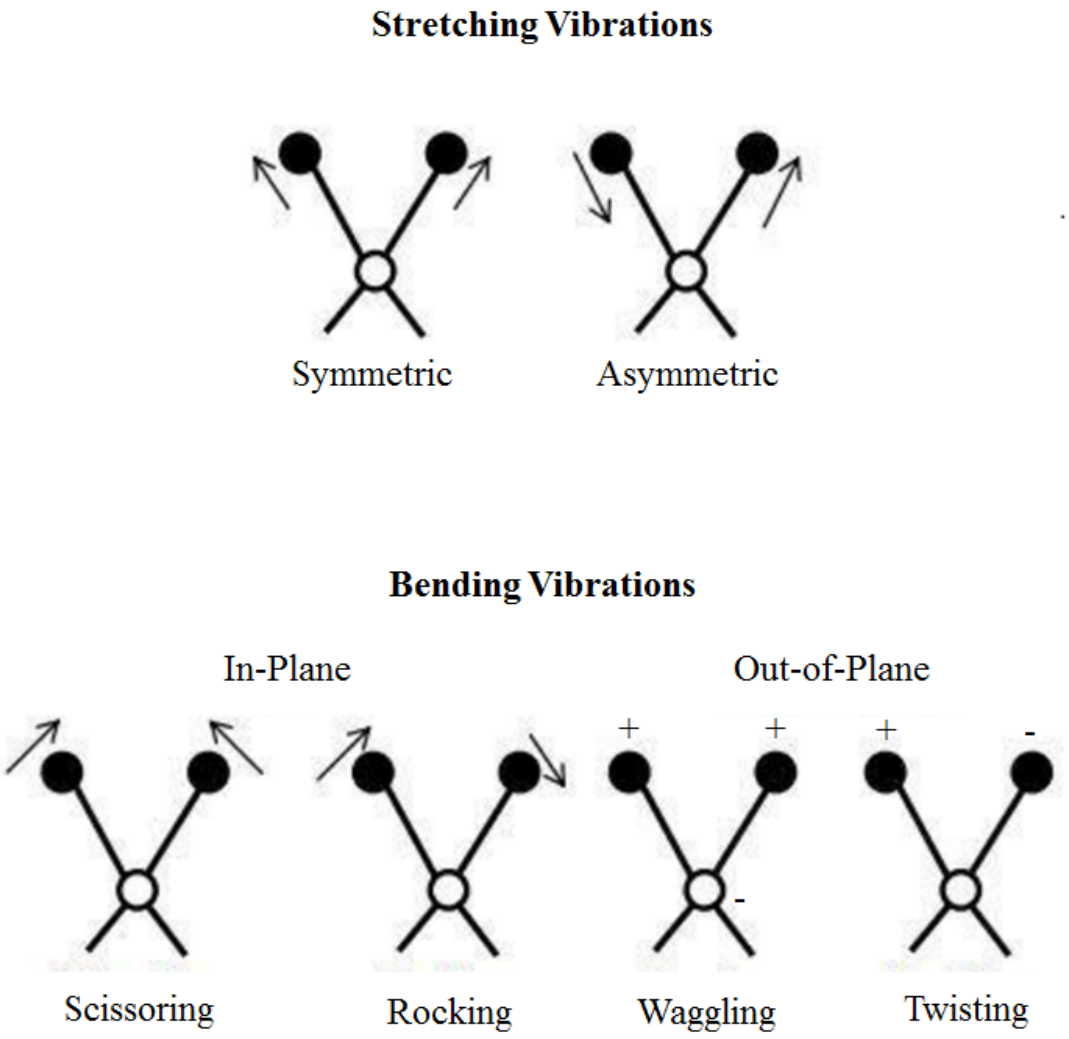

Figure 3.3: *The molecular vibrations of a CH_2 group.The arrows show the motions in the molecule'splane, while the + and - sings denote motion above and below the plain respectively*

3.3.2 Vibration Frequency

Molecular vibrations can be treated using Newtonian mechanics to calculate the correct vibration frequencies. The basic assumption is that each pair of atoms can be treated as though the atoms are masses connected by a spring. In the harmonic approximation the spring obeys Hooke's law: the force required to extend the spring is proportional to the extension. The proportionality constant is known as a force constant, k. Strong bonds have higher force constants, while weak bonds have lower force constants.

$$\vec{v} = \frac{1}{2\pi c}\sqrt{\frac{\kappa}{\mu}} = \frac{1}{2\pi c}\sqrt{\frac{\kappa\,(m1+m2)}{(m_1 * m_2)}}$$

Where V is the vibrational frequency, c is the speed of light and m_1 and m_2 are the atoms masses.

3.4 Infrared Spectrum

The IR spectrum can be divided into four different regions. The first region spreads from 4000 cm^{-1} to 2500 cm^{-1} and it is the area where X H bonds and absorb radiation. Typically, the N-H and C-H bonds absorb in the range 3300 - 3600 cm^{-1} while the CH bonds absorb near 3000 cm^{-1}. As it can be seen at Figure 3.4 the characteristic peak of the C-O of vanillin is easily spotted at 3600 cm^{-1}, while absorbance from C-H bonds can be spotted at 3000 cm^{-1}.

In the 2500-2000 cm^{-1} range absorbance is caused by triple bonds and radiation between 2000 and 1500 cm^{-1} is absorbed by double bonds stretching vibrations. Usually C = O and C = N absorb more radiation than C = C. This is due to the electronegativity difference at C = O and C = N which increases the change in bipolar vibration.

In the range below 1500 cm^{-1}, too many absorptions can be spotted, most of which cannot easily be attributed to particular stimuli. The complexity of this area makes it unique and distinct for each association, and it is called a fingerprint area. In the fingerprint area, absorbance is caused by single-link vibrations and all bending vibrations appear. It is easier to bend a molecule than stretch it, hence stretching vibrations have higher frequencies and require greater energy than bending modes.

It is also emphasized that strong bonds absorb at higher frequencies than the weaker ($triple > doubles > simple$), explained by the Hook law discussed earlier and X-H bonds absorb at very high frequencies due to a small reduced mass recalled that is inversely proportional to the absorption frequency.

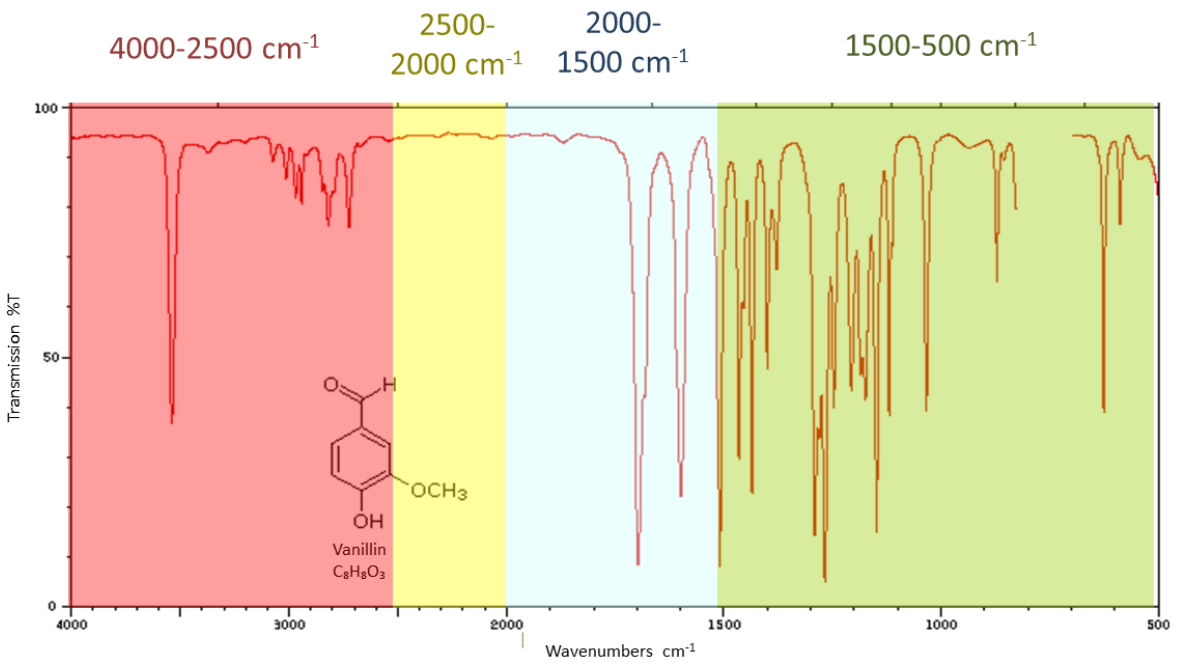

Figure 3.4: *The regions of the spectrum where each category of bonds typically absorbs electromagnetic radiation*

A bonds vibrational frequency is only affected by the type of the bond and the masses of the connected atoms. The chemical environment of the bond doesnt play a major role as to where the absorption picks will be located. However a peaks width for solid and liquid samples is determined by the number of intermolecular interactions. Figure 3.5 shows hydrogen bond in water molecules and these water molecules are in different chemical environments. Because the number and strength of hydrogen bonds differs with chemical environment, the force constant varies and the wavenumber differs at which these molecules absorb infrared light.

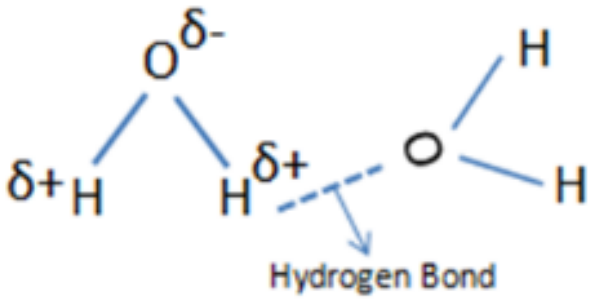

Figure 3.5: *Hydrogen bond formed between an oxygen atom and a hydrogen atom that belong in different molecules.*

In any sample where hydrogen bonding occurs, the number and strength of intermolecular interactions varies greatly within the sample, causing the bands in these samples to be particularly broad. This is illustrated in the spectrum of ethanol in Figure 3.6. When intermolecular interactions are weak narrow infrared bands are observed.

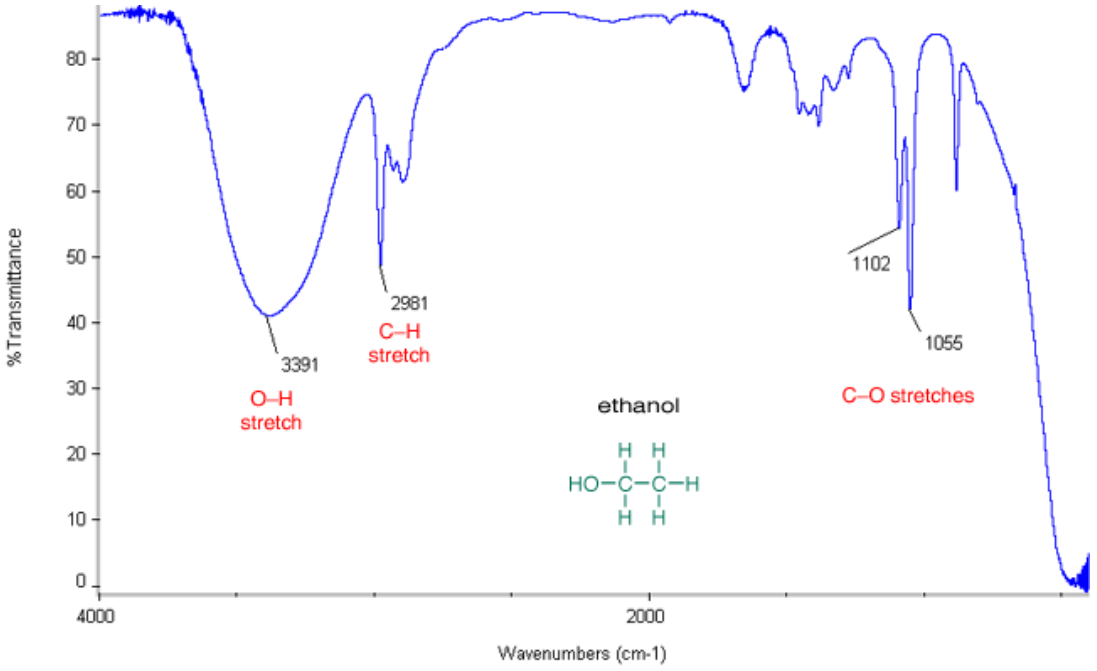

Figure 3.6: *Infrared spectrum of Ethanol with the charcteristic absorption frequencies*

Last but not least, the IR spectrum of Formaldehyde, CH2O (C2v) is analyzed as an example. Formaldehyde molecules have 3N 6 = 6 vibrational modes. Specifically a C-H symmetric stretching, a C-H asymmetric stretching, a C-O stretching, a H-C-H in-plane scissoring, a H-C-H in-plane rocking and a H-C-H out-of-plane wagging. Figure 3.7 shows Formaldehydes transmittance ratio for the infrared spectrum and the frequencies where absorption takes place can easily be located. We can see six peaks as expected, each one of them associated with a different vibrational mode.

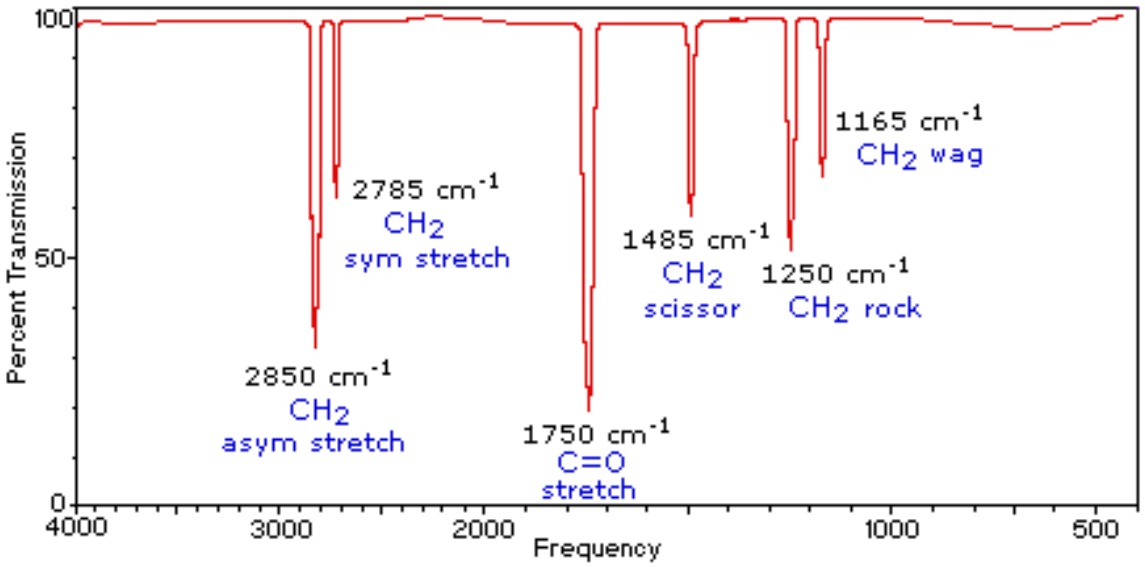

Figure 3.7: *Infrared spectrum of Formaldehyde with the charcteristic absorption frequencies*

The absorption peaks within this region are usually sharper when compared with absorption peaks from the ultraviolet and visible regions. In this way, IR spectroscopy can be very sensitive to determination of functional groups within a sample since different functional group absorbs different particular frequency of IR radiation. Also, each molecule has a characteristic spectrum often referred to as the fingerprint. A molecule can be identified by comparing its absorption peak to a data bank of spectra. IR spectroscopy is very useful in the identification and structure analysis of a variety of substances, including both organic and inorganic compounds. It can also be used for both qualitative and quantitative analysis of complex mixtures of similar compounds.

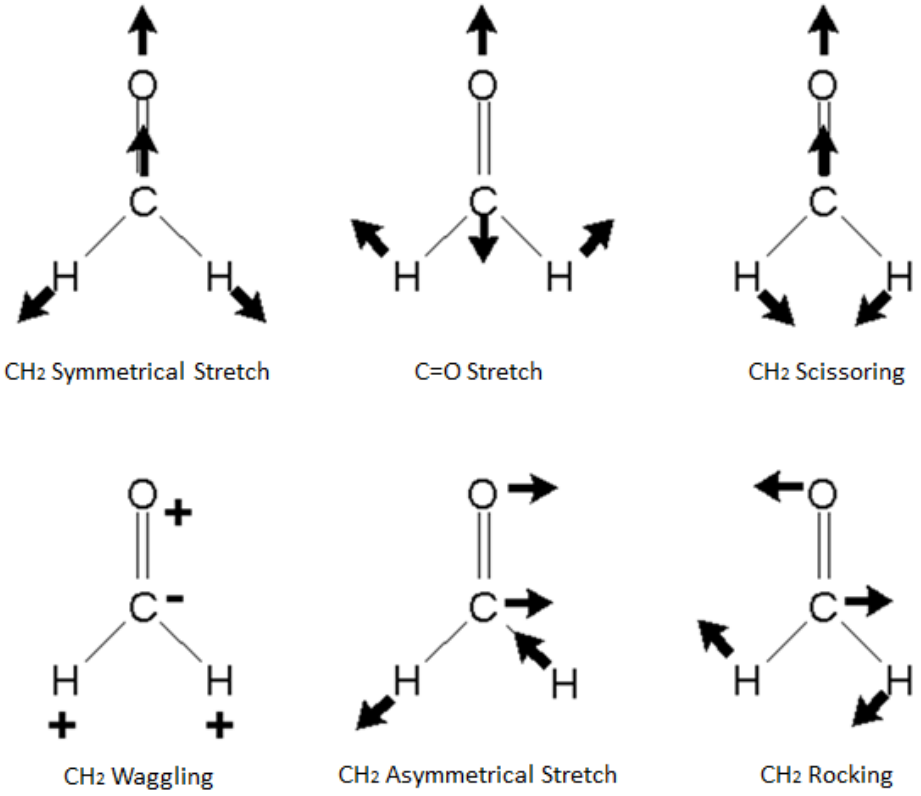

Figure 3.8: *Formaldehyde vibrations*

3.5 Advantages and Disadvantages of Infrared Spectroscopy

Advantages	**Disadvantages**
Infrared spectroscopy can be used in solid, liquid and gas compound analysis.	Atoms or monatomic ions do not have infrared spectra and thus can not be detected.
Peak positions, intensities, widths and shapes, all provide useful information about the tested sample.	Complex mixture and aqueous solutions are difficult to analyze using infrared spectroscopy.
Its a fast and easy technique.	Homonuclear diatomic molecules do not possess infrared spectra.
Peak positions, intensities, widths and shapes, all provide useful information about the tested sample.	
Great sensitivity can be achieved (Even micrograms of materials can be detected).	
Relatively inexpensive technique.	

Chapter 4

Fourier-Transform Infrared Spectroscopy

Fourier-transform infrared spectroscopy (FTIR) is a technique used to obtain an infrared spectrum of absorption or emission of a solid, liquid or gas. An FTIR spectrometer simultaneously collects high-spectral-resolution data over a wide spectral range. This confers a significant advantage over a dispersive spectrometer, which measures intensity over a narrow range of wavelengths at a time.

The term Fourier-transform infrared spectroscopy originates from the fact that a Fourier transform (a mathematical process) is required to convert the raw data into the actual spectrum.

4.1 Developmental Breakthrough

Up till FTIR spectrometers, there have been three generations of IR spectrometers. The first low-cost spectrophotometer capable of recording an infrared spectrum was the Perkin-Elmer Infracord, produced in 1957. This instrument covered the wavelength range from 2.5 m to 15 m (wavenumber range 4000 cm^{-1} to 660 cm^{-1}). The lower wavelength limit was chosen to encompass the highest known vibration frequency due to a fundamental molecular vibration. The upper limit was imposed by the fact that the dispersing element was a prism made from a single crystal of rock-salt (sodium chloride), which becomes opaque at wavelengths longer than about 15 m; this spectral region became known as the rock-salt region. Later instruments used potassium bromide prisms to extend the range to 25 m (400 cm^{-1}) and caesium iodide 50 m (200 cm^{-1}). The region beyond 50 m (200 cm^{-1}) became known as the far-infrared region; at very long wavelengths it merges into the microwave region. An additional issue was the need to

exclude atmospheric water vapor because water vapor has an intense pure rotational spectrum in this region. Far-infrared spectrophotometers were cumbersome, slow and expensive.

The second generation IR spectrometer was introduced to the world in 1960s. The advantages of the Michelson interferometer were well-known, but considerable technical difficulties had to be overcome before a commercial instrument could be built. Also an electronic computer was needed to perform the required Fourier transform, and this only became practicable with the advent of mini-computers, such as the PDP-8, which became available in 1965. Digilab pioneered the world's first commercial FTIR spectrometer (Model FTS-14) in 1969.

Nowadays FTIR spectroscopy offers a vast array of analytical opportunities in areas such as academic research, QA/QC (quality assurance, the set of processes used to measure and assures the quality of a product and quality control. In other words the process of ensuring products and services meet consumer expectations) and forensic labs. Deeply ingrained in everything from simple compound identification to process and regulatory monitoring, FTIR covers a wide range of chemical applications, especially for polymers and organic compounds.

4.2 FTIR Spectrometers

The parts of a typical FTIR spectrometer are: the source, the interferometer, the sample compartment, the detector, the amplifier, the A/D convertor, and a computer. The source generates radiation which passes the sample through the interferometer and reaches the detector. Then the signal is amplified and converted to digital signal by the amplifier and analog-to-digital converter, respectively. Eventually, the signal is transferred to a computer in which Fourier transform is carried out. Figure 4.1 shows a block diagram of an FTIR spectrometer.

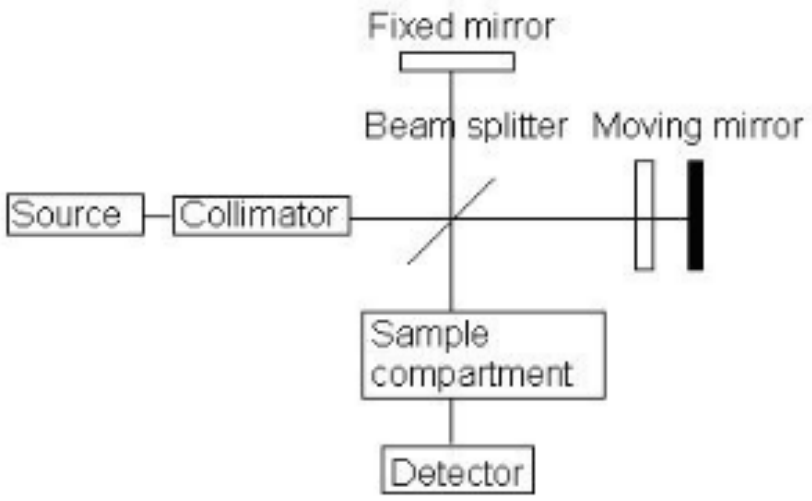

Figure 4.1: *Block diagram of an FTIR Spectrometer*

The major difference between an FTIR spectrometer and a dispersive IR spectrometer is the Michelson interferometer.

4.2.1 Michelson Interferometer

The Michelson interferometer, which is the core of FTIR spectrometers, is used to split one beam of light into two so that the paths of the two beams are different. Then the Michelson interferometer recombines the two beams and conducts them into the detector where the differences of the intensity of these two beams are measured as a function of the difference of the paths. Figure 4.2 shows a schematic of the Michelson Interferometer.

A typical Michelson interferometer consists of two perpendicular mirrors and a beamsplitter. One of the mirrors is a stationary mirror and another one is a movable mirror. The beamsplitter is designed to transmit half of the light and reflect half of the light. Subsequently, the transmitted light and the reflected light strike the stationary mirror and the movable mirror, respectively. When reflected back by the mirrors, two beams of light recombine with each other at the beamsplitter.

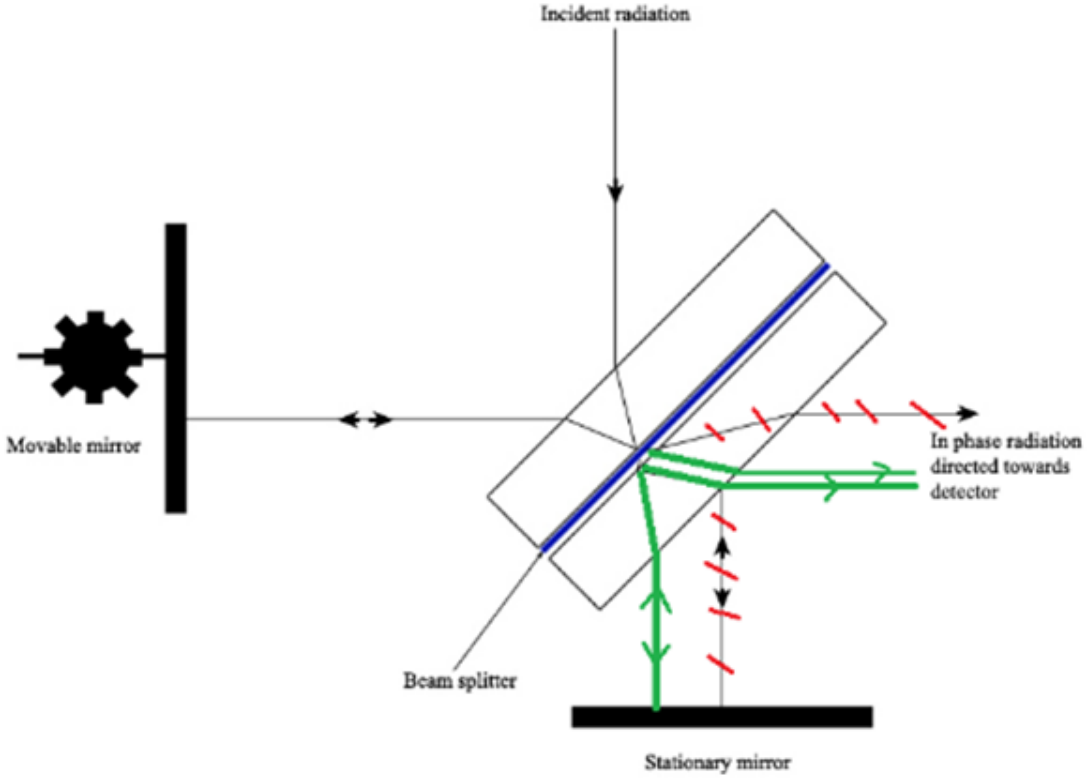

Figure 4.2: *Michelson Interferometer*

If the distances travelled by two beams are the same which means the distances between two mirrors and the beamsplitter are the same, the situation is defined as zero path difference (ZPD). But imagine if the movable mirror moves away from the beamsplitter, the light beam which strikes the movable mirror will travel a longer distance than the light beam which strikes the stationary mirror. The distance which the movable mirror is away from the ZPD is defined as the mirror displacement and is represented by Δ. It is obvious that the extra distance travelled by the light which strikes the movable mirror is 2Δ. The extra distance is defined as the optical path difference (OPD) and is represented by delta. Therefore,

$$\delta = 2\Delta$$

It is well established that when OPD is the multiples of the wavelength, constructive interference occurs because crests overlap with crests, troughs with troughs. As a result, a maximum intensity signal is observed by the detector. This situation can be described by the following equation:

$$\delta = n\lambda$$

Where n = 0,1,2,3...

On the contrary, when OPD is the half wavelength or half wavelength add multiples of wavelengths, destructive interference occurs because crests overlap with troughs. Consequently, a minimum intensity signal is observed by the detector. This situation can be described by the following equation:

$$\delta = \left(n + \frac{1}{2}\right)\lambda$$

Where n = 0,1,2,3...

These two situations are two extreme situations. If the OPD is neither n-fold wavelengths nor $\left(n + \frac{1}{2}\right)$-fold wavelengths, the interference should be between constructive and destructive. So the intensity of the signal should be between maximum and minimum. Since the mirror moves back and forth, the intensity of the signal increases and decreases which gives rise to a cosine wave.

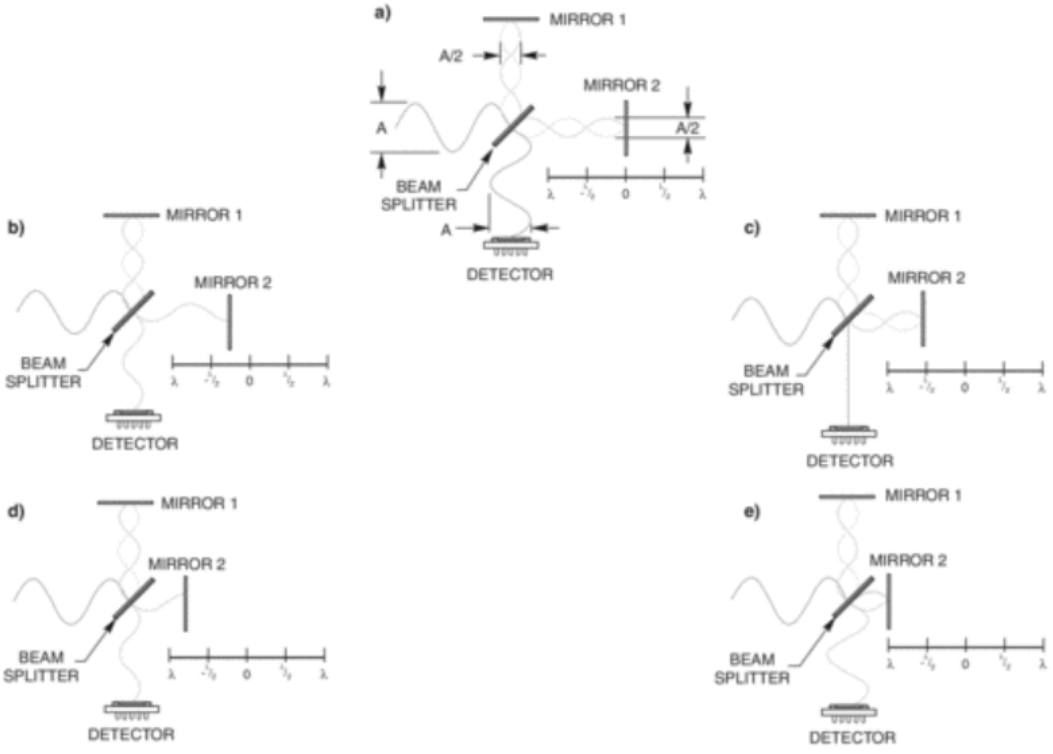

Figure 4.3: *Cosine waves based on the mirror's position*

The plot is defined as an interferogram. When detecting the radiation of a broad band source rather than a single-wavelength source, a peak at ZPD is found in the interferogram.

4.2.2 Michelson Interferometer

Interferogram is the name of the signal format acquired by an FT-IR spectrometer. It is usually significantly more complex looking than a single sinusoid, which would be expected if only a single wavelength of light was present. Figure 4.4 depicts the interferogram of a broadband light source.

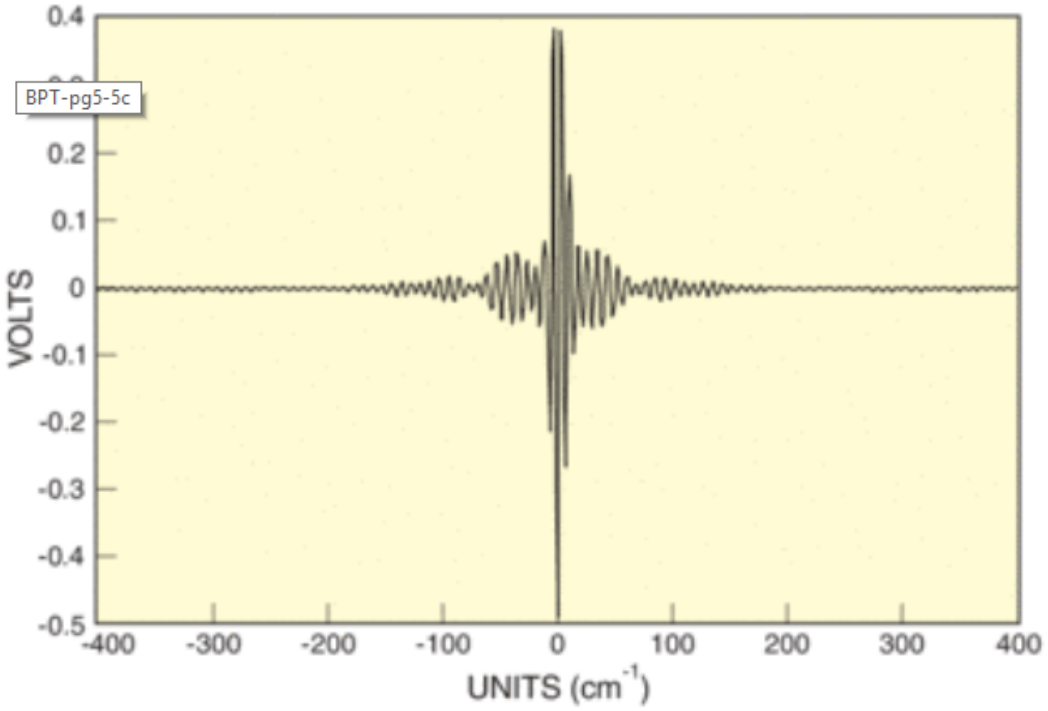

Figure 4.4: *Interferogram of a broadband light source*

The centerburst, the big spike in the center of Figure 4.4 is a telltale signature of a broadband source. Its origin lies in the fact that all wavelengths are in-phase at the ZPD. Therefore, their contributions are all at maximum and a very strong signal is produced by the systems detector.

As the optical path difference, OPD, grows different wavelengths produce peak readings at different positions and, for a broadband signal, they never again reach their peaks at the same time. Thus, as you move away from the center, the interferogram becomes a complex looking oscillatory signal with decreasing amplitude.

4.2.3 Fourier Transform of Interferogram to Spectrum

Once an interferogram is collected, it needs to be translated into a spectrum (emission, absorption, transmission, etc.). The process of conversion is through the Fast Fourier Transform algorithm. Figure 4.5 shows the Fast Fourier transform from an interferogram of polychromatic light to its spectrum.

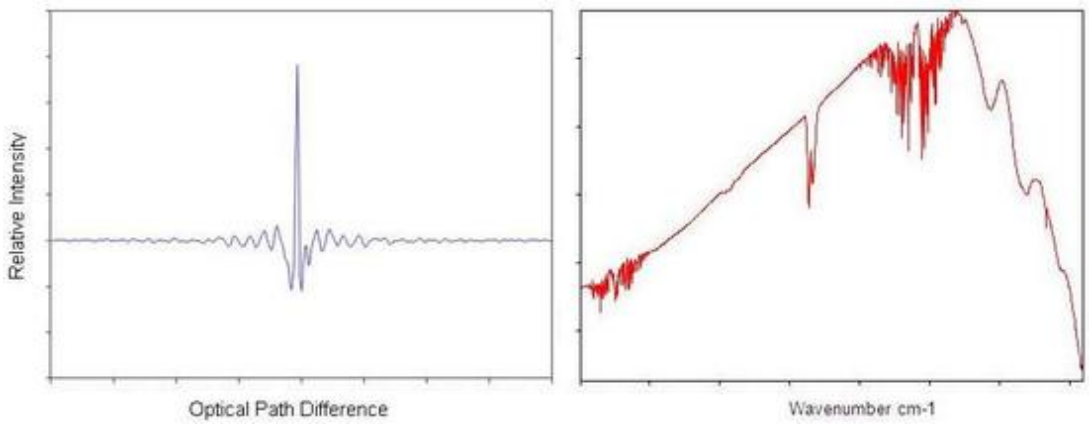

Figure 4.5: *Interferogram and spectrum of a broadband light source*

The first who found that a spectrum and its interferogram are related via a Fourier transform was Lord Rayleigh. He made the discovery in 1892. But the first one who successfully converted an interferogram to its spectrum was Fellgett who made the accomplishment after more than half a century. Fast Fourier transform method on which the modern FTIR spectrometer based was introduced to the world by Cooley and Turkey in 1965 followed by an explosive growth of computational power at affordable prices.

Fourier transform, named after the French mathematician and physicist Jean Baptiste Joseph Fourier, is a mathematical method to transform a function into a new function. The following equation is a common form of the Fourier transform with unitary normalization constants:

$$F(\omega) = \frac{1}{\sqrt{2\pi}} \int_{-\infty}^{\infty} f(t)\, e^{-\iota\omega t} dt$$

The following equation shows how f(t) is related to F(v) via a Fourier transform:

$$f(t) = \frac{1}{\sqrt{2\pi}} \int_{-\infty}^{\infty} F(v)\, cos\,(2\pi v t) dv$$

4.3 FTIR Advantages

FT-IR instruments hold three significant advantages over dispersive spectrometers:

- **Multiplex (Fellgett) Advantage:** In a dispersive spectrometer, wavenumbers are observed sequentially, as the grating is scanned. In an FT-IR spectrometer, all the wavenumbers of light are observed at once. When spectra are collected under identical conditions (spectra collected in the same measurement time, at the same resolution, and with the same source, detector, optical throughput, and optical efficiency) on dispersive and FT-IR spectrometers, the signal-to-noise ratio of the FT-IR spectrum will be greater than that of the dispersive IR spectrum by a factor of $\sqrt{M}$, where $\sqrt{M}$ is the number of resolution elements. This means that a 2 cm^{-1} resolution 800 - 8000 cm^{-1} spectrum measured in 30 minutes on a dispersive spectrometer would be collected at equal S/N on an FT-IR spectrometer in 1 second, provided all other parameters are equal.

- **The Throughput (Jacquinot) Advantage:** For the same resolution, the energy throughput in an interferometer can be higher than in a dispersive spectrometer, where it is restricted by the slits. In combination with the Multiplex Advantage, this leads to one of the most important features of an FT-IR spectrometer: the ability to achieve the same signal-to-noise ratio as a dispersive instrument in a much shorter time.

- **Precision (Connes) Advantage:** The wavenumber scale of an interferometer is derived from a HeNe (helium neon) laser that acts as an internal reference for each scan. The wavenumber of this laser is known very accurately and is very stable. As a result, the wavenumber calibration of interferometers is much more accurate and has much better long term stability than the calibration of dispersive instruments.

- **No discontinuities Advantage:** Because there are neither grating nor filter changes, there are any discontinuities in the spectrum.

- **Negligible stray light Advantage:** Because there is no grating or filter changes, there are any discontinuities in the spectrum.

- **Constant resolution Advantage:** Resolution is constant at all wavenumbers in the defined spectral range but the signal-to-noise ratio varies across the spectrum. FT-IR instruments have a much higher optical throughput than dispersive instruments and do not use slits to define the resolution. Instead, the resolution is defined by the J-stop (Jacquinot stop) aperture size, which does not change during data collection. In dispersive instruments, throughput is typically optimized by adjusting the slit width during the scan. Thus, signal-to-noise is constant but resolution varies.

- **Non Destructive Method Advantage:** the light doesn't fragment the sample; it just excites it at various frequencies so that the molecules vibrate at certain intensities depending on how close the current frequency is to the resonant frequency. In most cases, the samples used for FTIR spectroscopic investigations can be completely recovered and used for further analysis elsewhere.

4.4 FTIR Disadvantages

However, FTIR spectrometers have some disadvantages as compared to dispersive instruments:

- **Multiplex (Fellgett) Disadvantage:** This arises because all regions of the spectrum are observed simultaneously. Therefore, if noise occurs in one part of the radiation from the infrared source, it will be spread throughout the spectrum. In a dispersive system, the noise would be seen only in the region of the spectrum in which it arose.
- **Single Beam Disadvantage:** FTIR instruments have a single beam, whereas dispersive instruments usually have a double beam. Assuming there is no change in atmospheric conditions throughout the experiment, this does not cause a problem. However, for highly sensitive experiments, or experiments that take a long time, changes in infrared absorbing gas concentrations can severely affect the results.
- **Sample Size Disadvantage:** The size of the item that needs to be scanned must be small enough to enter the spectrometers cavity. Most of the times this is not the case and as a result a sample must be taken.
- **Sample Preparation Disadvantage:** Cases when samples are too concentrated, practically absorbing all infrared radiation, must be diluted by mixing with infrared transparent diluters, such as KBr for diffuse reflectance measurements. While the sample is not destroyed in this procedure, it is intimately combined with KBr making it unrecoverable. This is particularly important when examining the chemical composition of unique, non-reproducible samples such as in forensic analysis, or in the analysis of artwork and historical artifacts.
- **Gas Analysis Disadvantage:** Special equipment is required in order to acquire the spectra of gases via FTIR spectrometry. Figure 4.6

Figure 4.6: *A complete FTIR-based gas analysis system*

Chapter 5

Thermal Cameras and Quantum Cascade Lasers

Thermal Imaging is the process imaging using Mid Infrared or Far Infrared radiation ($7000 - 14000nm$), which is the radiation emitted from every material at room temperature. The energy of the electromagnetic radiation in this region is not enough to cause ionization or to excite the electrons of a camera sensor to the conduction zone. As a result thermal cameras are taking advantage of different, macroscopic, properties of specific materials. One such property is photoresistance. Radiation in the $7 - 14\mu m$ band can rise the temperature of a conductors material and as a result change the conductors resistance. MIR and FIR radiation can be calculated from the changes in a materials temperature.

Thermal Imaging can be achieved with two ways:

- Passive Thermography: Depicting the object as a thermal source
- Active Thermography: Depicting the object as it is being heated by an external source.

Active thermography is mostly used in non-destructive evaluation (NDE). When a sample is heated, faulty areas have different temperature than the non-fault ones and thus can be identified. These areas can also be below the surface.

5.1 Thermal Sensors

Temperature is the measure of the average kinetic energy of the molecules of a gas, liquid, or solid. A thermal sensor is a device that is specifically used to measure temperature. In this way, thermal sensors are able to give us a quantifiable way to describe the substance, whether it is an object, the environment in which an object is placed or the environment in which an object is distributed.

5.1.1 Thermistors

Resistance thermometers are also known as resistance temperature detectors, or RTDs. They are typically made of a single pure metal [8]. Each metal has a material property of electrical resistance that is a function of temperature. The most accurate resistance thermometers are ones that use metals that have a very linear relationship with temperature, such as platinum. By using the relationship curves between electrical resistance and temperature, when the resistance of the metal is measured, a temperature can be calculated. A thermistor is a specific type of resistance thermometer. Thermistors are made of metal wires connected to a ceramic base made of several sintered, oxide semiconductors [9]. Like other resistance thermometers, the change in temperature can be calculated from the change in resistance. But unlike traditional resistance thermometers, the relationship is not very linear. Thus, the temperature range in which thermistors can be used is small compared to traditional resistance thermometers. But thermistors have the advantages of being small in size, inexpensive to buy and very sensitive to temperature changes, so they can be ideal to use in many electronics applications [9].

Thermistors are divided into two categories:

- Negative temperature coefficient (NTC) whose resistance is reduced as temperature rises.
- Positive temperature coefficient (PTC) whose resistance rises as temperature rises.

A common problem with thermistors is that they can be damaged due to (self)-heat. PTCs have an advantage because when they are heated by infrared radiation their resistance rises. As a result, less current goes through the thermistor and the temperature developed is less.

5.1.2 Bolometers

In thermal cameras, each pixel behaves like a small thermometer. Using a special lens which is created from special materials, with the ability to focus infrared radiation, the thermal image is projected on the sensor. The sensors area is covered by thermistors which convert the infrared radiation to voltage or current change.

Nowadays, the sensors most commonly used are called bolometers. Bolometers are so popular due to the fact that they dont need cooling and as a result are cheaper, smaller and simpler than other types of thermistors.

Every pixel (figure 5.1) on the sensor area is made of a material (usually Vanadiunoxide (VOX) or amorphous silicon) with small mass which also absorbs infrared radiation. This material is placed on small laminates in order to reduce the temperature loss caused by induction. The smaller the sensors mass, the less radiation is needed to achieve a measurable change of resistance. A reflective layer is placed under the sensor, in order to reflect radiation that isnt absorbed back to the sensor and increase its sensitivity.

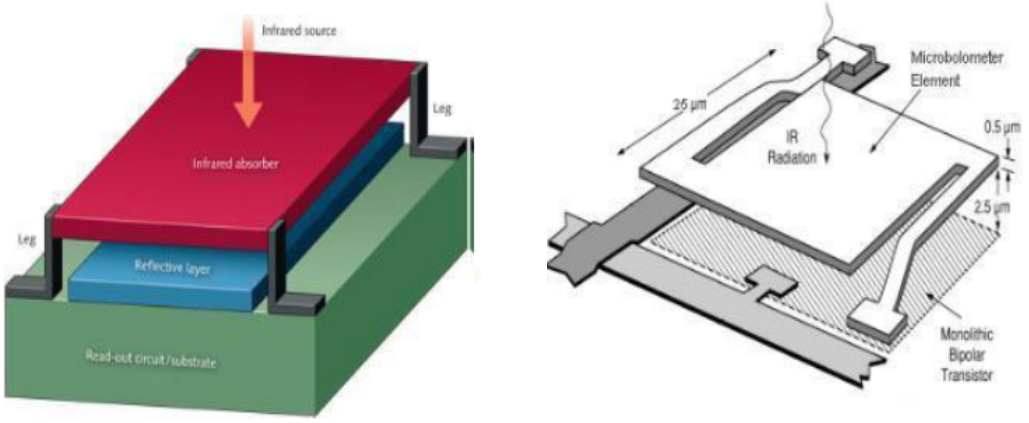

(a) *Bolometer depiction* ***(b)*** *Bolometer scetch*

Figure 5.1: *Bolometers that cover a sensor's area*

5.2 Quantum Cascade Lasers

Quantum Cascade Lasers (QCLs) are semiconductor lasers that emit in the mid- and long-wave IR bands. They were first demonstrated in 1994 by the Bell Labs Team of Jerome Faist, Federico Capasso, Deborah, Sivco, Carlo Sirtori, Albert Hutchinson, and Alfred Cho [14]. Since their invention in 1994, QCLs have reached maturity. They now are a well-established class of opto-electronic devices that can produce coherent radiation in a wide part of the infrared spectrum, although the best performances are obtained in the 5 to 13 μm wavelength range. Their wide tuning range and fast response time allow for faster and more precise compact trace element detectors and gas analyzers that are replacing slower and larger FTIR, mass spectroscopy, and photothermal microspectroscopy systems. Unlike typical interband semiconductor lasers that emit electromagnetic radiation through the recombination of electronhole pairs across the material band gap, QCLs are unipolar and laser emission is achieved through the use of intersubband transitions in a repeated stack of semiconductor multiple quantum well heterostructures [15].

The thickness of such a quantum well is typically $5 - 20nm$. Such thin layers can only be fabricated with molecular beam epitaxy (MBE) or metal-organic chemical vapor deposition (MOCVD). There are at least two techniques by which quantum well structures can be grown, molecular beam epitaxy (MBE) [16], and metal-organic chemical vapor deposition (MOCVD) [17]. Both can achieve a layer thickness control close to about one atomic layer. MBE is essentially a very high vacuum technique in which beams of the constituent atoms or molecules (e.g., Ga, Al, or As) emerge from ovens, land on the surface of a heated substrate, and there grow layers of material. Which material is grown can be controlled by opening and closing shutters in front of the ovens. For example, with a shutter closed in front of the Al oven, but open shutters in from of the Ga and As ovens, GaAs layers will be grown. Opening the Al shutter will then grow the alloy AlGaAs, with the relative proportion of Ga and Al controlled by the temperatures of the ovens. With additional ovens and shutters for the dopant materials, structures of any sequence of GaAs, AlAs, and AlGaAs can be grown with essentially arbitrary doping. MOCVD is a gas phase technique at low pressure. In this case the constituents are passed as gasses over a heated substrate, with the resulting composition being controlled by the relative amounts of the appropriate gasses. There are many different materials that can be grown by these techniques, and many of these have been used to make quantum well structures. MOVPE reactors offer the possibility of multiwafer deposition and can be maintained without needing long baking cycles to recover from atmospheric contamination, meaning less down time. Also, simplification of the growth of phosphide materials, measns that the whole structure including cladding can be grown in one step with the use of faster cladding growth rate, thus reducing the total growth time. One significant restriction is that it is important to ensure that the lattice constants (essentially, the spacing between the atoms) of the materials are grown similarly in the heterostructure. If

this is not the case, it will be difficult to retain a well-defined crystal structure throughout the layers and the growth will not be "epitaxial".

5.2.1 Quantum Wells Physics

Within a bulk (3D) semiconductor crystal, electrons may occupy states in one of two continuous energy bands - the valence band, which is heavily populated with low energy electrons and the conduction band, which is sparsely populated with high energy electrons. The two energy bands are separated by an energy band gap in which there are no permitted states available for electrons to occupy. The simplest model for absorption between the valence and conduction bands in a bulk semiconductor is to say that we can raise an electron from the valence band to the conduction band (a "vertical" transition) by absorbing a photon. Conventional semiconductor laser diodes generate light by a single photon being emitted when a high energy electron in the conduction band recombines with a hole in the valence band. The energy of the photon and hence the emission wavelength of laser diodes is therefore determined by the band gap of the material system used.

QCLs however differ in a fundamental way from traditional semiconductor diode lasers. The lasing medium is a superlattice which consists of thin layers of a semiconductor medium called well, embedded between other semiconductor layers of wider band gap between valence and conduction bands called barriers (examples: GaAs quantum well embedded in AlGaAs, or InGaAs in GaAs). Both electrons and holes see lower energy in the "well" layer, hence the name (by analogy with a "potential well"). This layer, in which both electrons and holes are confined, is so thin (typically smaller than 100 A, or about 40 atomic layers) that the fact that the electrons and holes must only exist in particular energy states cannot be neglected, the system is quantized, hence the name "quantum well".

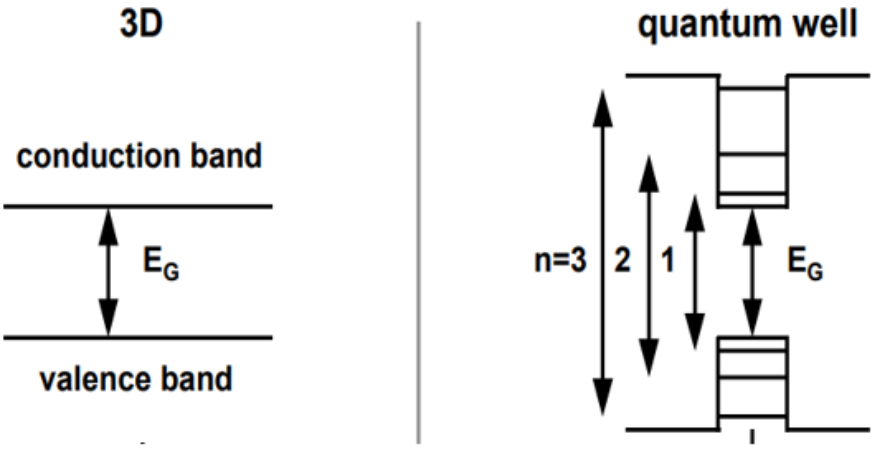

Figure 5.2: *Electron energy levels of a bulk semiconductor vs a quantum well*

5.2.2 Light Emission

When no external force is applied, the conduction band diagram of the structure that was described will have an overall sawtooth shape. However, if voltage of the appropriate polarity is applied, the conduction band diagram acquires a staircase shape as shown in the Figure 5.3.

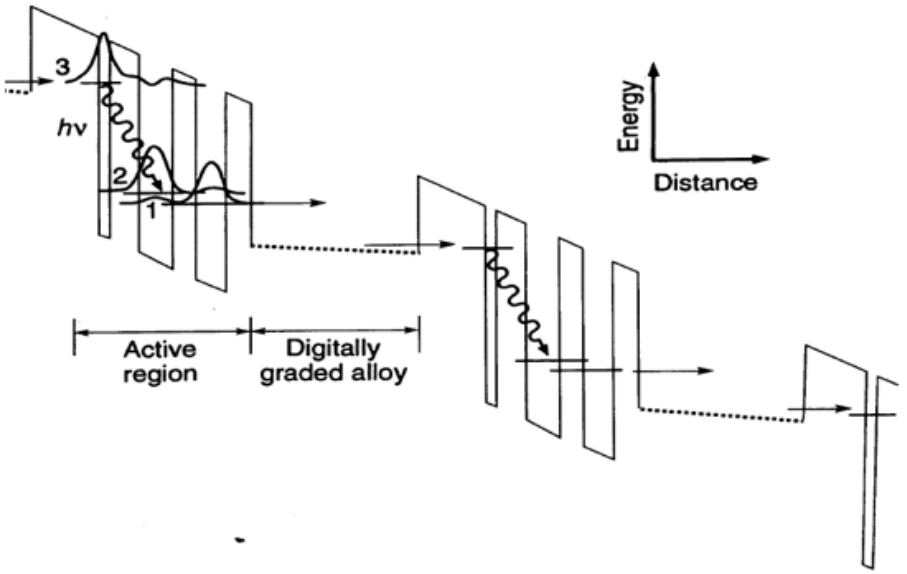

Figure 5.3: *Schematic conduction band diagram of a quantum cascade laser. Each stage of the structure consists of an active region and a relaxation/injection region. Electrons can emit up to one photon per stage*

The voltage difference at the edges of the medium makes the electrons to move through the quantum wells, then relax at the graded region and afterwards are injected by tunneling to the n = 3 excited state. Taking this into account we can consider the quantum well region as a three state laser system where the laser transition is between two adjacent quantum wells. As a result the wavelength of the emitted photons is determined by the energy gap between the conduction and the valence band of the well layer.The active region, which in this case consisted of three coupled QWs, is a three-level system in which population inversion between levels 3 and 2 is achieved by engineering of the lifetimes The nonradiative relaxation time between levels 3 and 2 is increased by employing a transition with a reduced spatial overlap of the wavefunctions (diagonal transition), and the lifetime of state 2 is minimized by making the spacing with level 1 resonant with the optical phonon energy. The active region is left undoped because the presence of dopants significantly broadens the lasing transition by introducing a tail of impurity states. The relaxation/injecton region has several functions. It is in this region that the electrons relax after the optical transition and are injected in the next period by resonant tunnelling. It also introduces an additional energy drop between the lower state of the laser transition and the ground state of the period, thus reducing the thermal backfilling of the former. Finally, it is doped to act as an electron reservoir, insuring that the integrated negative charge in the

structure is compensated by the positive donors, even in the situation of strong injection to prevent the formation of space-charge domains.

he wavelength of the emitted photons is determined by the following equation:

$$\lambda = \frac{1.24}{E_g}$$

Moreover, emission wavelength is not depending only on the band gap of constituent materials, but can be tuned by tailoring the layer thickness. This seems rather unusual if we attempt to explain it with standard physics. Quantum Cascade Lasers however are semiconductor double heterostructure lasers that the thickness of the active layer is less than the de Brogile wavelength of electrons and as a result quantum size effects exist and lead to discretization of energy levels in the potential well. Furthermore, the gap between the energy states defined as valence and conduction band tends to decrease when the thickness of the active layer is increased, as seen in Figure 5.4, where a typical relation between energy gap and wells width is represented.

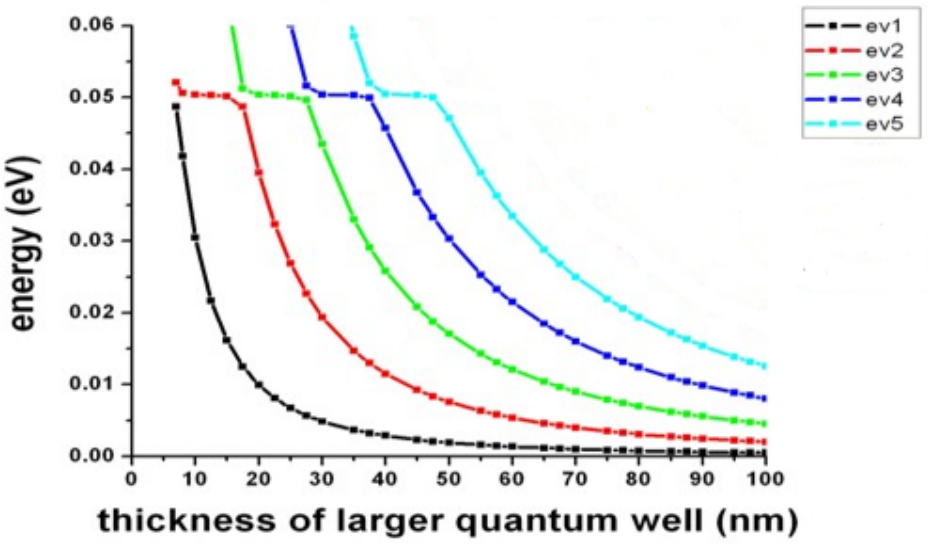

Figure 5.4: *Energy level scheme of an asymmetrical double quantum well structure*

It is worth mentioning that for each well width different number of states is supported (for example between 10μm and 15μm only two energy states are supported) and the bandgap varies greatly even for minor changes in the wells width. If band gap changes, then the emission wavelength changes although the same material system is used. This is one of quantum lasers most important properties and has great consequences as far as implementations of this technology are concerned because it is very easy to tailor the materials layer during the fabrication process and with great precision using techniques like the ones seen in previous chapters. This point can be illustrated with the help of an example:

A very commonly used laser material combination used (figure 5.5) is the superlattice created from Indium Gallium Arsenate matched to Indium Phosphate substrate (InGaAs/InP).

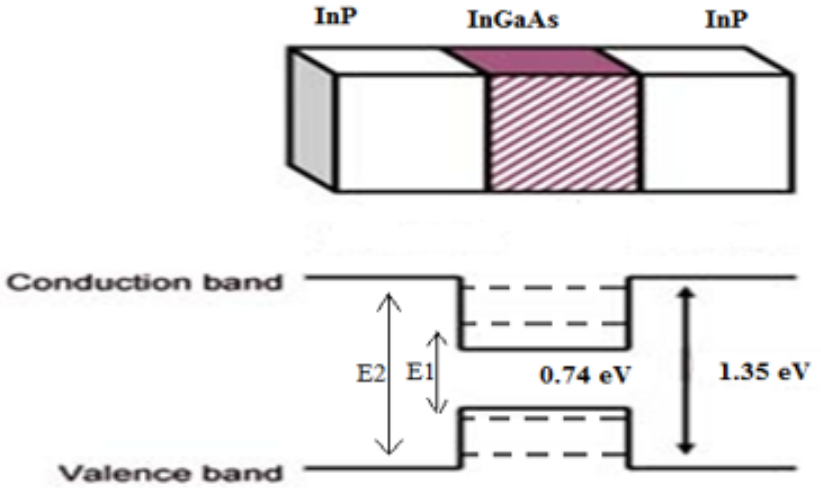

Figure 5.5: *Indium Gallium Arsenate matched to Indium Phosphate substrate*

For a bulk double heterostructure (wide enough to ensure that no quantum effects occur, greater than 100 A wide) the allowed energy levels are discrete but are so close to each other that are essentially continuous and therefor the effective band gap is ,as shown in Figure 5.5, approximately $Eg = 0.74eV$ for InGaAs and $E_g = 1.35$ eV for InP. Consequently the emitted light has a wavelength equal to $\lambda = \frac{1.24}{0.74} = 1.67\mu$m [18].

On the other hand, if the InGaAs layer is reduced to 100 A wide, the heterostrucure is a quantum well, which means that the allowed energy levels are discretized and are represented by dashed lines in Figure. The new energy band gap is $E1 = 0.8eV$ and the emitted wavelength is equal to $\lambda = \frac{1.24}{0.8} = 1.55\mu m$. Following the same procedure we can calculate the emitted wavelength, if the InGaAs layer is 80 A. The new energy band gap is $E_1 = 0.84eV$ and the emitted wavelength is equal to $\lambda = \frac{1.24}{0.84} = 1.46\mu m$.

5.2.3 External Cavity Quantum Cascade Lasers

Last but not least, another fundamental feature of QCLs is the multistage cascade scheme, whereby electrons that travel through the superlattice under the influence of the applied voltage are recycled after each time they take part in a photon emission, contributing each time to the gain. Thus each electron injected above threshold can generate, in principle, Np laser photons, where Np is the number of active regions.

However, commercial QCLs are designed to emit at a vast area of the electromagnetic spectrum. This means that not all quantum wells are of the same width and as injected electrons pass

through them photons of different wavelengths are emitted. In order to achieve that only one wavelength is emitted every time, the laser gain chip is placed inside a tunable external cavity, with the tuning element typically being a diffraction grating. By mechanically rotating the diffraction grating, the precise center wavelength of the emission can be tuned across a broad range ($> 100cm^{-1}$ typically).

Optical feedback is used in many external-cavity QCLs in order to ensure that monochromatic radiation is emitted [19]. This can be achieved by pointing the beam on a grating which re-injects only one wavelength, providing an easily tunable light source. The wavelength can be shifted by changing the incident angle on the grating, other factors that affect the spectrum of the emitted beam are the length of the cavity and the amplitude of the voltage which is applied at the lasing medium. Figure 5.6.

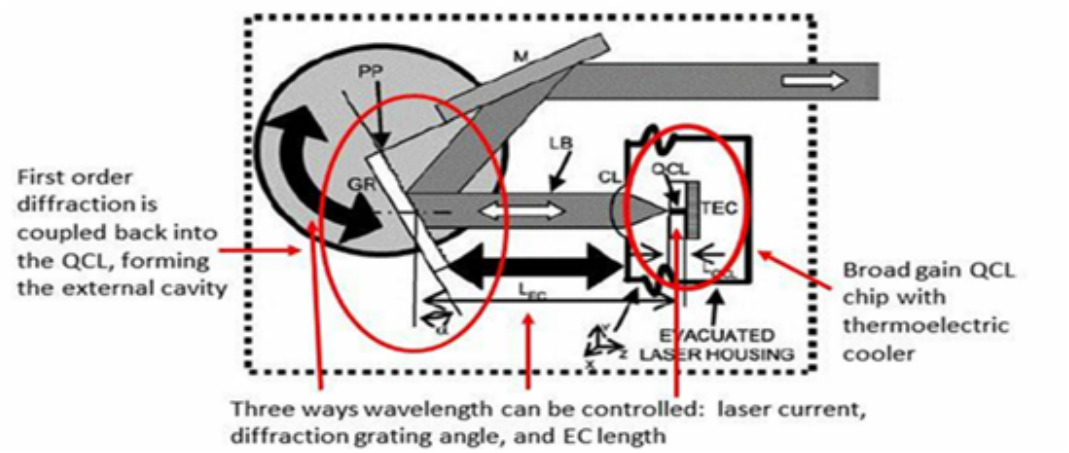

Figure 5.6: *Methods that wavelenght tailoring can be achieved in external cavity QCLs*

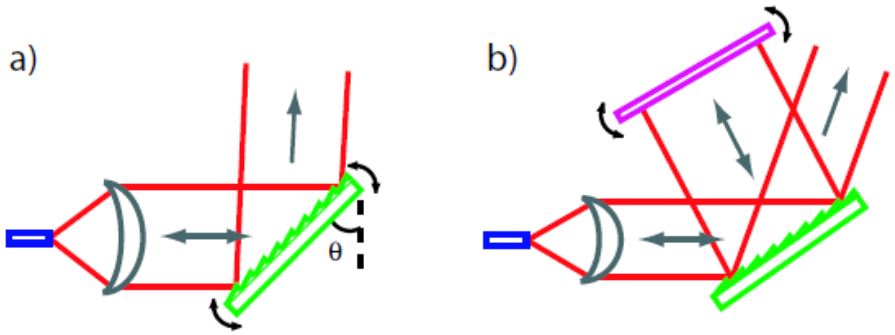

Figure 5.7: *a) Littrow and b) Littman external cavity configurations. The large grey arrows indicate the directions of propagation of light and the small black arrows show how coarse tuning is achieved.*

The most common grating-coupled external cavity configurations for semiconductor lasers are the Littrow and Littman-Metcalf [40] configurations illustrated in Figure 5.7. In the Littrow setup, the first-order diffracted beam from the grating is directly fed back into the chip. Coarse tuning is achieved by rotating the grating. This has the advantages of requiring only two optical elements, a lens and a diffraction grating, hence making the alignment easier, and providing a strong feedback since light is diffracted only once by the grating. In the Littman setup, the first-order diffracted beam is sent back to the grating by an additional mirror to be diffracted again and the first-order beam of this second diffraction is sent back into the chip. Coarse tuning is usually achieved by rotating the mirror since it allows to keep unchanged the direction of the zeroth order, which can be used for extraction. The double-pass on the grating results in an increased wavelength selectivity, but it has the drawback of decreasing the feedback strength.

Chapter 6

Advantages of QCL-Based Spectrometer over FTIR Spectrometer

In recent years, the interest for mid-infrared spectroscopy instrumentation beyond classical FTIR has dramatically increased. New technologies such as the synchrotron, the supercontinuum, and external-cavity quantum cascade laser light sources have emerged and are already gaining a reputation as viable alternatives to the traditional thermal black-body emitter (Globar). Especially when it comes to remote interrogation of samples as well as hyperspectral imaging at diffraction-limited spatial resolution (microspectroscopy) these new technologies have certain advantages over FTIR spectroscopy. Consequentially these different light sources are gaining more and more popularity for such applications. In the following chapter, the theoretical maximum achievable signal-to-noise ratio (SNR) of FTIR using synchrotron or supercontinuum light vs. that of a tunable quantum cascade laser will be compared.

Great emphasis has been placed by a great part of the scientific community on the field of infrared microscopy and great effort is being made in order for a combination between vibrational spectroscopy and microscopy to be achieved. Infrared spectroscopy is used in many biological and medical applications due to the fact that it is a non-destructive method and has the advantage that small volumes of tissue can be analyzed.

Spatially resolved mapping of infrared spectra can provide chemically resolved images of the distribution of key biological components, such as extracellular matrix proteins, nucleic acids and phospholipids [21].

6.1 Alternatives to FTIR

From a technical point of view, infrared microspectroscopy generally involves combining a single-point spectroscopy technique such as Raman or Fourier Transform Infrared (FTIR) with some form of beam scanning to build up a 2-D image. FTIR however was originally evolved at a time when the mid-infrared (mid-IR) light source of choice was a spatially incoherent black-body and only single-element detectors were available. The sensitivity of FTIR comes from its multiplex (i.e., Fellgett) advantage relative to filtering the light source with a narrow-line monochromator. The lack of spatial coherence, however, is a major problem in high spatial resolution image acquisition, because the optical power per diffraction limited spot is low.

To overcome the spatial coherence barrier, a great deal of interest is currently directed toward synchrotron radiation. The synchrotron uses a beam of relativistic electrons to generate spatially coherent broad-band light, which is an ideal light source to illuminate an infrared microscope, because all the infrared power can be brought to a single, diffraction-limited focus. Although, those devices have some advantages, synchrotron radiation is clearly impractical for the majority of lab-based experiments and all field-based work and there are only 50 synchrotron facilities worldwide. Its difficult to gain access to a synchrotron facility and often such facilities might not be developed sufficiently to integrate the requirements of a biological laboratory. The time-consuming nature of individual experiments within a limited beam time allocation currently minimizes the number of replicates achievable, which lessens the robustness of the findings. Consequently, the approach of infrared spectroscopy to biological or environmental questions often appears exotic and niche.

Another type of source has recently gained attention, which is mid-infrared supercontinnum radiation. This approach involves propagating a sub-ps laser pulse through a highly nonlinear medium, most practically a photonic crystal fiber. Mid-infrared supercontinuum shares the high spatial coherence and broad bandwidth of synchrotron radiation, but in a table-top form factor. Sources using silica or fluoride work best at the shorter end of the mid-infrared band, below 5 microns and Chalcogenide fiber can generate supercontinuum up to 10 μ m, covering a major part of the biological fingerprint region. But, a part of the region of interest cant be accessed with the use of aupercontinuum radiation.

Last but not least, one more potential light source has been developed: the external-cavity tunable quantum cascade laser. Combining such sources with microscopy allows the spatial mapping of infrared spectra.

6.2 Comparing QCL Based Systems with FTIR Spectrometers

Prior to the invention of QCLs there were no commercially available lasers that could provide light across the fingerprint region in the mid-IR. Fourier transform IR (FTIR) spectrometers have been the standard equipment used for decades to obtain the spectral characteristics of substances, but new QCL-based spectroscopic instruments have significant benefits over these devices.

First of all, the brightness that QCLs provide is notably higher than any of the other light sources in the mid-IR. The spectral radiance, as a function of wavelength of the QCL, is approximately seven orders of magnitude greater than the FTIR source. Figure.

Based on this property QCL based systems can be used in applications that require noncontact sensing, and analysis of highly absorbing or scattering targets. The dimensions of the output facets of QCLs are so small that the light emitted can be imaged to essentially diffraction-limited spots, allowing the analysis of tiny targets even hundreds of meters away while at the same time the coupling to small diameter fibers with very little optical coupling loss is also possible. For example, in pharmaceutical cleaning verification, QCL spectroscopy can be used to scan the walls of production vessels to ensure that they have been properly cleaned between production batches. On the contrary, FTIR spectrometers cannot be used in noncontact or standoff applications [27].

Radiance is defined as:

$$L = \frac{d^2\Phi}{dAd\Omega cos\theta} \approx \frac{\Phi}{A\Omega cos\theta}$$

Where: L is the observed radiance, Φ is the total radiant flux or power emitted, θ is the angle between the surface normal and the specified direction, A is the area of the source and is the solid angle subtended by the observation on measurement.

6.2.1 Comparing Scanning Speed

In a recent study, a new commercial EC-QCL, the LaserTune (Block Engineering Inc.), has been used for infrared microspectroscopy. The thing that makes this device special is the fact that it has an advanced cavity tuning mechanism and thus it can reduce the spectral acquisition time to 3 seconds. The laser was combined with a 2-D MCT focal plane array detector in order to create a complete hyperspectral imaging system. This systems SNR was compared with the SNR of versus a conventional imaging FTIR microscope also using an FPA detector (Stingray

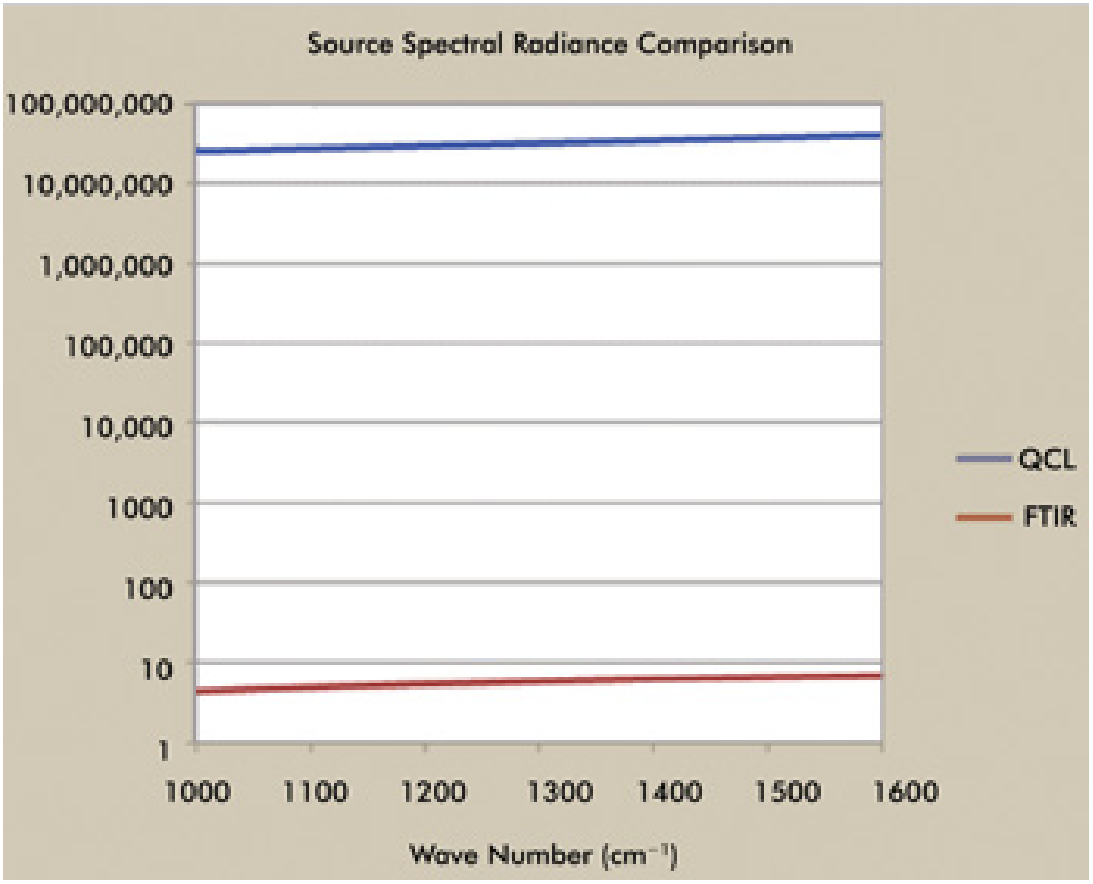

Figure 6.1: *Brightness comparisson of an FTIR-based system and a QCL-based system*

620-IR, Agilent Inc., Santa Clara, CA, USA). Pixel size and integration time was different for each system and that was taken into account before they concluded that the home-built EC-QCL microscope could collect spectral scans of a sample in half the time than the FTIR system. Moreover, the EC-QCL has the ability to scan over specific, targeted regions. FTIR systems, on the other hand, cannot achieve such targeted spectral scanning [23].

Another study was conducted around the same time comparing a Spero IR microscope with an FTIR system. It was shown that a Spero microscope was able to collect single-wavenumber images of a breast tissue microarray that contains more than 26 million spectra in 540 seconds, compared with more than 17 hours using an FTIR microscope [24]. This allowed an entire biopsy sample covering an area of 20x24 mm to be imaged with 4 micron pixel size in 9 minutes.

Although, to be fair, only one wavelength is collected by the QCL based system, whereas the FTIR system produces a true spectrum at each pixel. This results in a loss of information when the FTIR system isnt used, which might be useful for the application. But this is a problem with a relatively simple solution: more wavelengths can be added by stepping the emission wavelength of the tunable laser until enough data to recreate the full spectrum are collected. Obviously, with the 9 minute acquisition time will increase proportionally with the number of additional wavelengths. This highlights an obvious limitation of these previous studies in

that they compare dissimilar systems such as, both the source and detector in the QCL-based systems and those in the FTIR systems, and also the spectral range of the information. This makes a quantitative performance comparison difficult.

6.2.2 Comparing SNR

Transmission mid-IR spectroscopy measures the absorbance of a sample in absorbance units (AU) and are calculated by the equation absorbance (AU) = $\log_{10} \frac{I_0}{I}$, where I_0 is the intensity of the illuminating beam and I that of the transmitted beam. If overall noise is dominated by measurement noise on I (denoted σ_I), then the baseline absorbance noise in AU (i.e., the fluctuation seen on a 100% transmissive sample) $\sigma_{AU} = 0.434 * \frac{\sigma_I}{I}$. Hence the absorbance noise is essentially the reciprocal of the SNR figure-of-merit, defined as the ratio of the total detectable power emanating from the sample divided by the noise on the measurement of the transmitted power. In the UV to NIR spectral region, the measurement noise is often dominated by shot noise on the detected power. In the mid-IR, however, the measurement noise is generally receiver-noise limited and so is independent of the signal amplitude. The receiver noise itself is generally limited by noise in the infrared detector and generally is found to scale as the square-root of the detector area [25].

The classic formula for the SNR of an FTIR spectrometer illuminated by a black-body is generally:

$$SNR = \frac{U_{\vec{\nu}}(T)\,\theta \Delta\vec{\nu} D t^{\frac{1}{2}} \xi}{A_D^{\frac{1}{2}}}$$

Where U_ν(T) is the spectral radiance of the black-body (W cm^{-1} sr^{-1})whose absolute temperature is T, θ is the system optical etendue (cm^2 sr), is the spectral resolution (sr^{-1}), t is the spectral acquisition time (s), ξ is the optical efficiency (0 to 1.0), and AD is the detector area (cm^2). The product on the numerator $U_{\vec{\nu}}\theta\xi$ is the continuous radiant intensity falling on the detector, per unit bandwidth. If, for simplicity, we assume that U is independent of ν (as thermal sources are typically far broader in bandwidth than the measurement window) and that the FTIR interferogram is recorded using radiation that spans a total of N spectral bins, each of bandwidth $\Delta\vec{\nu}$ then the product $U_{\vec{\nu}}\theta\Delta\vec{\nu}\xi$ is simply
phi_e, where $\frac{\phi_e}{N}$ is the total radiant flux (W) falling onto the detector. In FTIR spectroscopy, this flux has been passed through a Michelson interferometer equipped with a scanning mirror before illuminating the sample, and this flux is then recorded by a single-element infrared detector. The detector records an interferogram at N equally spaced temporal sample points during the mirror scan, with each point thus being sampled for a period of $\frac{t}{N}$ i.e. with a measurement

bandwidth B = $\frac{t}{N}$. Because $\frac{A_D^{\frac{1}{2}}}{D}$ is simply the noise-equivalent-power of the detector ($\frac{W}{\sqrt{Hz}}$) and hence $\frac{A_D^{\frac{1}{2}}B^{\frac{1}{2}}}{D}$

An alternative scheme to measure the N-point spectrum is using a tunable laser whose linewidth is $\Delta\vec{\nu}$ and which is tuned over the spectral range N*$\Delta\vec{\nu}$. The spectrum will be constructed by the records taken from the detector at N discrete times. Taking into account that the spectrum is collected in the same time t as the FTIR spectrum and that the measurement bandwidth B hasnt change, it can be deduced that the value of will also remain the same in both occasions. As a result, the SNR for the EC-QCL is SNR = ϕ_e/σ. From equation (1) it is clear that, if ϕ_e is unchanged, then for the FTIR instrument to match the SNR of the tunable-laser spectrometer the acquisition time t must be increased N times.

Chapter 7

Mid Infrared Hyperspectral Imager

The developments of the MidInfrared Hyperspectral Imaging System is analyzed in this chapter. More specifically, the hardware parts of the system and their function and the software that was developed specifically for the purposes of this application and exploits the full potential of the hardware. Lastly, all the measurements conducted for the purposes of this research are presented and analyzed.

7.1 The Set-Up

During the process of building a Mid Infrared Hyperspectral Imaging System it was necessary to design the set-up. The experimental procedure consists of a few basic elements which are: a coherent light source, i.e. laser, a light expander and a camera used to capture the images.

7.1.1 The Camera

For the needs of this study an Optris PI 640 thermal camera (Figure 7.1) was used. It is a state of the art thermal camera with an optical resolution of 640x480 pixels with the ability to deliver pin-sharp radiometric pictures and videos in real time. The thermal imager Optris PI 640 is the smallest measuring VGA infrared camera worldwide with a body sized 45x56x90 mm and weighing only 320 grams (lens included) and counts among the most compact thermal imaging cameras on the market.

Optris PI 640 makes accurate measurements in the temperature range from -20^oC to 900^oC. Due to its low weight and high resolution, thermal imaging camera is the best choice for the integration into a drone or UAV (unmanned aerial vehicle). Moreover, the high resolution

Figure 7.1: *Optris PI 640*

infrared camera finds use in all industrial applications, where pin-sharp infrared pictures and videos are of essence for process monitoring and optimization. The real-time thermographic images prove especially valuable for surveillance and quality assurance in the automotive sector, in the plastics branch, and in the semi-conductor as well as photovoltaic industries.

Technical Details of the optris PI 640

- Scope of supply:
  USB camera,
  USB cable (1 m),
  table tripod,
  PIF cable incl. terminal block (1 m),
  software package optris PI Connect,
  Rugged outdoor transport case (IP67)
- Detector: FPA, uncooled (17 µm x 17 µm)
- Optical resolution: 640x480 pixel
- Spectral range: 7.5 - 13 µm
- Temperature ranges:
  -20 °C...100 °C
  0 °C...250 °C
  150 °C...900 °C
  additional range: 200 °C...1500 °C (option)
- Frame rate: 32 Hz
- Optics:
  33° x 25° FOV / f = 18.7 mm or
  15° x 11° FOV / f = 41.5 mm or
  60° x 45° FOV / f = 10.5 mm or
  90° x 64° FOV / f = 7.7 mm
- Thermal sensitivity (NETD): 75 mK
- Accuracy: ±2 °C or ±2 %
- PC interface: USB 2.0
- Process interface (PIF):
  Standard PIF: 0-10 V input, digital input (max. 24V), 0-10 V output
  Industrial PIF: 2x 0-10 V inputs, digital input (max. 24 V), 3x 0-10V outputs, 3x relay (0-30 V/ 400 mA), fail safe relay
- Ambient temperature (T_{Amb}): 0°C...50°C
- Storage temperature: -40°C...70°C
- Relative humidity: 20 - 80%, non condensing
- Enclosure (size / rating): 46 mm x 56 mm x 90 mm / IP 67 (NEMA 4)
- Weight: 320 g, incl. lens
- Shock / vibration: 25G, IEC 68-2-29 / 2G, IEC 68-2-6
- Tripod mount: 1/4-20 UNC
- Power supply: USB powered

Part number: optical resolution / frame rate / thermal resolution

- **OPTPI640**: 640x480 pixel / 32Hz / 75 mK

Figure 7.2: *Optris PI640 characteristics*

7.1.2 Coherent Light Source

The light source that was used in our system is a LaserTune, a Widely Tunable Mid-Infrared Quantum Cascade Laser, developed by Block Engineering. This light source was made for scientific applications such as chemical detection and gas analysis. Moreover, it offers the widest gap free tuning range available on the market of 5.4 - 12.8 microns (1850 770 cm^{-1}) which is a really exciting feature when it comes to infrared spectroscopy, because a broader spectral region can be studied.

A tunable external cavity laser with a broadband QCL chip is the engine inside of the LaserTune IR Source. The external cavity is a Littrow configuration with back extraction, with a grating as the tuning element. The angle of the grating selects the wavelength of the diffracted light, which couples back into the QCL chip and creates a Laser at a single wavelength. The QCL chip is driven with pulsed current, typically with $\sim$ 200 kHz repetition rate, $\sim$ 200 ns pulse width and $\sim$ 3.5% duty cycle.

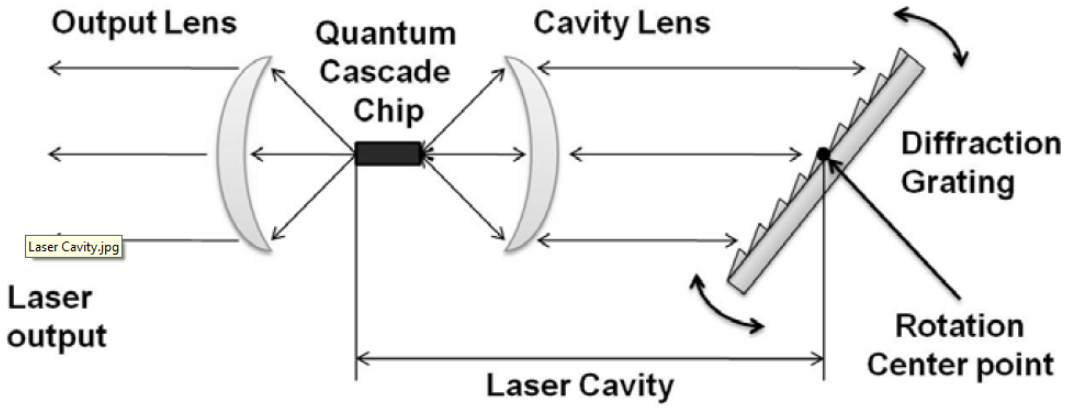

Figure 7.3: *LaserTune cavity*

When used as a spectrometer with the External IR Detector, light from the QCL interacts with a sample, is absorbed or reflected at particular wavelengths, and is measured by the detector. The detector signal as a function of wavelength generates a spectrum. Advantages of using a QCL for such measurements include narrow band emission, high brightness, small and collimated output beam, linear polarized output, and insensitive characteristics to stray light due to high speed pulsing of the laser enable extremely sensitive standoff measurements.

The maximum average power output of a LaserTune can be as high as 20 mWatts depending on the operating parameters. An exemplary average power output curve of standard configuration LaserTune operated at 5% duty cycle is shown in the Figure 7.4.

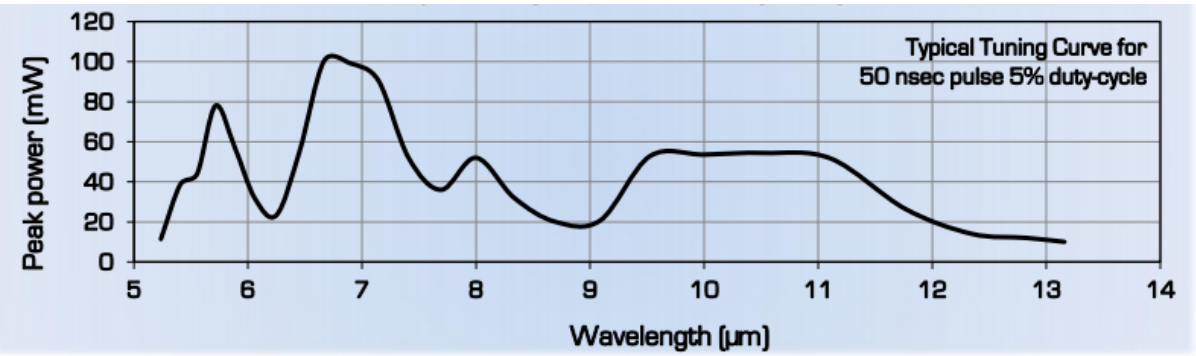

Figure 7.4: *LaserTune's intensity level*

Another advantage that LaserTune possesses is its extremely small size, while at the same time no external power supply or control peripherals are required. Additionally, the instrument comes with wireless capability for remote control so it can be programmed via an iPad or other computer peripheral. The software provides the user with the ability to adjust critical laser parameters including thermal control of the QCL, pumping current, pulse parameters and both internal as well as external triggering.

Figure 7.5: *LaserTune*

The LaserTune software comprises four main operating modes: TUNE, REMOTE, CONFIG and SYSTEM. If the External IR Detector is used, an additional ACQUIRE mode is also available. All of these modes are accessed via the HOME screen.

- **Tune Mode :** Allows the user to operate the LaserTune source in the various tuning modes (manual move, step, and sweep) and to alter laser pulse and trigger settings.
- **System Mode:** Provides general system information and troubleshooting alerts.
- **Config Mode:** Allows the user to modify various software settings and alter laser drive parameters such as temperature and pump voltage.
- **Remote Mode:** Allows the user to operate the system remotely via Ethernet link to a PC.

Last but not least, the LaserTune can be programmed to operate in several modes including Move Tune (manual control), Step Tune with programmable steps, and Sweep Tune with programmable sweep parameters. LaserTune offers an extremely fast sweep capability at 25 cm-1 per millisecond. The system supports pulse durations of between 20 to 500 nsec, a repetition rate of up to ∼3 MHz, and a duty-cycle of up to 15%. The pulses can be internally triggered at regular intervals with an available sync-out signal. External triggering is also supported. The beam size is roughly 2 mm x 4 mm with industry leading pointing stability.

Mechanical Interface & Dimensions

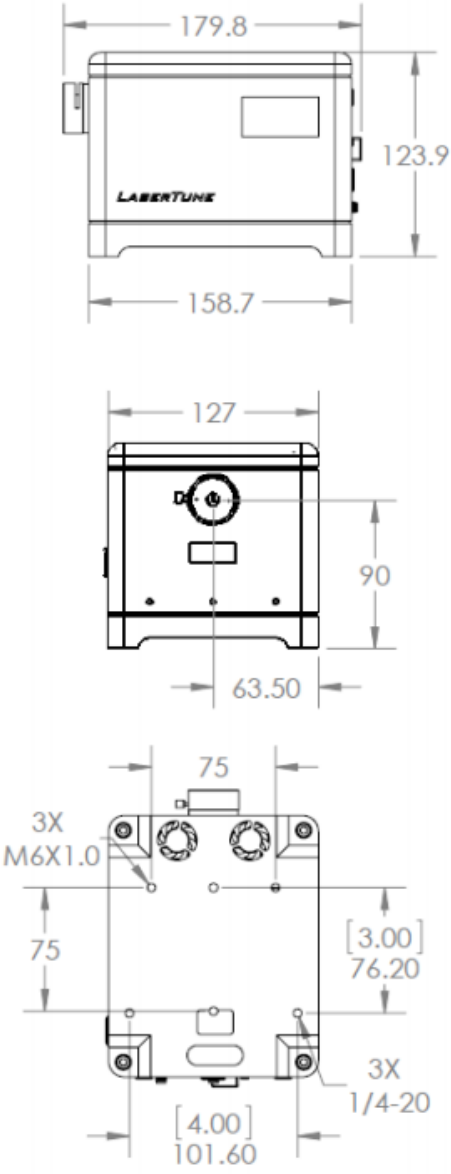

All dimensions in mm [inches]

LASERTUNE™
Tunable Mid-IR Laser Source Specifications

Gap-Free Tuning Range	λ ≈ 5.4 – 12.8 µm (Δν > 1050 cm^{-1}) (typical) (system can be configured with up to 4 tuners)
Spectral Linewidth	2 cm^{-1} (typical)
Spectral Accuracy / Repeatability	< 2 cm^{-1} / < 0.5 cm^{-1} (typical)*
Maximum Peak Power	Up to 150 mW depending on selected wavelength range **
Average Power	0.5 – 10 mW typical at 5% duty-cycle
Power Stability	< 10% pulse-to-pulse (typical)
Pulse Width	30 – 300 nsec ▫ continuously variable with External Pulse Control ▫ 10-ns-resolution with Int. & Ext. Triggering
Pulse Repetition Frequency	Up to 3 MHz
Maximum Duty Cycle (DC)	2.5 – 15% (depending on pulse width, period, & tuner)
Beam Quality	Single spatial mode
Beam Diameter	2 x 4 mm, collimated output
Beam Divergence	< 5 mrad
Pointing Stability	< 1 mrad over 99% of tuning range
Polarization	Vertically polarized, 100:1 extinction
Tuning Modes	Move Tune – manual control at one wavelength Step Tune – programmable linear steps Sweep Tune – variable sweep speed
Step Tune Speed	100 cm^{-1} step in <15 msec
Sweep Tune Speed	Linear sweep up to 15 cm^{-1}/msec
Computer Control	Ethernet; HTML/SOAP interface
Synchronous Pulse Control	Trigger input – with Sync-Out and adjustable offset Trigger output – for laser pulse & wavelength tune Digital input for pulse control – directly controls rising & falling edges
Dimensions	Approx. 6.25 × 5 × 4.9 inches → Volume = 2.6 liters
Weight	2 kg (4.5 lbs)
Cooling	Active cooling via fans
Temperature Range (Operating / Storage)	10 to 30 °C / -10 to 70 °C
Electrical Power	100 – 240 Volts (50/60 Hz) 2.5 Amp

* At 25°C with temperature stabilization
** Contact a sales representative to discuss power specifications in more detail.

Figure 7.6: *LaserTune's characteristics*

7.1.3 Light Beam Expander

A Zinc Selenide (ZnSe) lens was used in order to expand the laser beam. Lenses made from this material are ideal for a wide variety of infrared applications including thermal imaging, FLIR, and medical systems.

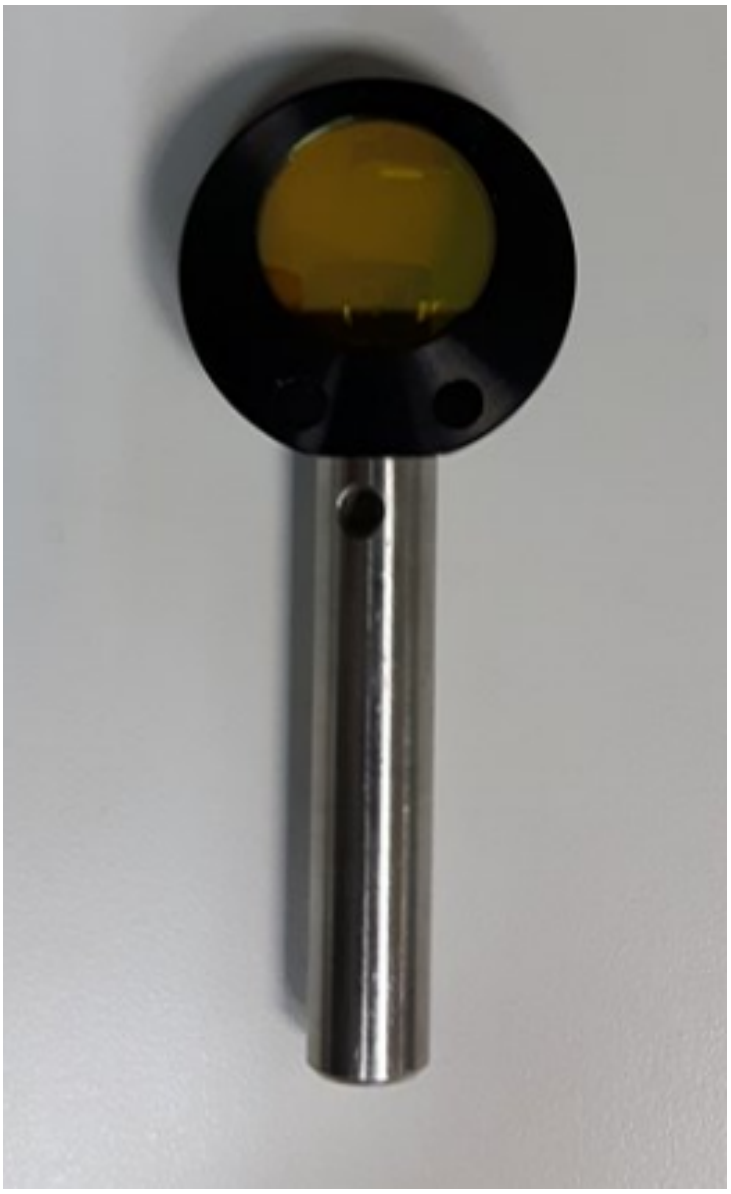

Figure 7.7: *Zinc Selenide beam expander*

This chemically vapor deposited material has wide usage in high power infrared laser systems because of its low absorption coefficient and high resistance to thermal shock. As it is shown in the Figure below, Zinc Selenide is transmissive from the whole spectrum of infrared radiation that LaseTune can emit (5.4 - 12.8 microns).

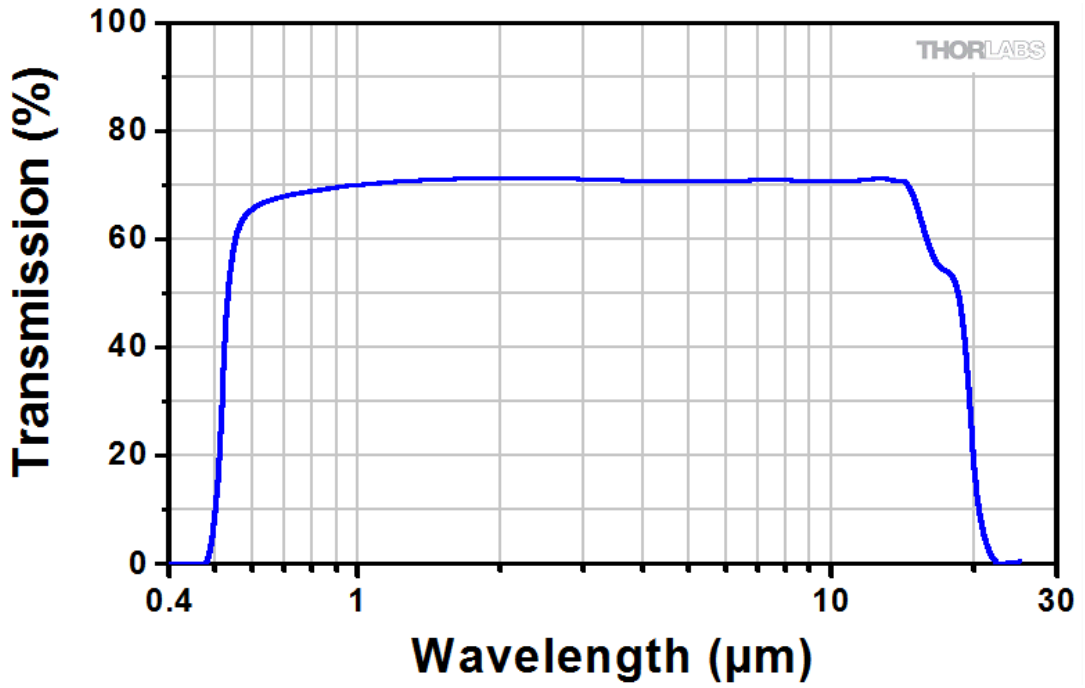

Figure 7.8: *Zinc Selenide infrared spectrum*

7.2 Software Development

A hyper-spectral imaging system is presented with the ability to acquire and real-time display of spectral images in the range of 5.4 - 12.8 μm. Synchronized spectral scanning and image storing makes possible the collection of a stack of calibrated spectral images, from which a fully resolved spectrum per image pixel can be calculated and displayed.

Specially developed software is employed for the control of the laser-camera system as well as for the spectral image analysis. In order to gain complete control of both the thermal camera and the quantum cascade laser an interface was developed with the use of the Microsofts Visual Studio platform. For that purpose, IRImagerDirect was used, which is software developed jointly by Evocortex GmbH and Optris GmbH and grants its user access to all cameras featured in the Optris PI series. This library enables a software developer to process a camera's data stream with C/C++. Moreover, LaserTune is a smart, discoverable, networked device, accessible via ubiquitous networking, and controllable via a SOAP API. This means that control is managed via XML-formatted messages exchanged over HTTP (TCP/IP).

The system operates in two modes: the view (Figure 7.9) and the acquisition mode (Figure 7.11). The image acquisition with this system is completely computer controlled. The first enables the selection, real-time visualization of desired spectral images and calculation of one full spectrum per image pixel, while the second performs synchronized spectral scanning and image capturing.

7.2.1 Acquisition Mode

When the program opens, the following window appears and when the On button is pressed it establishes a connection between the two devices by opening a socket. A TCP based protocol is used for the exchange of messages between the two devices.

Also, the data stream which the camera provides is displayed on the black area. Our system can acquire, process and display the data stream with a frame rate of 32 frames per second (fps). In order for an imaging system to be considered real time a common deadline is that the screen be updated at least 30 times per second; hence our system is considered a real - time imaging system.

Additionally, although the data from the camera are displayed originally in black and white form, the user can choose to apply a pseudo-color to the displayed data just by clicking on the Pallete button. The software maps each of the grey levels of a black and white image into an assigned color. This colored image, when displayed, can make the identification of certain features easier for the observer. Artificially coloring an image can reveal textures and qualities within the image that may not have been apparent in the original coloring.

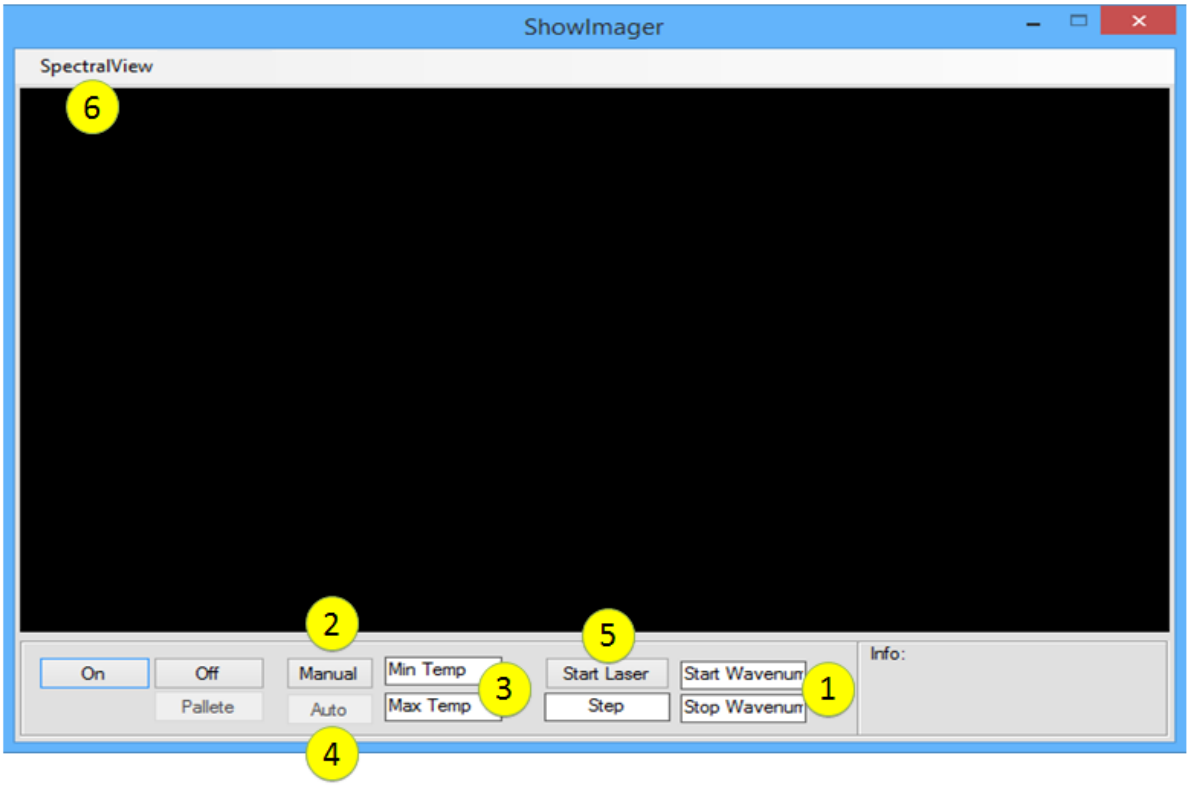

Figure 7.9: *Acquisition Mode*

The user must give the range of the spectrum that will be scanned as well as the step as input (1). Those parameters are typed at the appropriate text areas (Start Wavenumber, Stop Wavenumber, Step).

Optionally the user can also choose the dynamic range of the camera or let it be set automatically by pressing the Manual, (2), or Auto, (4), button respectfully. If Manual mode is chosen then the dynamic ranges boarders must be typed at the text areas Min Temp and Max Temp, (4). Temperatures must be given in the Celsius scale. However, if Auto mode is selected a command is given to the laser and a quick scan (sweep) of the selected spectral band begins. The scan lasts about 1.5 seconds and during that time the maximum and minimum temperature detected by the camera define the dynamic range. That ensures that the lowest detected temperature (room temperature) will be depicted as black and the highest detected temperature will be depicted as white, as a result all the gray values in between will be used.

If all the parameters described above are set and the user presses Start Laser, (5), a message, containing the information about the range of the spectrum and the step, is sent through the socket to the laser. The laser emits a beam tuned to the beginning of the band and after one second informs the interface with another message through the socket. Furthermore, an image is stored at .png format and a message is sent to the laser in order to emit a beam of a different frequency. This process is executed repeatedly until the whole spectral range is covered.

Finally, when SpectralView, (6), is pressed the program switches to spectral view mode.

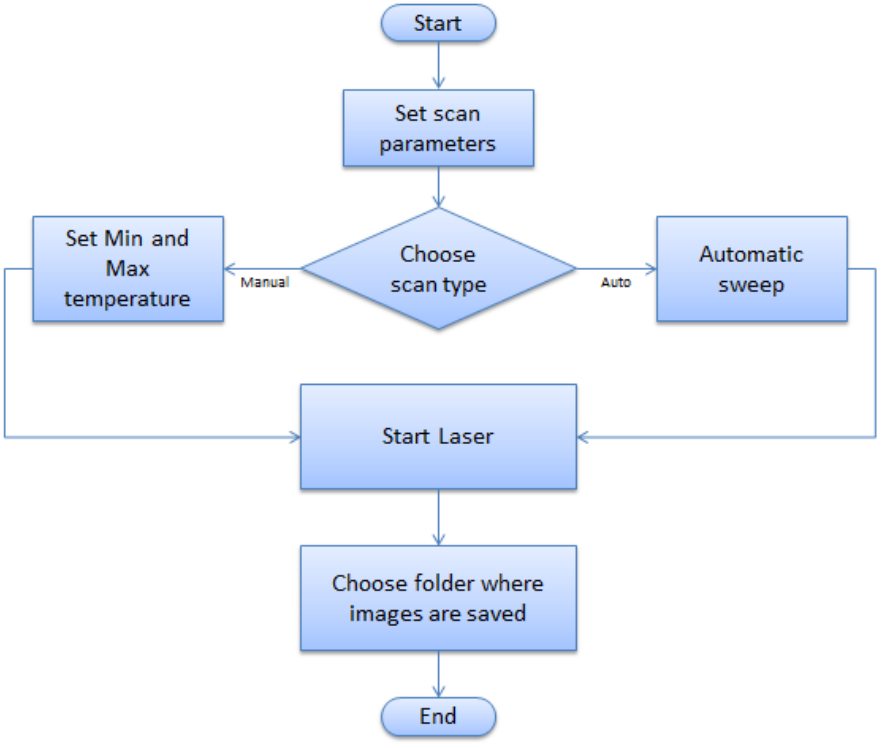

Figure 7.10: *Flowchart that describes the process of acquiring a spectral cube*

7.2.2 Spectral View Mode

In order to load the spectral cube the user choses the file where the images are saved, (1). The spectra are calculated automatically from the gray values of the selected pixel. The spatial resolution of the detector determines the number of the spectra that can be collected in one experiment run.

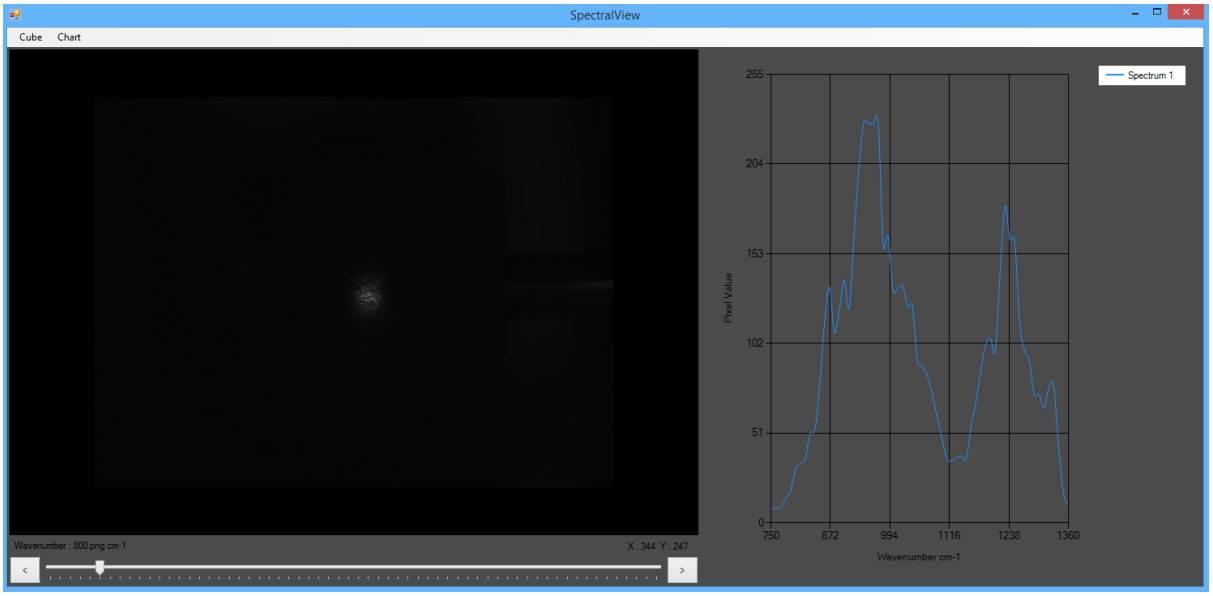

Figure 7.11: *Spectral View Mode, single spectrum displayed*

The bars bellow the picture, (2), allows the user to quickly browse through the images. The wavenumber of the image on display is shown at the top left of the bar. At the top right of the bar we can see the pixel where the mouse is located.

While hovering the mouse through the picture the spectrum shown in the chart changes as it corresponds to the spectrum of the pixel at which the cursor points at any given time, (3). Although, if a single click is pressed then program stops acquiring spectrums and displays the clicked pixels spectrum.

Moreover, if the user wishes to examine or compare more than one spectrum he can double click on the desired pixels and then multiple graphs will be drawn on the chart, (4).

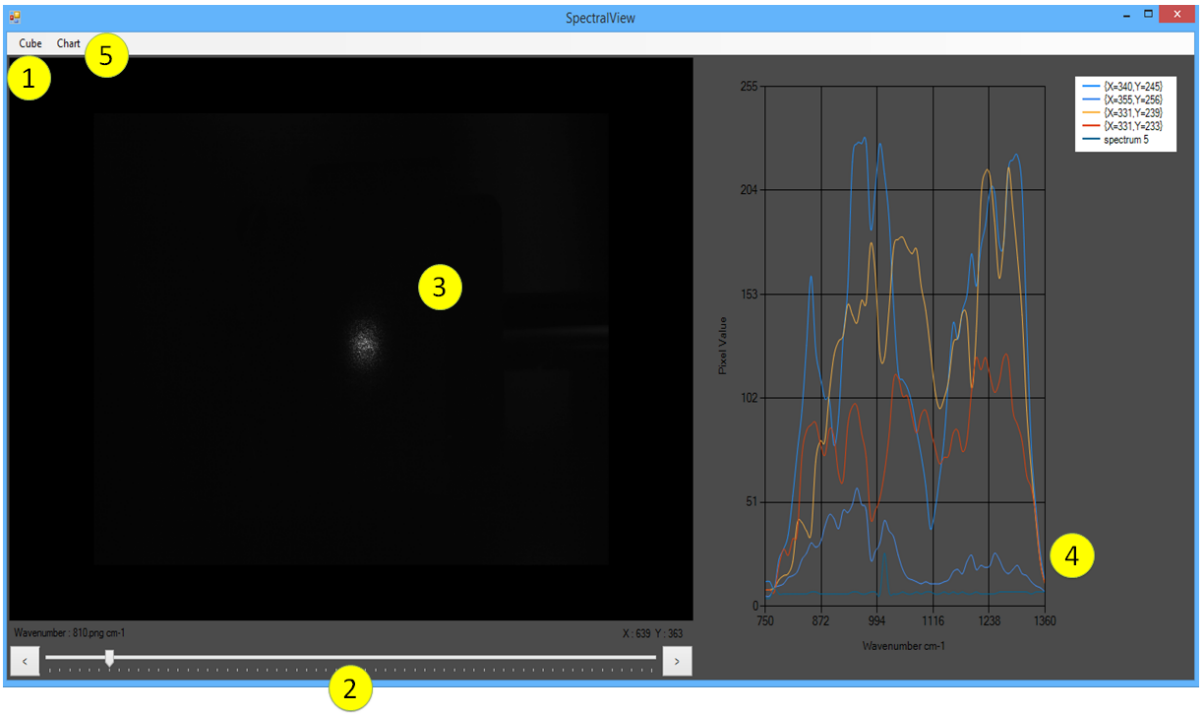

Figure 7.12: *Spectral View Mode, multiple spectra displayed*

At the top right corner, we can see from which pixel each chart was generated. In order to drop a spectrum chart the user has to press a right click. And in order to clear the chart from all the displayed spectrums has to press Chart, (5), and Clear.

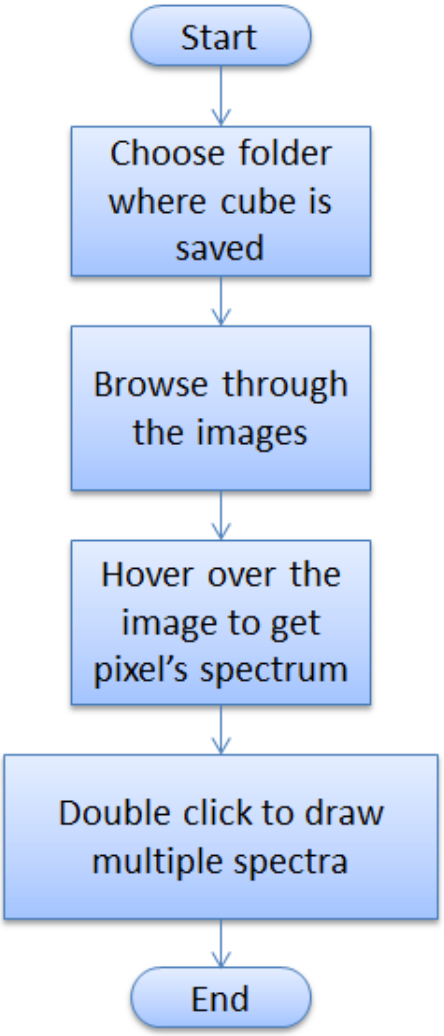

Figure 7.13: *Flowchart thhat describes the spectral view mode*

7.3 Scanning Procedure

7.3.1 Golden Plate Reflectance

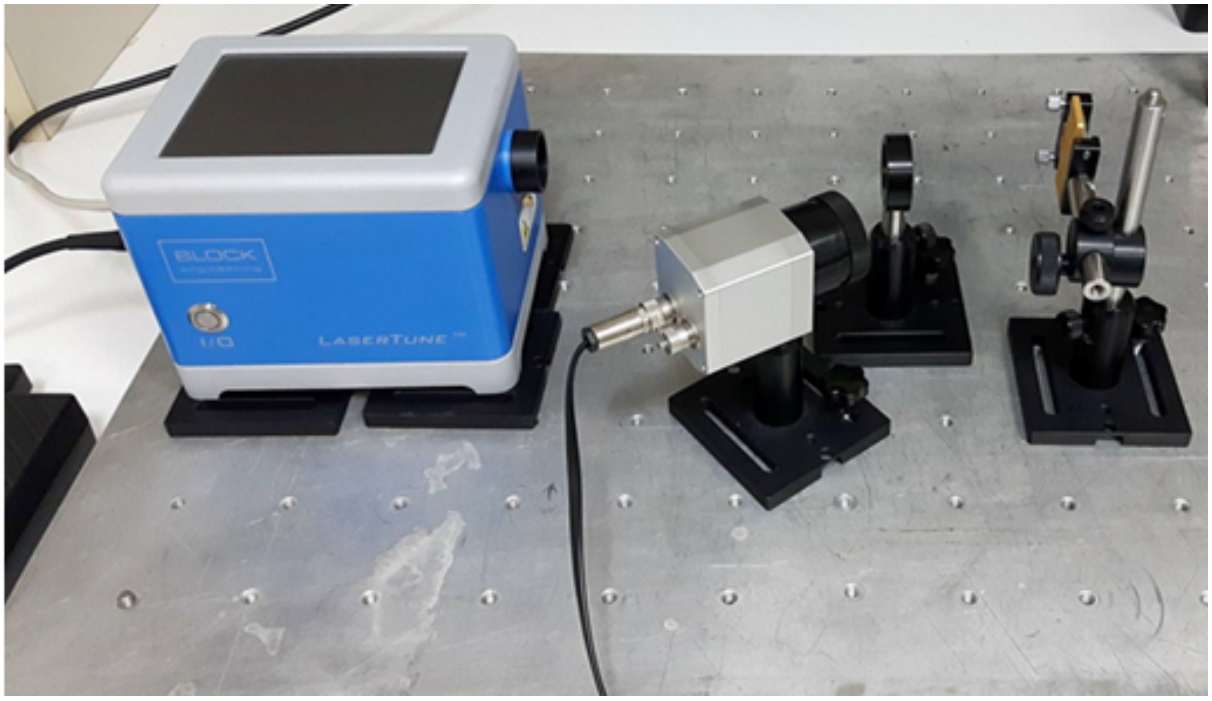

Figure 7.14: *The set up described above*

The specimen of choice was a golden plate (Figure 7.15) . We chose this material because of certain optical properties that it possesses in the mid infrared region. To be more specific, gold was chosen due to the fact that its reflectance behavior when it interacts with mid-infrared radiation is almost total. As we can see in Figure 7.16 infrared radiation is reflected at a rate greater than 99% [28].

Figure 7.15: *Gold Plate*

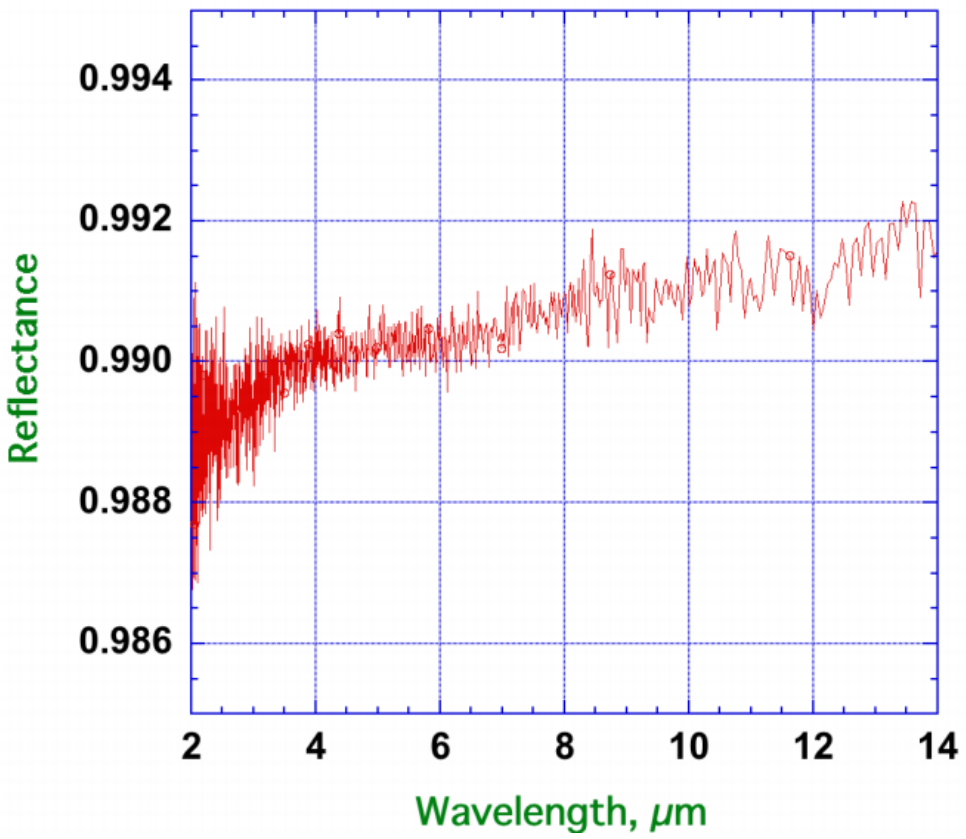

Figure 7.16: *Infrared spectrum of gold*

The specimen is placed in the field-of-view (FOV) of the lens and the beam expander is used. A total scan of the spectral range with a step of 10 cm^{-1} is performed. The spectral cube consists of 58 images that were acquired in 60 seconds.

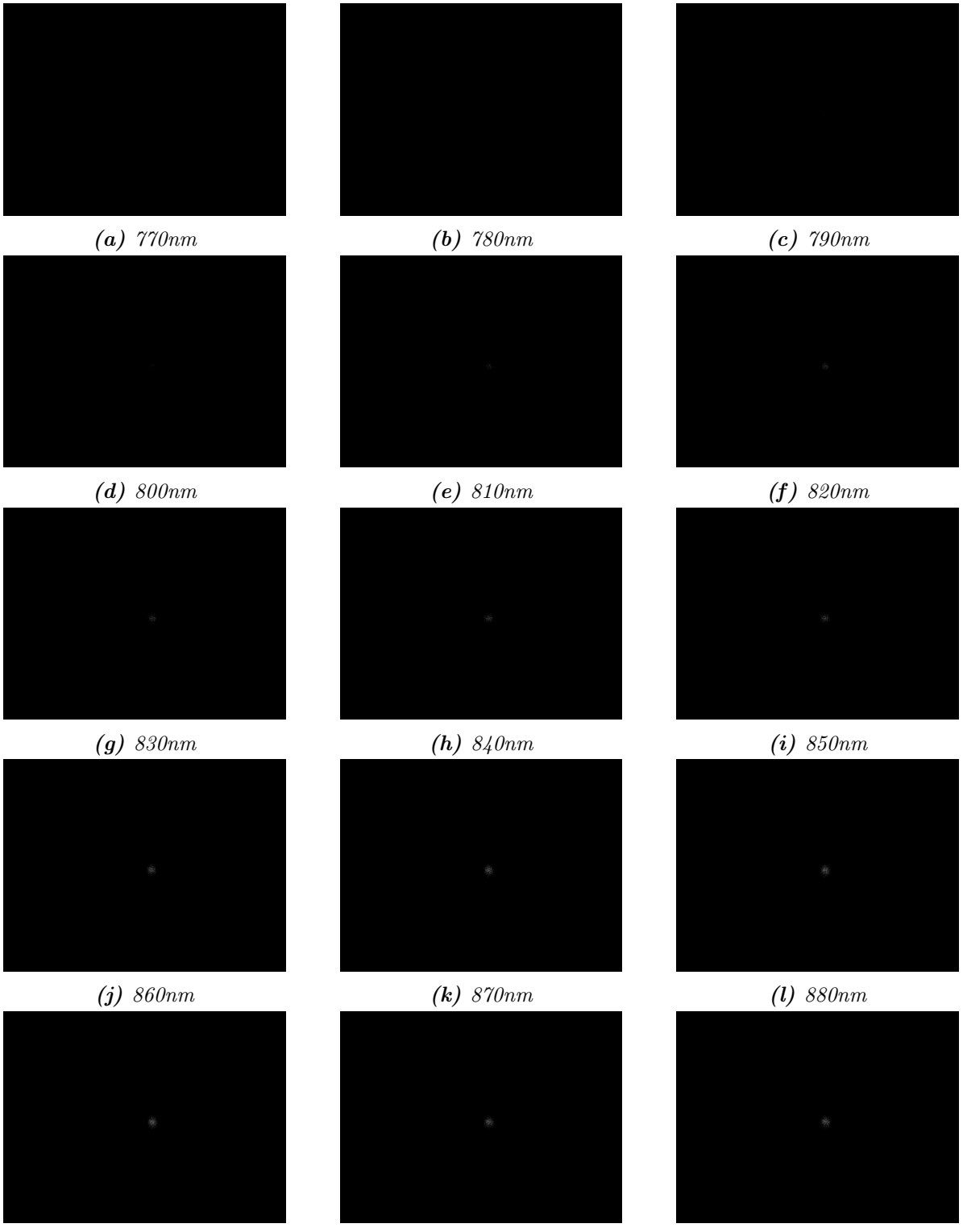

(a) *770nm* ***(b)*** *780nm* ***(c)*** *790nm*

(d) *800nm* ***(e)*** *810nm* ***(f)*** *820nm*

(g) *830nm* ***(h)*** *840nm* ***(i)*** *850nm*

(j) *860nm* ***(k)*** *870nm* ***(l)*** *880nm*

(m) *890nm* ***(n)*** *900nm* ***(o)*** *910nm*

Figure 7.17: *Scanning Procedure(1)*

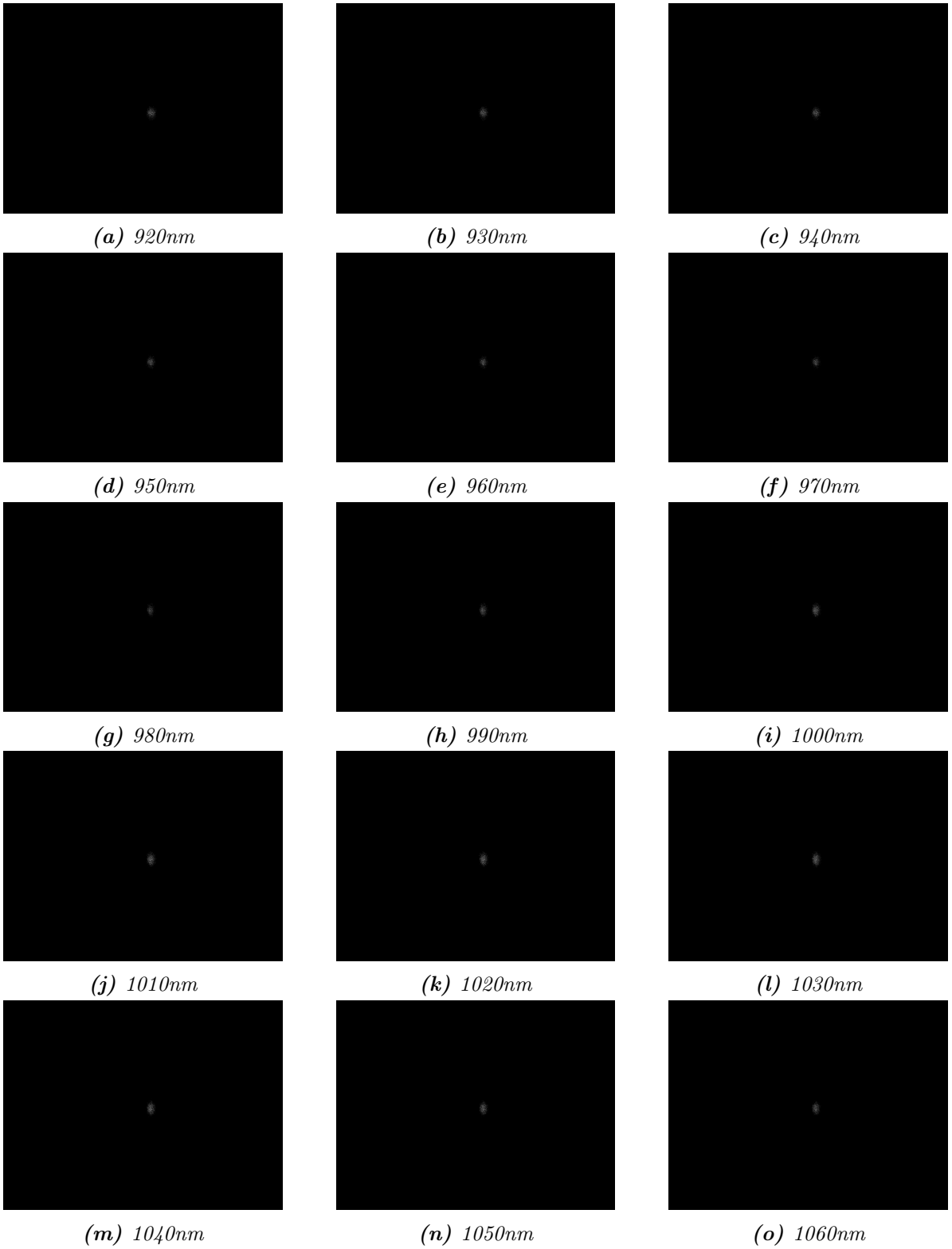

(a) *920nm* ***(b)*** *930nm* ***(c)*** *940nm*

(d) *950nm* ***(e)*** *960nm* ***(f)*** *970nm*

(g) *980nm* ***(h)*** *990nm* ***(i)*** *1000nm*

(j) *1010nm* ***(k)*** *1020nm* ***(l)*** *1030nm*

(m) *1040nm* ***(n)*** *1050nm* ***(o)*** *1060nm*

Figure 7.18: *Scanning Procedure(2)*

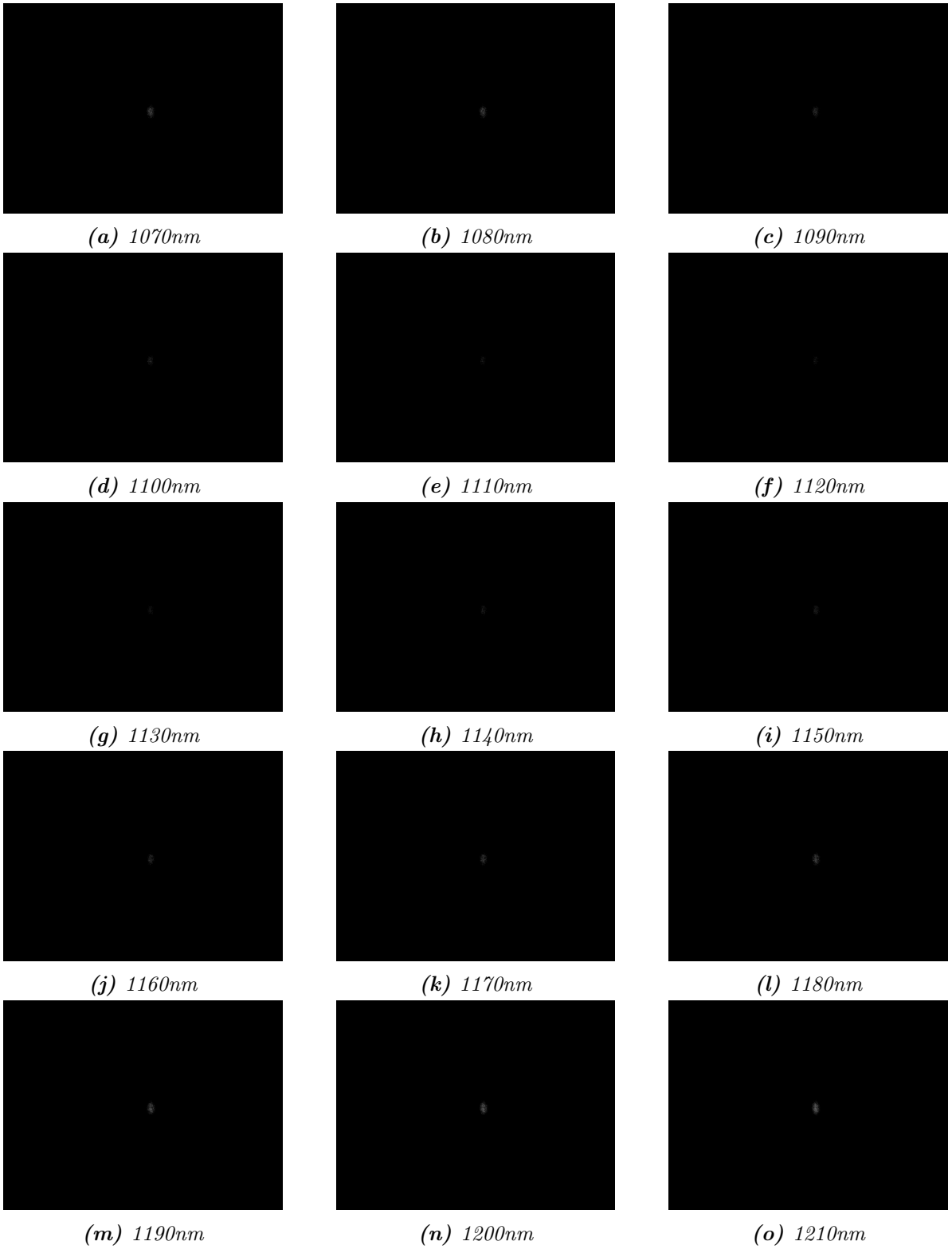

(a) *1070nm* ***(b)*** *1080nm* ***(c)*** *1090nm*

(d) *1100nm* ***(e)*** *1110nm* ***(f)*** *1120nm*

(g) *1130nm* ***(h)*** *1140nm* ***(i)*** *1150nm*

(j) *1160nm* ***(k)*** *1170nm* ***(l)*** *1180nm*

(m) *1190nm* ***(n)*** *1200nm* ***(o)*** *1210nm*

Figure 7.19: *Scanning Procedure(3)*

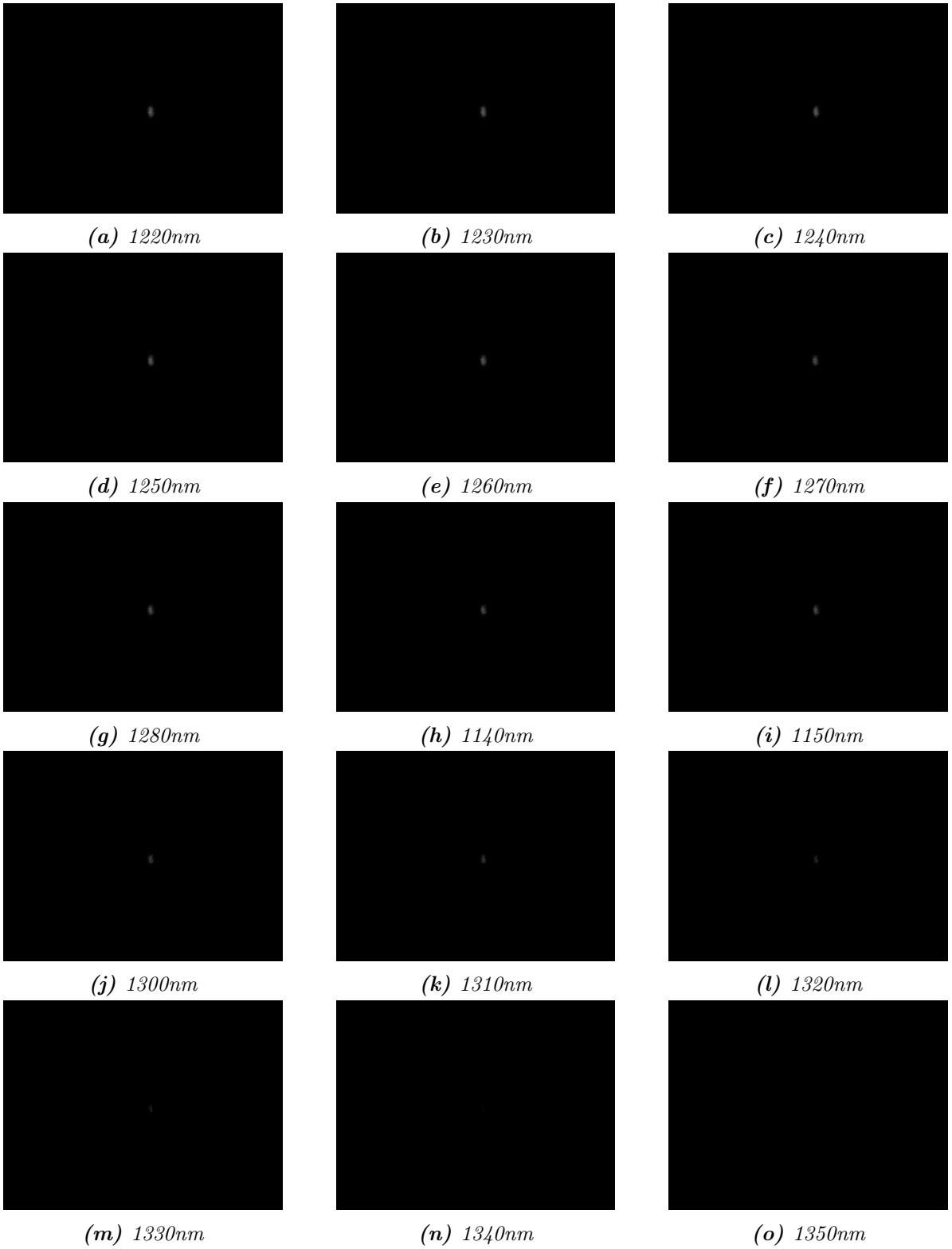

(a) *1220nm* ***(b)*** *1230nm* ***(c)*** *1240nm*

(d) *1250nm* ***(e)*** *1260nm* ***(f)*** *1270nm*

(g) *1280nm* ***(h)*** *1140nm* ***(i)*** *1150nm*

(j) *1300nm* ***(k)*** *1310nm* ***(l)*** *1320nm*

(m) *1330nm* ***(n)*** *1340nm* ***(o)*** *1350nm*

Figure 7.20: *Scanning Procedure(4)*

From the stored stack of spectral images, a spectrum is calculated and displayed. Each spectrum is calculated from the gray values of the selected pixel spectral column. The recorded spectrum is generated from the reflectance of the laser beam on the gold plate. As a result, it should be identical with the power output curve of LaserTune configuration given by Block Engineering.

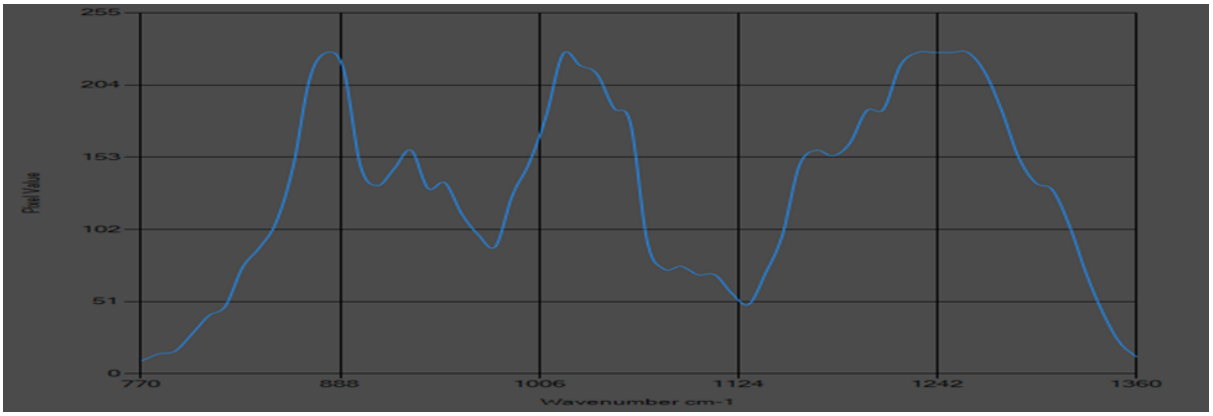

Figure 7.21: *Spectrum generated from the acquired images*

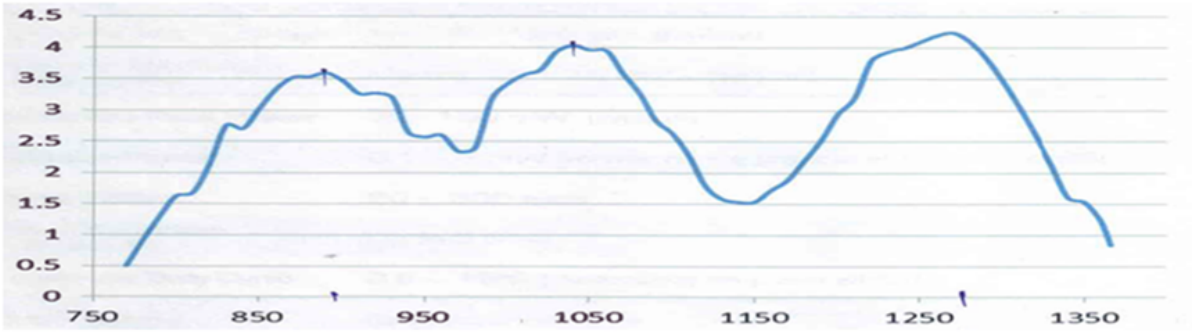

Figure 7.22: *LaserTune's spectrum as it was given from Block Engineering*

It is obvious that the two spectra are almost identical. Most importantly, the three peaks at 880 cm^{-1}, 1030 cm^{-1} and 1280 cm^{-1}, which are the characteristic peaks of the LaserTune spectrum according to its manufacturers, can easily be spotted. This is a very important observation and can be used as proof that our system works properly. Comparing the data acquired with the data given from the laser manufacturer is solid evidence that our system can provide totally reliable spectra.

7.3.2 Polystyrene Film Transmission

Nevertheless, additional experiments have been conducted in order to prove the functionality of this system. In the following experiment the specimen of choice was polystyrene.

Figure 7.23: *The polystyrene film used*

Polystyrene films have been a popular wavelength reference for mid-infrared spectrometers for many years and have been used to qualify Mid IR - FTIR spectrophotometers for wavelength accuracy over the range 3.2 μm to 18.5 μm (3125 cm^{-1} to 540 cm^{-1}).

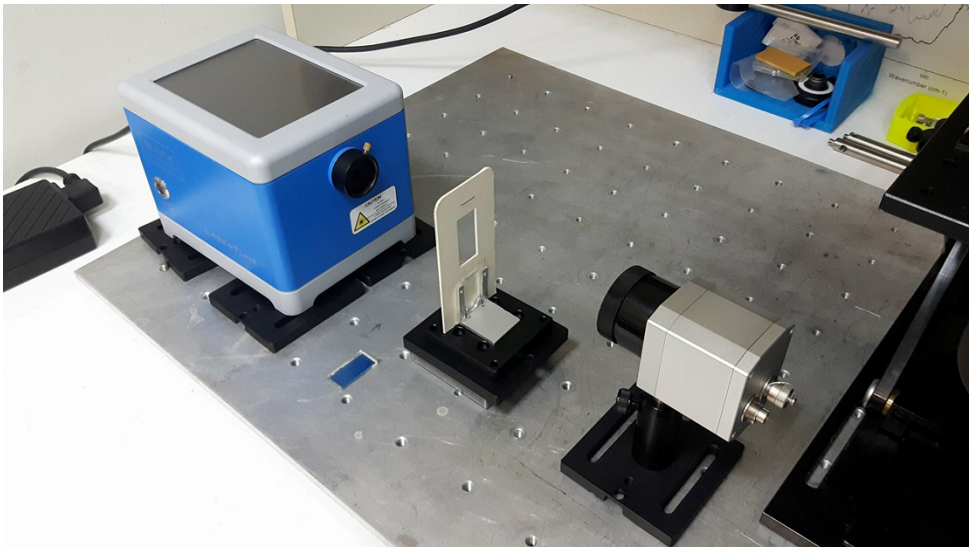

Figure 7.24: *The set up used to acquire the spectrum of polystyrene*

The specimen is placed in the field-of-view (FOV) of the lens. A total scan of the spectral range with a step of 10 cm^{-1} is performed in 60 seconds.

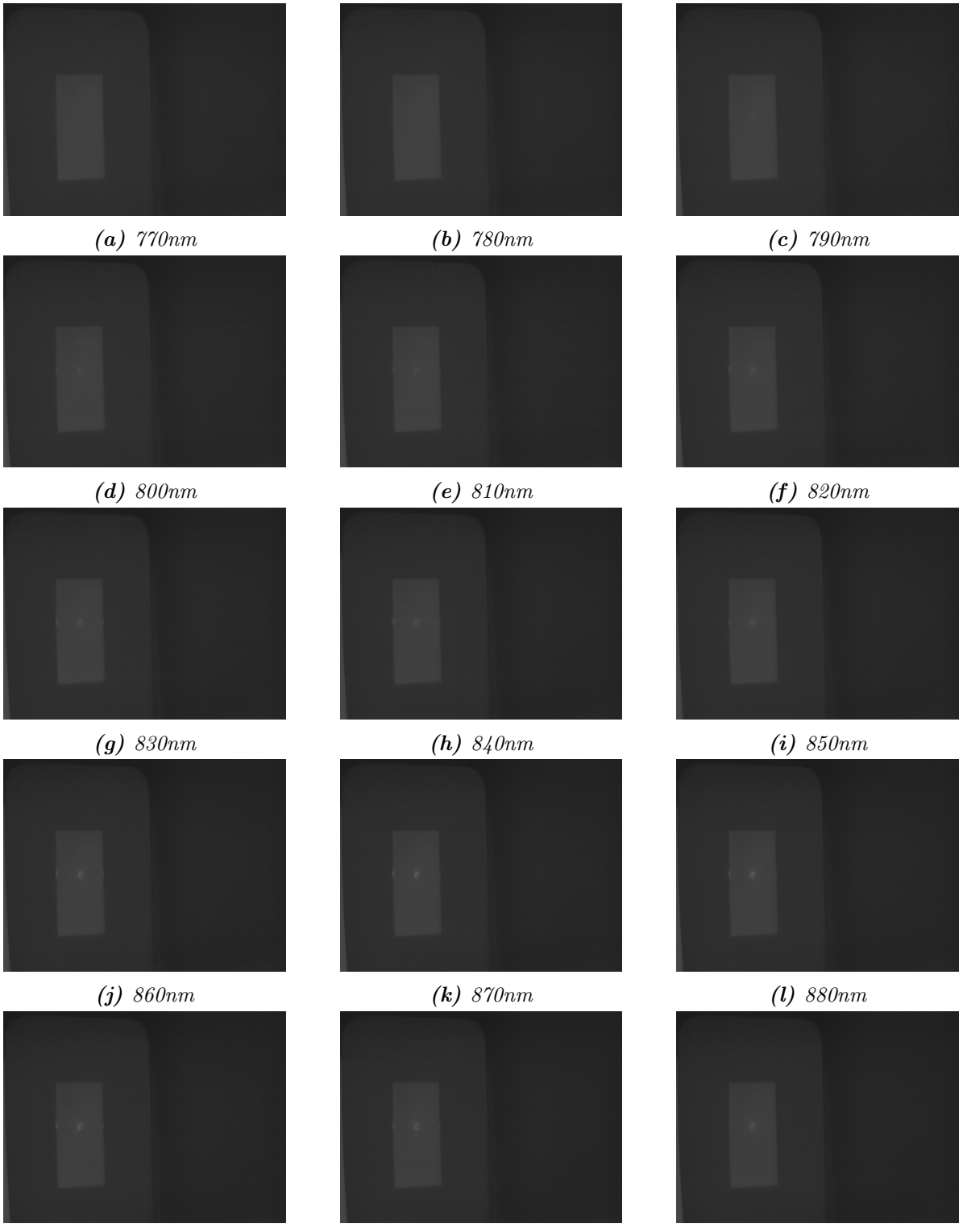

(a) *770nm* ***(b)*** *780nm* ***(c)*** *790nm*

(d) *800nm* ***(e)*** *810nm* ***(f)*** *820nm*

(g) *830nm* ***(h)*** *840nm* ***(i)*** *850nm*

(j) *860nm* ***(k)*** *870nm* ***(l)*** *880nm*

(m) *890nm* ***(n)*** *900nm* ***(o)*** *910nm*

Figure 7.25: *Scanning Procedure(1)*

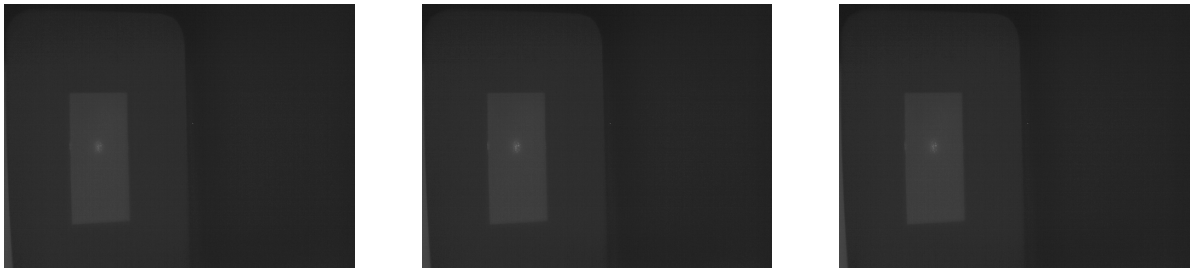

(a) *920nm* ***(b)*** *930nm* ***(c)*** *940nm*

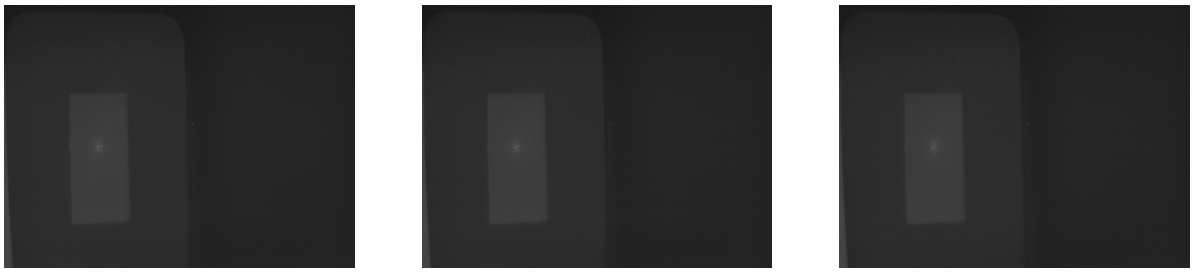

(d) *950nm* ***(e)*** *960nm* ***(f)*** *970nm*

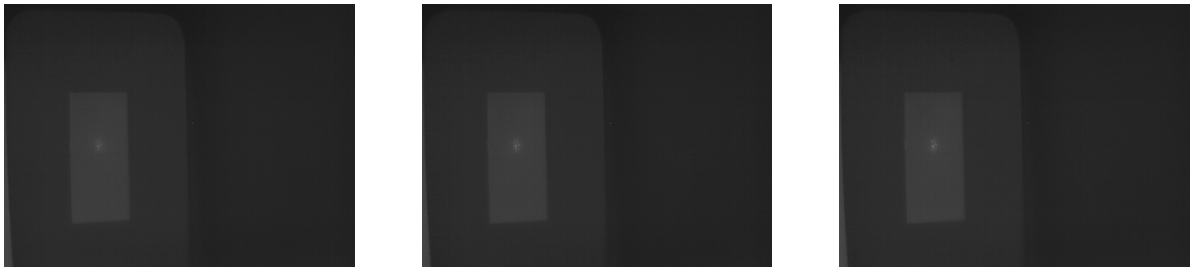

(g) *980nm* ***(h)*** *990nm* ***(i)*** *1000nm*

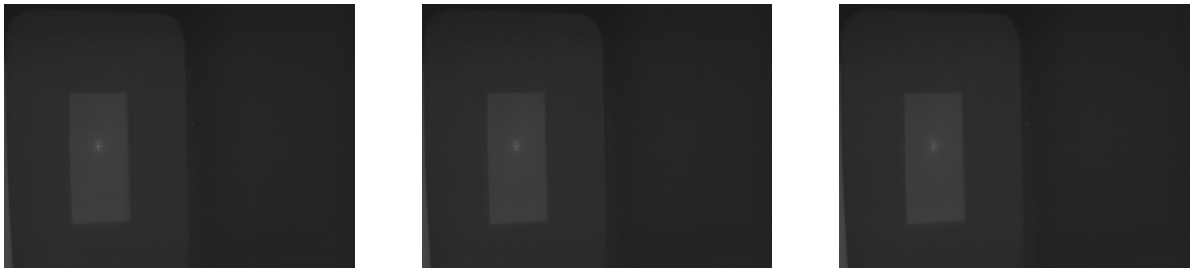

(j) *1010nm* ***(k)*** *1020nm* ***(l)*** *1030nm*

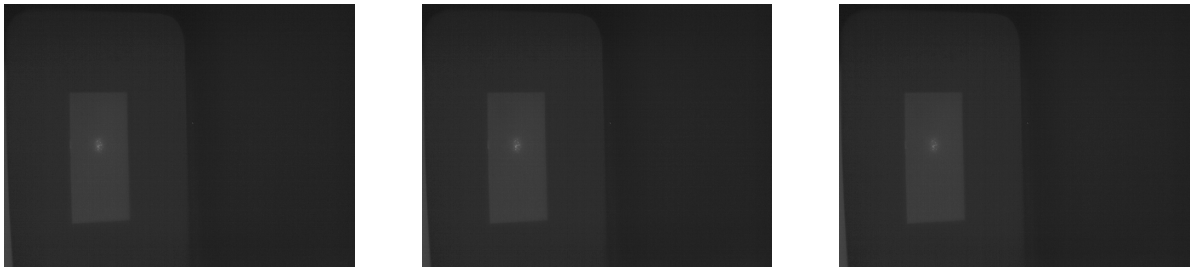

(m) *1040nm* ***(n)*** *1050nm* ***(o)*** *1060nm*

Figure 7.26: *Scanning Procedure(2)*

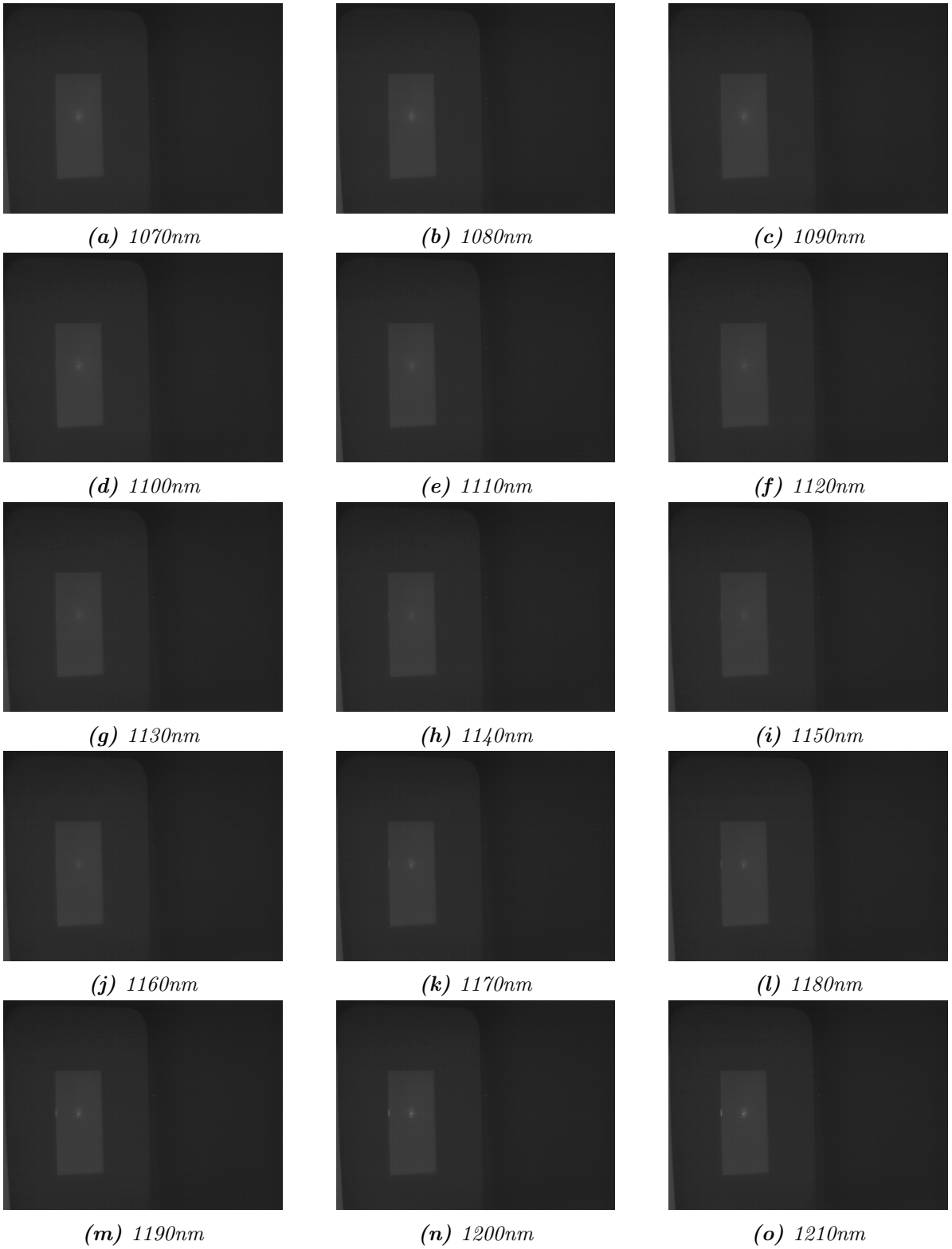

(a) *1070nm* ***(b)*** *1080nm* ***(c)*** *1090nm*

(d) *1100nm* ***(e)*** *1110nm* ***(f)*** *1120nm*

(g) *1130nm* ***(h)*** *1140nm* ***(i)*** *1150nm*

(j) *1160nm* ***(k)*** *1170nm* ***(l)*** *1180nm*

(m) *1190nm* ***(n)*** *1200nm* ***(o)*** *1210nm*

Figure 7.27: *Scanning Procedure(3)*

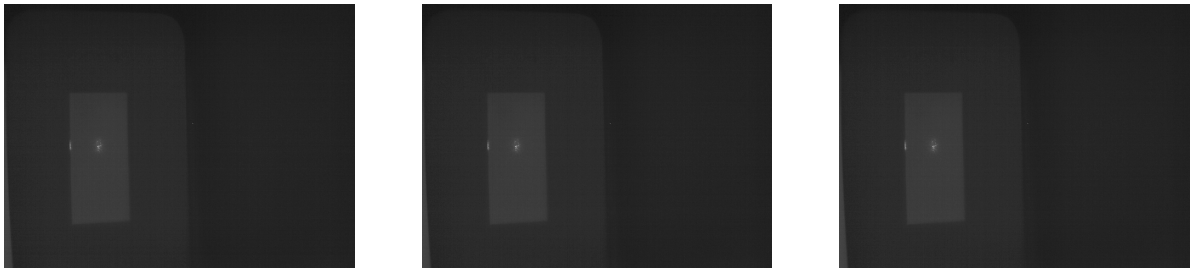

(a) *1220nm* ***(b)*** *1230nm* ***(c)*** *1240nm*

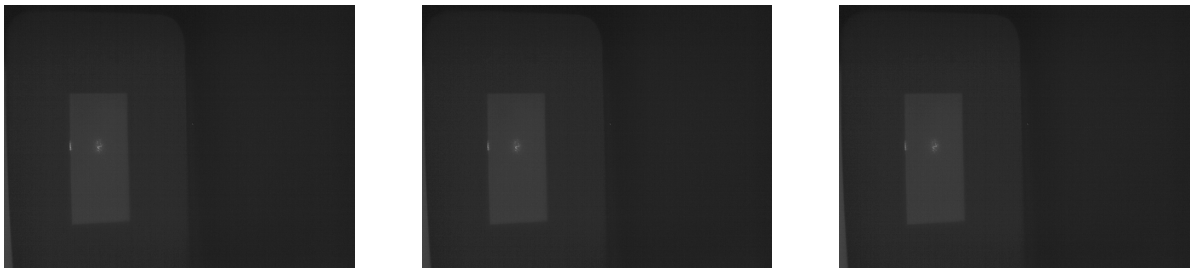

(d) *1250nm* ***(e)*** *1260nm* ***(f)*** *1270nm*

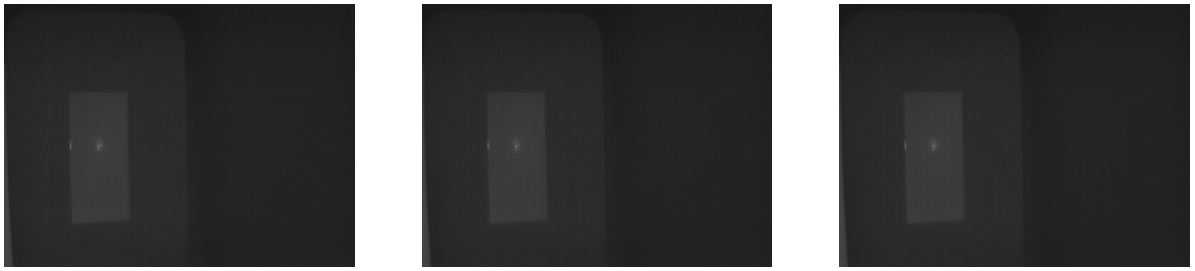

(g) *1280nm* ***(h)*** *1140nm* ***(i)*** *1150nm*

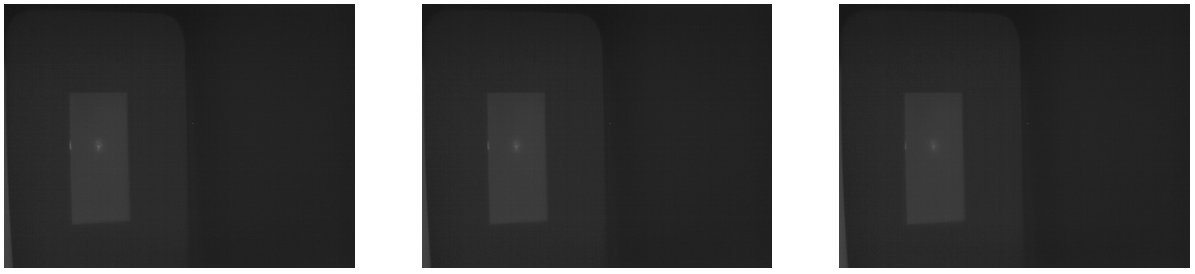

(j) *1300nm* ***(k)*** *1310nm* ***(l)*** *1320nm*

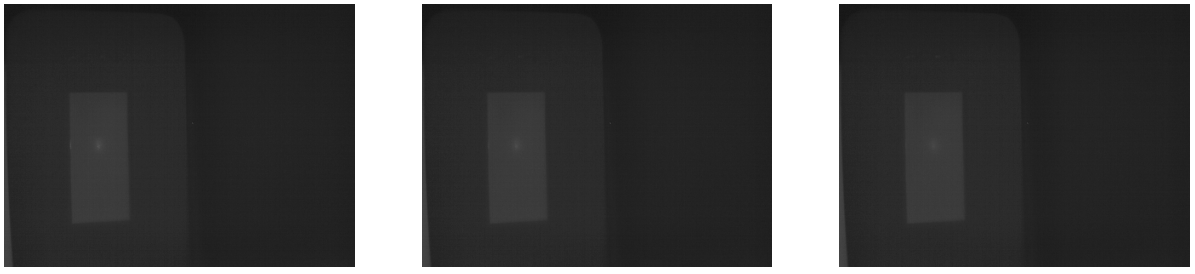

(m) *1330nm* ***(n)*** *1340nm* ***(o)*** *1350nm*

Figure 7.28: *Scanning Procedure(4)*

According to NIST fourteen certified peaks are available for wavelength qualification purposes in the Mid-IR: 539, 842, 907, 1028, 1069, 1155, 1583, 1601, 1943, 2849, 3001, 3026, 3060, and 3082 cm^{-1} [39].

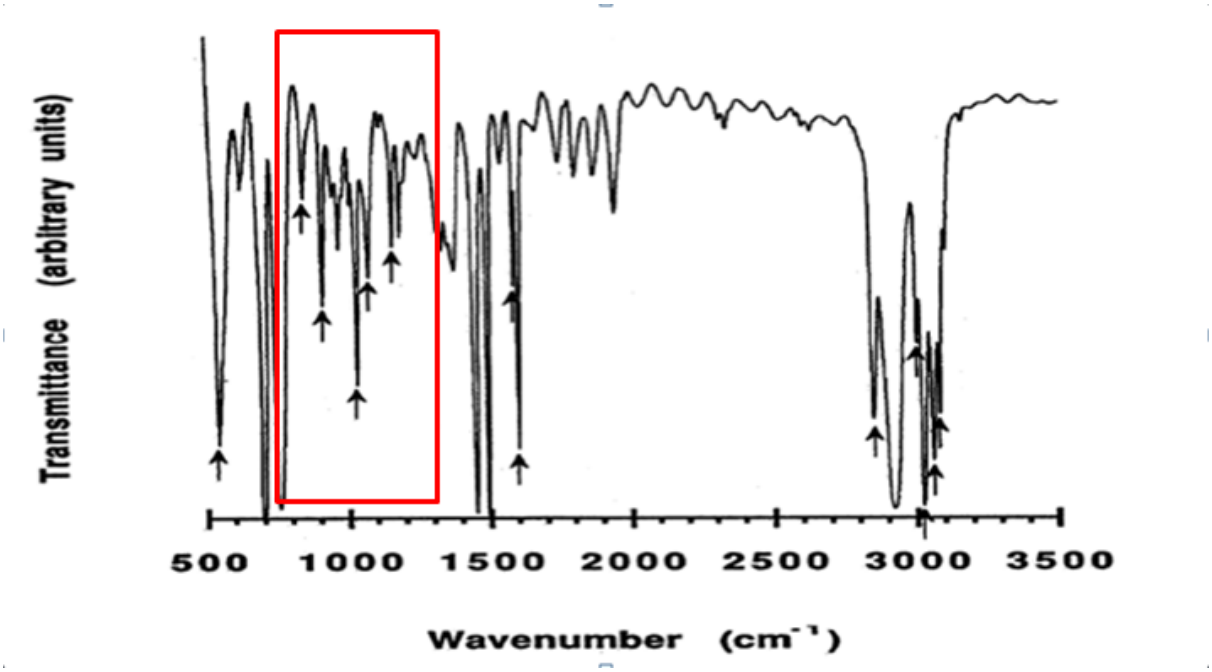

Figure 7.29: *Spectrum of polystyrene film showing locations of certified absorption peaks. The red box contains the wavenumbers that LaserTune can emit*

However our system operates in the 1360 770 cm^{-1} region; consequentially the only frequencies that can be identified are: 842, 907, 1028, 1069 and 1155 cm^{-1}.

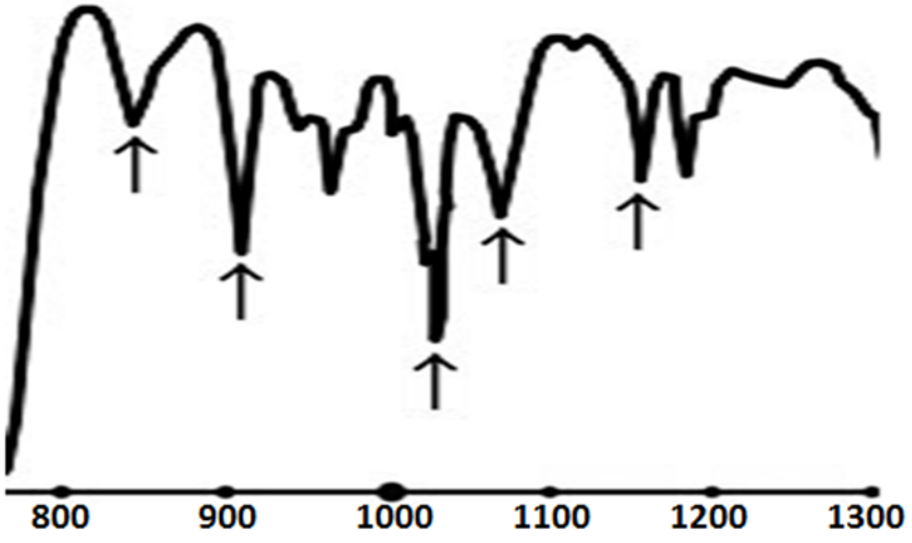

Figure 7.30: *Area of interest from the spectrum of polystyrene film showing locations of certified absorption peaks*

From the stored stack of spectral images, a spectrum is calculated and displayed. Each spectrum is calculated from the gray values of the selected pixel spectral column.

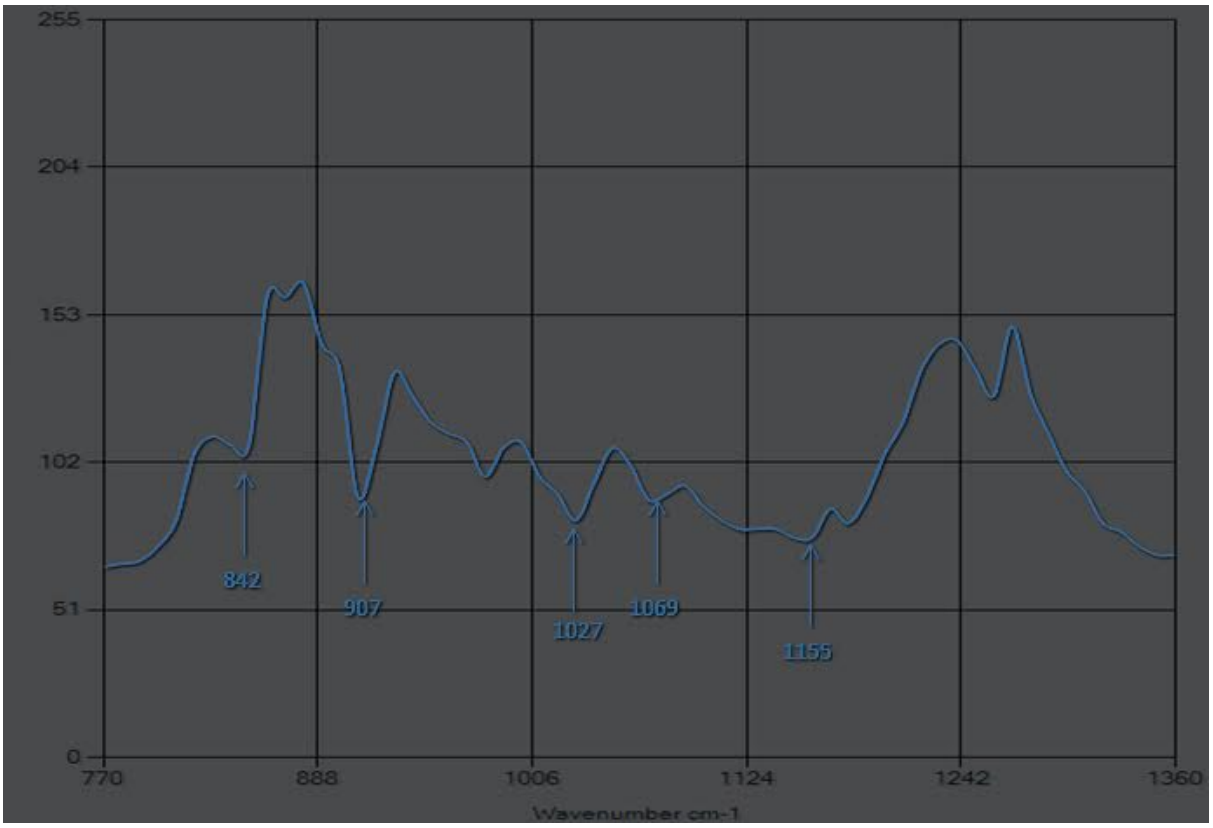

Figure 7.31: *Spectrum generated from the acquired images. It shows the absorption of the laser beam when it passes through a polystyrene film*

The displayed spectrum is generated from the transmission of the laser beam through the polystyrene film. The characteristic peaks mentioned above can easily be spotted. Evidence that proves that this spectrum is undoubtedly generated from polystyrene are the two peaks that can be spotted at the 1240 - 1260 cm^{-1} region. Differences in the hight of the peaks between this spectrum and the one given by NIST are observed, but that is because the spectra in thsese two cases were acquired from different angles.

To sum up, it is shown without a doubt that our system is a real-time mid infrared hyperspectral imaging system with excellent spatial and spectral resolution. Another important characteristic is that spectral cubes can be acquired either be transmission measurements or reflection measurements.

7.4 The Speckle Problem

After paying close attention to the acquired images it was obvious that the reflection of the expanded beam on the gold plate, presents very high speckle intensity.

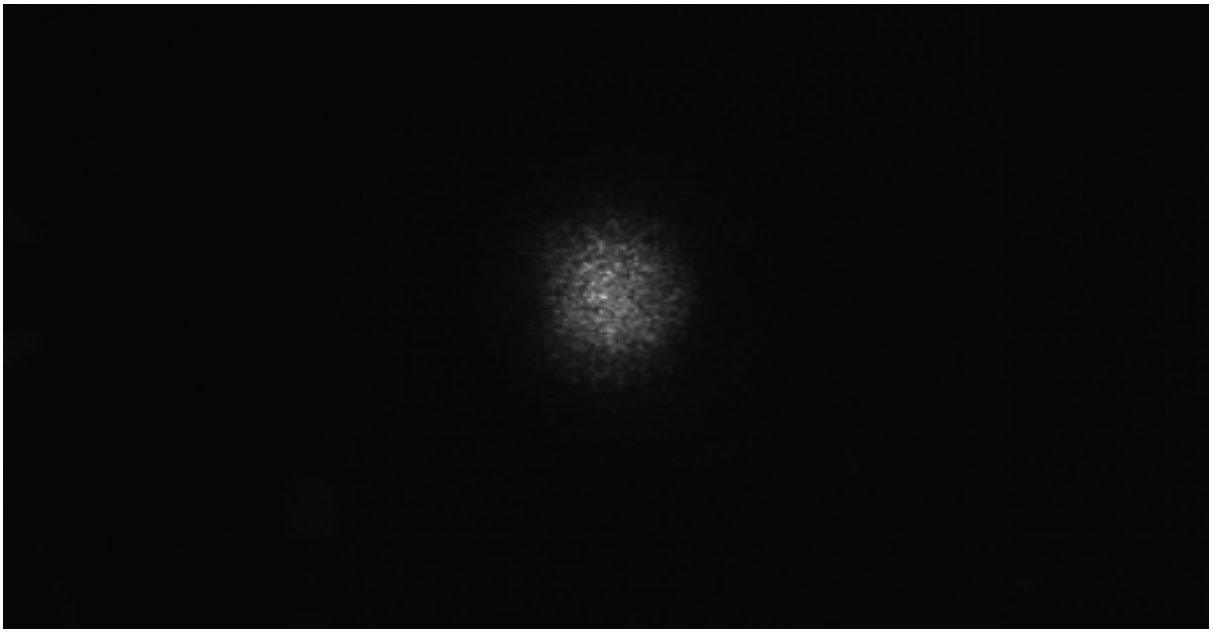

Figure 7.32: *The laser beam recorded after reflected on a golden plate obviously the speckle is very intense*

7.4.1 The Speckle Pattern

According to diffraction theory, each point on a surface that is illuminated by a light wave will behave as a source of secondary waves. The light detected by a sensor will be made of waves which could have been scattered from each point on the illuminated surface. Taking also into account that the surface of gold is rough enough to create path-length differences exceeding one wavelength, the amplitude, and hence the intensity, of the resultant light at each pixel of the detector varies randomly [29]. As a result the speckle pattern is an intensity pattern produced by the interference of many waves of the same frequency, having different phases and amplitudes, which add together to give a resultant wave whose amplitude, and therefore intensity, varies randomly [30]. Speckle patterns typically occur in diffuse reflections of monochromatic light such as laser light.

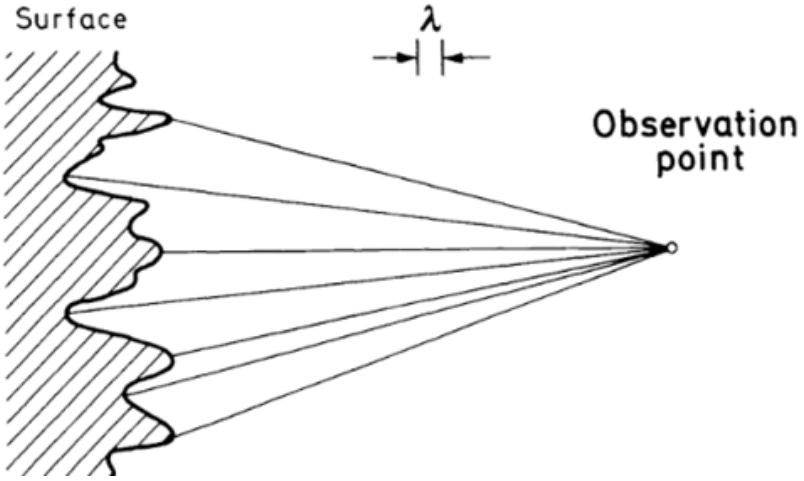

(a) *Physical origin of the speckle for an imaging system*

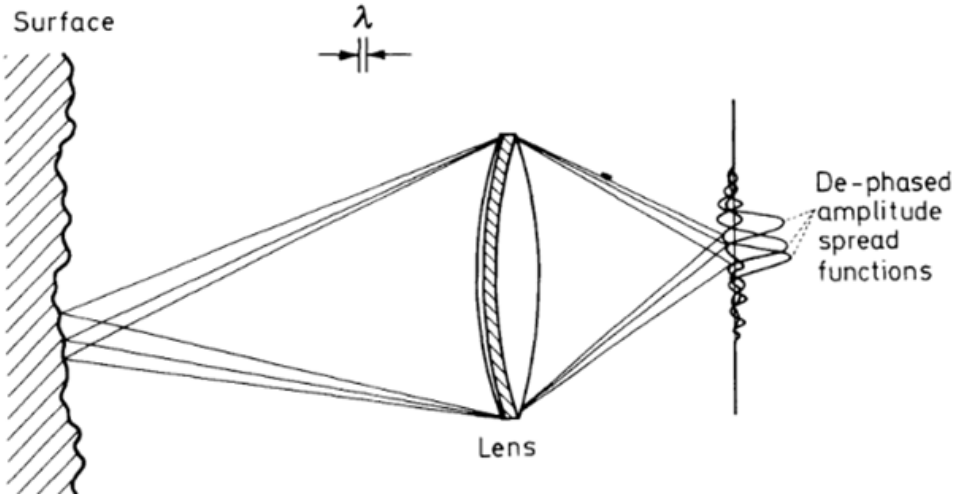

(b) *Free-space propagation for an imaging system*

Figure 7.33: *Origin of speckle*

The problem is that the image quality can be severely degraded because of the speckle phenomenon.

7.4.2 Speckle Reduction Techniques

When it comes to conventional lasers, the reciprocal motions of photons before they exit the cavity will result in photons coming out with different phases at each different point of time. Consequentially the speckle pattern changes and is a dynamic phenomenon. This is extremely useful as far as speckle reduction is concerned, because by taking multiple images and applying an averaging algorithm it is possible to eliminate the speckle contrast. Taking the average of multiple images smoothens the spectral pattern.

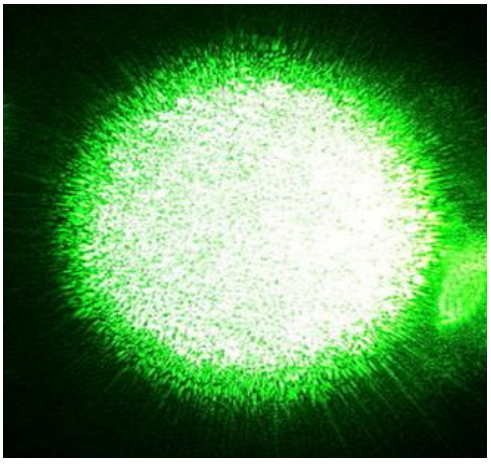

(a) *Speckle pattern of a laser beam*

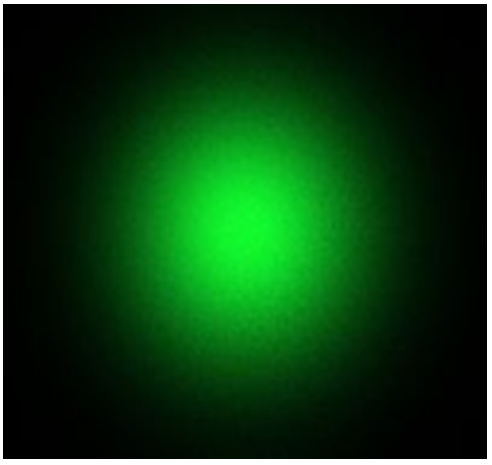

(b) *Average of many images of the laser beam*

However, this technique wont have the desired effects if applied by our system. The reason is that quantum cascade lasers do not have a cavity and as a result the phase of the photons wont change randomly. The speckle is static and taking the average of multiple images doesnt produce the desired effect.

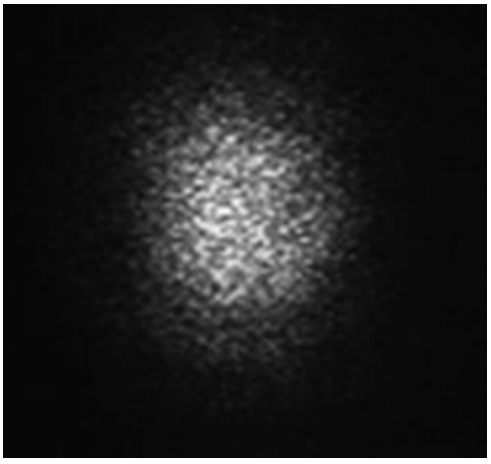

(a) *Speckle pattern of the laser beam of our system*

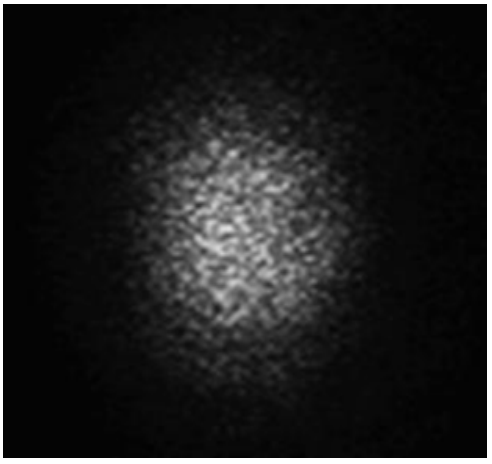

(b) *Average of many images of the laser beam of our laser system*

The technique described at [31] uses a rotating diffuser, which is randomly scratched, in order to create independent speckle patterns at any given time.

Chapter 8

Conclusion and Future work

Hyper-spectral imaging in mid infrared band of the spectrum possesses the advantage of acquiring an entire spectrum of information at each pixel of the examined object. Recent studies have shown the potential contribution that this technology can offer in the field of biomedicine and more specifically in the development of more sophisticated diagnostic devices and techniques. It is a non-destructive and non-invasive method, and hence appropriate for applications that require quality inspection and monitoring in real time.

However, mid-IR hyper-spectral imaging is complex because of the huge amount of data gathered, and it requires large storage capacity and fast computers to process and analyze the huge amount of data acquired.

Although the potential of hyper-spectral imaging might seem unlimited, certain limitations do exist, such as the equipments high cost, large volume of acquired data and use of sophisticated algorithms for processing of the data; all resulted in neglecting of this technology by the industry and only partial installation in real-time applications in the commercial world. Nowadays, technological advancements in the aforementioned fields, as well as a continuously raising interest of the scientific community in using mid-IR spectral imaging in biomedical applications have paved the ground in order for mid-IR spectral imaging to become a widely exploited and booming field of research in the near future.

In this thesis, we have studied a mid-infrared hyperspectral imaging system based on a quantum cascade laser theoretically and experimentally, and discussed different methods for solving problems that occur due to high speckle intensity. We developed a fully operational spectrometer and developed software that not only exploits all the abilities of the hardware in order to acquire high quality images or video, but also has the ability to generate spectral cubes from a set of images. This approach leads to a reconstruction method that obtains very good results and appears suitable for any kind of hyper-spectral camera.

8.1 Future Work

The HSI system that has been presented so far is fully equipped with the functions of hyper-spectral scanning and reconstruction of spectral cubes, which could find prospective application on fields such as medicine, security, leak detection and pharmacology. The principal conclusion is that this type of imaging system is able to provide functional hyper-spectral and single-spectral images across the mid infrared band of the electromagnetic spectrum divided into many more close bands, beyond the scope of human eye. The spectral response of the depicted material/sample conveys useful information as far as its composition and behavior are concerned, which is strictly associated with non-invasive and non-destructive analysis.

The image reconstruction has to be as fast as possible. Despite the fact that the HSI system provides live display of the hyper-spectral scanning procedure, the reconstruction of the images is not real-time procedure. The hyper-spectral scanning process must finish in order for image reconstruction to begin. Hyper-spectral images, although providing abundant information of the object, also bring high computational burden to data processing. The curse of dimensionality is a thing that must be taken into account when managing this type of data. Despite the fact that the development of a fully operational hyper spectral imaging system was completed within the requirements of this thesis, does not by any means indicate that there is not any potential of further improvement and perfection. The potential of this device would better be exploited if it was used as the basis of an infrared microscope. The reasons why this specific application is recommended are many and will be presented in detail.

First of all, mid infrared spectroscopic imaging is rapidly emerging as a technique in biomedical research and clinical diagnostics. This happens due to the fact that in the infrared spectrum information can be extracted about the unique molecular fingerprint of cells, tissue and biofluids in order to provide a detailed biochemical mapping with spatial resolution that exceeds the m and without the need of staining. Researchers have been able to proceed to objective classification of biological material at a molecular level [32]. Whereas with other microscopy methods one needs a priori knowledge of the sample to be interrogated to facilitate the tracking of a prescribed biomolecule, unlimited by this restriction, infrared microspectroscopy is a discovery-based method. However, at the same time, the inability to track specific molecules with infrared microspectroscopy means that it should be used as a complementary tool to optical microscopy, not as a replacement for it.

Moreover, an infrared spectrometer attached to a microscope can be used in microbiology to differentiate, classify, and identify microbial species and strains [33]. IR spectra are useful to detect in situ intracellular compounds or structures such as inclusion bodies, storage materials, and endospores, [34] monitor and quantify metabolically released CO_2 in response to various

different substrates, and [35] characterize growth dependent phenomena and celldrug interactions. This method is really useful for various reasons, such as the fact that it can be applied to practically every microorganism which can be grown in culture. Required biomass can be scaled down to even microcolonies as small as 20 m in diameter. Meaning that only a few hundred cells can be analyzed and give results within minutes [36]. This is partially achieved due to the fact that, detection, enumeration, classification, and identification can be conducted with the use of one single instrument, the IR microscope.

Furthermore, another field that infrared microscopy can be of assistance is tumor diagnostics, where the most common diagnostic tool, and the indisputable golden standard, is even today the simple visual examination of stained tissue material in the visible region. The specimens are examined and characterized based on criteria like the morphology of the tissue and nuclear polychromasia. Microscopes have improved the spatial resolution for this type of histology. Now, IR spectrometry could be used to detect analogous criteria in the form of spectral signatures and yet IR micro spectroscopy is still in the initial stages of development for use as a supplementary method in pathology. This is not absurd because the techniques that had been used so far (FTIR spectroscopy) possessed many disadvantages that had been stated in the previous chapters. One more is that biopsy samples in all the examples cited above, has to be taken and specially prepared for IR spectroscopic analysis. However, as we have seen in previous chapters the majority of those problems have been solved with the development of the next generation of infrared microscopes, those based on quantum cascade lasers. The fact that neither labeling nor staining of the sample is required combined with the fact that shinning infrared light on a sample is a non-destructive way of extracting information, means that the need for tissue samples required for a biopsy will significantly scale down, because multiple tests will be conducted on the same specimen.

A report from U. Bindig and G. Muller demonstrates an attempt for tissue identification as well as to differentiate between malignant and healthy tissue in vivo [37]. Although for the purposes of this research a microscope based on an FTIR spectrometer was used; part of this research will be described in order to highlight the potential benefits that infrared microscopy has to offer when it comes to oncology and detection of cancer, regardless of the means that were used in order to acquire the spectra.

Bladder cancer is the fourth leading cause of cancer in men and seventh leading cause of death from cancer in the United States. The techniques that can be used in evaluation of bladder cancer are intravenous pyelography, computed tomography scanning, magnetic resonance imaging and more commonly, cystoscopy and cytological examination of the urine. The biochemical detection of bladder cancer may be affected by urinary tract infections or stone diseases. As a result urinary cytology has a low sensitivity for low-grade carcinoma. Also, the tissue sampling required for histological examination is painful for the patient and takes time.

Fresh bladder tissue samples from biopsies were acquired and put under dry-air conditions in a dark room for a whole day. The average thickness of the dehydrated tissue was reduced from 10m to 3μm and no fixation or freezing media were used, to avoid artifacts or alteration of the specimens. Initially, twenty two healthy tissue specimens and eleven tumor specimens from different parts of the colon were used to generate the spectra, and the different parts of the tissue were divided in six categories for correlation-coefficient analysis; those categories were: tumor, necrotic tissue, muscle tissue, connective tissue and dysplasia. The analysis of the spectra was focused at a part of the fingerprint region of the spectrum, from 1500 to 900 cm^{-1}. The mean spectra of the major tissue categories are shown in Figure 8.1.

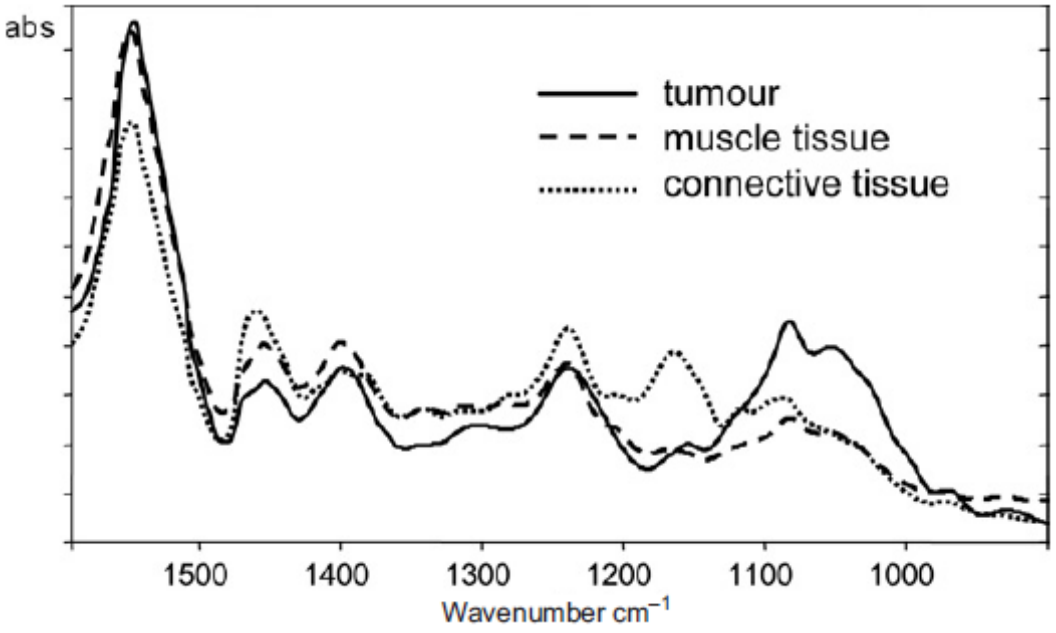

Figure 8.1: *IR mean spectra of tumour, muscle tissue and connective tissue from bladder tissue (IR microscope, transmission mode, 10m thin dried sections)*

In order to interpret the graph, it must be taken into account that collagen is the most common family of proteins in the human body. Collagen which is a part of healthy tissue and not affected by tumor is usually absorbing light with wavenumbers around 1240 cm^{-1}. However, rapid degeneration of the malignant tissues means that a smaller proportion of collagen will be detected and therefore they will show less absorption at 1240 cm^{-1} region. The reduction in the spectrum intensity can be observed in malignant tissue at 1204, 1240 and 1283 cm^{-1}. In addition to this, the mean spectrum of malignant tissue shows higher absorption than normal tissue at approximately 1070 cm^{-1}. The absorbance at 1547 cm^{-1} is attributed to the amide-II proteins.

Based on these observations an effort was made to divide the specimens into the aformentioned categories. Special pathologists were also consulted in order to categorize the specimens and

provide a bench mark. The pathological assessment was compared with the results from the correlation-coefficient analysis, and it showed that 30% of the tumorous tissue areas were assigned correctly. The rest of the cancerous areas were classified as dysplasia or as a mixed class of tumorous and connective tissue. The error rate was expected because the tumorous tissue often does not fill up the total aperture; it is usually mixed with connective tissue. Moreover, the resolution of the visible pictures from the IR microscope could not give an optimal picture for the classification. A smaller aperture would lead to increased positional resolution but would also result in a lower intensity and the signal/noise ratio would decrease dramatically.

It was possible to make a re-constructed picture based on the main tissue components defined. The IR-data analysis was further evaluated using quadratic discriminant analysis; 1831 spectra were used (1105 spectra for the tumor group and 726 for the normal tissue group). In this procedure, the univariate discriminant analysis was restricted to the two wavenumber ranges given in Figure 8.2 where the mean spectra of both groups are shown (from 1444 to 1412 cm^{-1} and from 1090 to 1062 cm^{-1}).

The band at 1746 cm^{-1} indicates the carboxylic stretching band of lipids. There seems to be a higher content of fatty tissue compared to the normal tissue specimens. In the range from 1430 to 1400 cm^{-1} and from 1100 to 1000 cm^{-1} significant differences can be found. The morphological structures were discernible. Correct classification as tumor or non-tumor (normal) was made with over 90% success using correlation-coefficient analysis. The results of the quadratic discriminant analysis using dry tissue cryosections have an error quotient of 2%.

The results of this research indicate that infrared microscopy can be of assistance in histopathology and tissue identification. Specific vibrational signatures can lead to an objective decision. Obviously, Fourier transform infrared (FT-IR) microscopy coupled with machine learning approaches has the potential to be a powerful technique for detecting abnormalities in human tissue.

However, despite recent technological breakthroughs in FT-IR microscopy obstacles such as sample throughput and acquisition speed are key and are yet to be overcome. Wide-field quantum cascade laser (QCL) infrared imaging systems with the ability to utilize discrete frequency imaging have made reduce the time needed for the procedure imaging of large tissue microarrays (TMA) in the order of minutes. This ground breaking technology is still in its infancy, and its applicability for routine disease diagnosis is, as yet, unproven.

A report from Michael J. Pilling, Alex Henderson, and Peter Gardner reported in 2017, has shown that by using QCL imaging and interpreting the spectra acquired from breast tissue samples between 912 and 1800 cm^1, can give accurate results and categorize the tissue between 4 different classes, epithelium, stroma, blood and necrosis. [38].

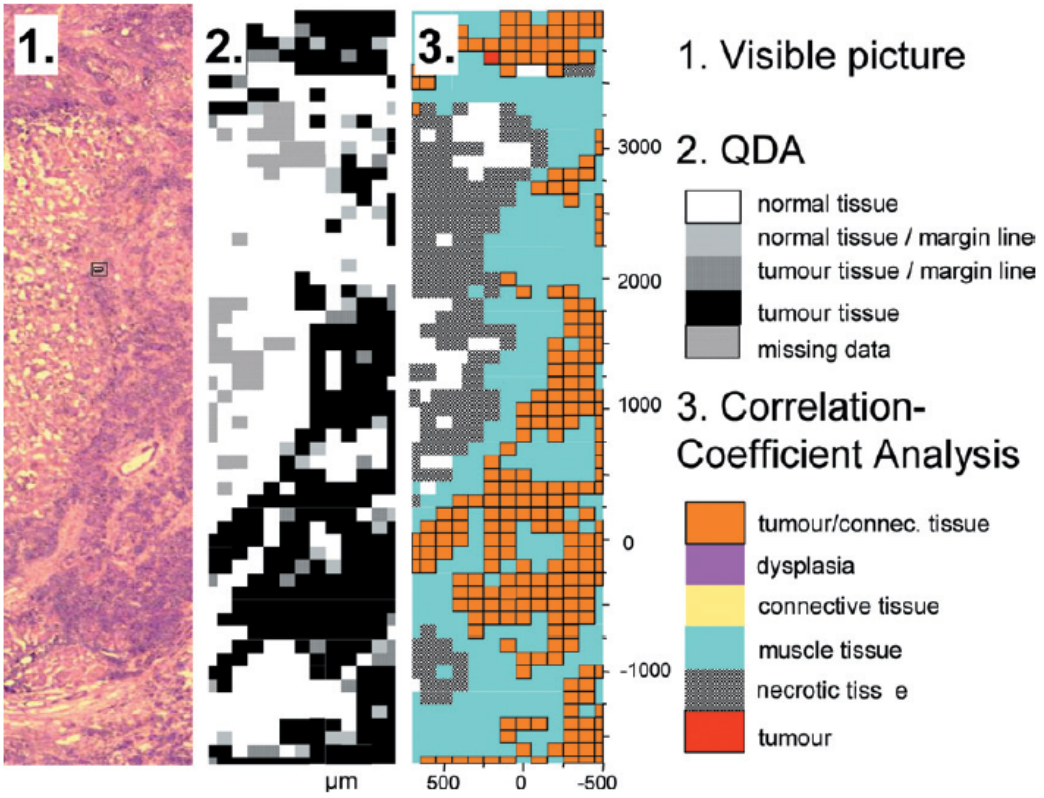

Figure 8.2: *Result of the image re-construction ((1) Visible image of the post HE-stained native tissue section(2) QDA (3) Correlation-coefficient analysis)*

Serial sections of formalin fixed paraffin embedded breast tissue microarray (TMA) cores were acquired from US Biomax, Rockville, MD, (TMA ID BR20832). A 5m section was floated onto a standard histology slide, dewaxed, and underwent hematoxylin and eosin (HE) staining. An adjacent section was floated onto a BaF_2 slide (Crystran Ltd., Poole, UK) and did not undergo any deparaffinization. Retaining the sample in wax removes the risk of chemical alteration of the sample from clearing solvents and is known to minimize resonant Mie scattering due to refractive index matching. So far, there is not a single large scale study about diagnostic accuracy for QCL based microscopy systems. To address this, the study presented here investigates the discriminatory power of QCL based imaging systems for categorizing malignant and healthy tissue in a large number (207 biopsy cores) of samples.

A literature review indicated that the efforts to identify malignant tissue should be focused on the epithilium tissue samples. On contraire, some recent studies have questioned this approach and suggest that stroma, specifically adjacent stroma, may have a key role to play in the initiation and progression of cancer. This approach seamed rather interesting and a choice was made to use stroma rather than epithelium to test the device's capabilities as a tumor diagnostic tool. The method that the team followed is briefly described: to begin with, 74 cores were separated randomly as training and testing cores using an 80:20 split which resulted in 59 training and 15 test cores. A Random Forest classifier was created from the training samples

and categorized each spectrum in the four categories mentioned before. After it was proved that the algorithm works as intended, stromal spectra were isolated from each of the 207 cores using the Random Forest classifier to remove all pixels belonging to any other class.

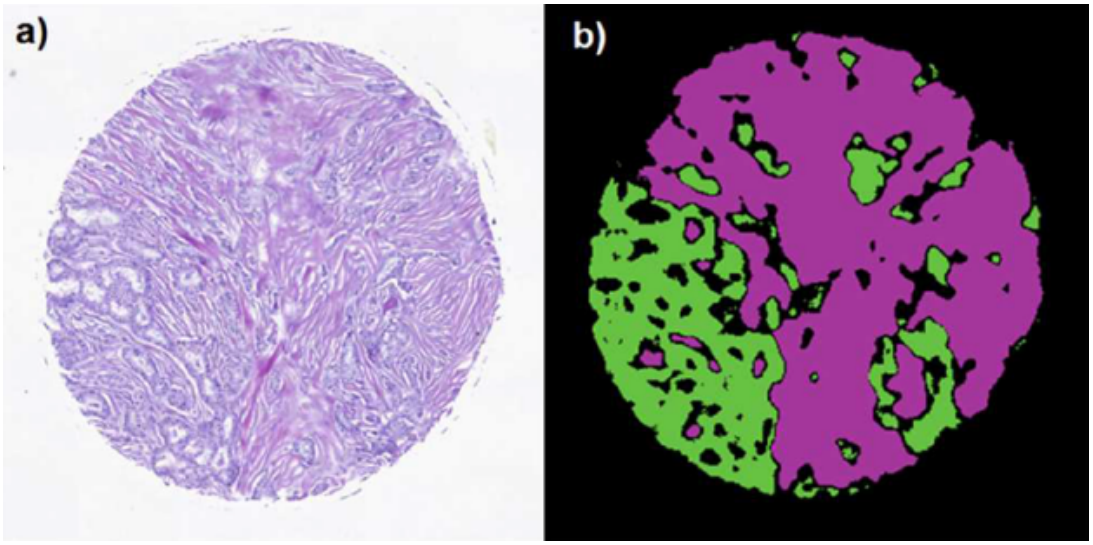

Figure 8.3: *(a) Brightfield image of HE stained serial section for core and (b) false color image of the classified core rendered using green (epithelium) and purple (stroma)*

A second Random Forest classifier was constructed with bias minimized by using approximately 140.000 malignant spectra and an equal number of randomly selected non-malignant spectra. The classifired was able to distinguish that for almost every patient the proportion of malignant stroma is close to 1. A bar chart displaying the proportion of stroma pixels classified as malignant for each of the malignant cores is displayed in Figure 8.3. Out of 192 malignant cores, four did not have any identifiable stroma (as determined by Random Forest) and could not be classified. The mean proportion of malignant stroma for the remaining malignant cores is 95.3%, suggesting stroma is an effective indicator of malignancy.

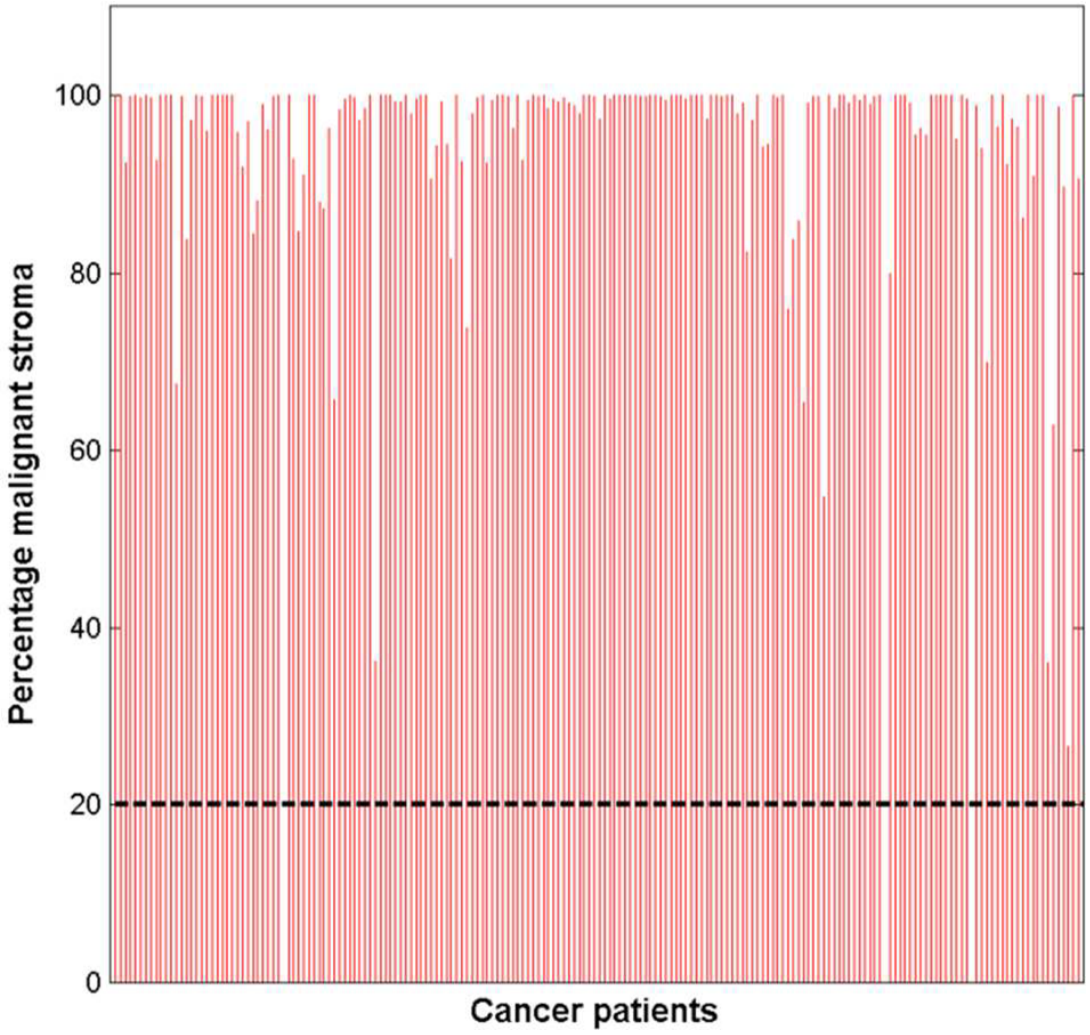

Figure 8.4: *Bar chart showing malignant stroma pixels as a percentage of total stroma pixels for each of the 192 cancer patients. The dashed line represents a threshold of 0.2)*

Applying a threshold of 0.2 to the bar chart in Figure 6 enables 100% accurate classification of all cores which had identifiable stroma. Recall that 4 cores out of 192 did not contain any stroma and could not be classified. An important conclusion that can be extracted is that there are no false negatives (malignant diagnosed as nonmalignant), which is a key feature as far as cancer screening is concerned. In the healthy tissue case, the stroma could be identified in all cores, although 2 false positives (nonmalignant diagnosed as malignant) results were generated, which reduced the specificity to 86.67%.

Taking into account the high specificity shown by this method, high throughput automated screening seems viable and it would enable biopsies to be triaged for pathological review. Screening methods that are used for cancer detection must ensure that all cases are detected, because otherwise the patient will not receive proper care. As it was stated before, a success rate of 86.67% is achieved by the use of this method. This is acceptable because only the rest 13.33% cases would need to be further examined by trained pathologies in order to conclude if there

are traces of nonmalignant tissue. The key advantage of screening with this system is that the nonmalignant cores that were correctly classified would not need to be reviewed by a pathologist. Moreover, it was shown that malignant and nonmalignant stroma spectra can be easily discriminated with 93.56% sensitivity and 85.64% specificity on an independent test set.

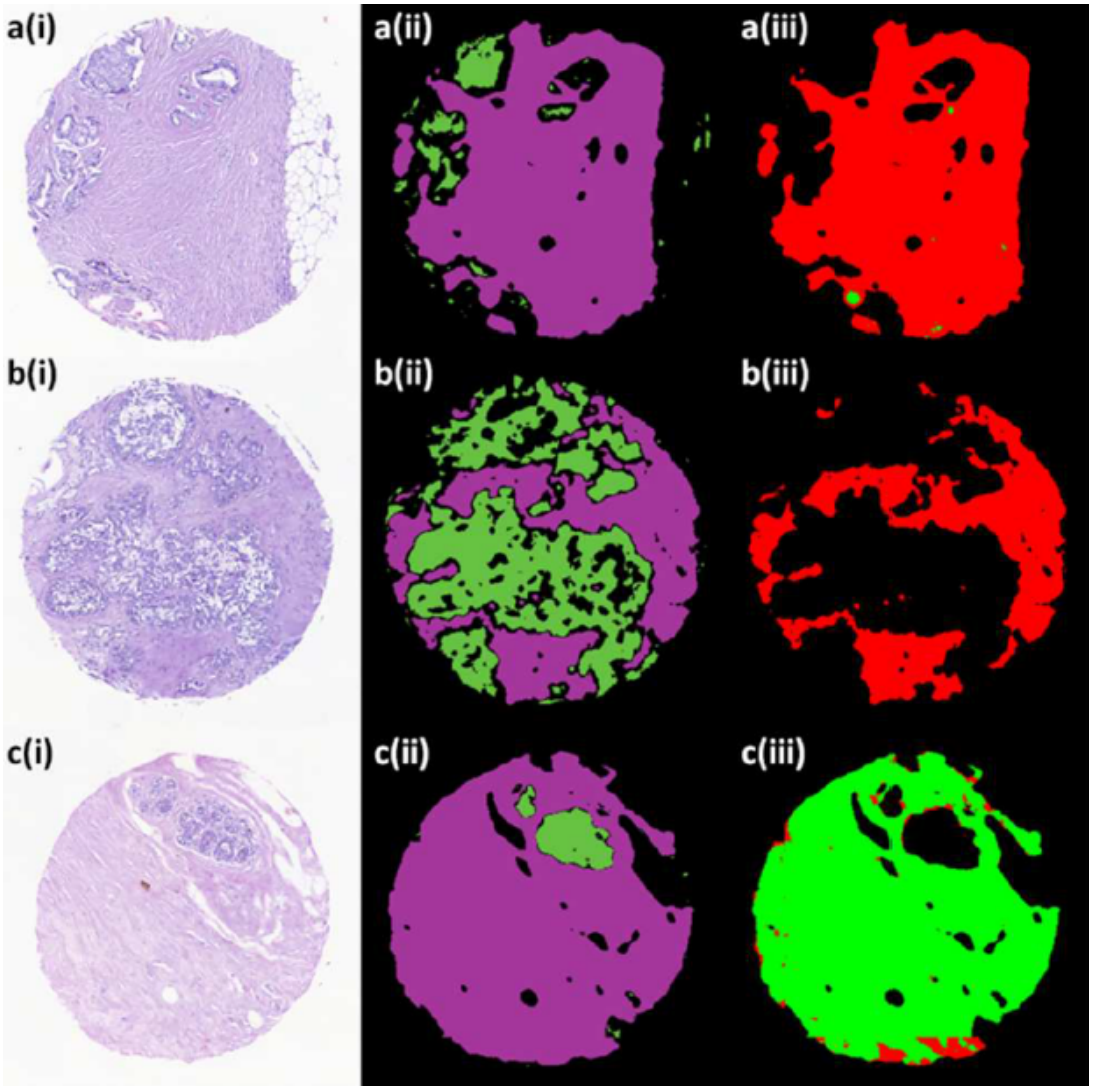

Figure 8.5: *a(i), b(i), c(i) Brightfield image of HE stained section of two malignant and one nonmalignant core, a(ii), b(ii), c(ii) false color image of histology rendered using green (epithelium) and purple (stroma) to illustrate predicted histological class, and a(iii), b(iii), c(iii) false color image of malignancy rendered using green (nonmalignant stroma) and red (malignant stroma)*

It has been proved that an FPA-based QCL imaging system can accurately discriminate between malignant and nonmalignant stroma. With the use of infrared chemical imaging complementary information can be provided in order to aid diagnosis and lead to better treatment for patients. But in order to fully exploit the potential of this method, further research has to be conducted. Clinical trials with greater number of patients over several separate TMAs are necessary to

demonstrate the advantages of this method in clinical medicine. At the present state the most critical drawback seems to be the ability of this method to reduce the time required for continuous frequency imaging and whether or not the throughput provided is enough. A possible solution to the throughput problem could be to optimize the range from which the spectra are acquired. This could be illustrated by an example, 207 breast tissue biopsy cores were scanned in a period of time equal to 13.6 h, meaning that each core was scanned in 3 minutes and 56 seconds. Optimizing the acquisition parameters would translate to each core being acquired in approximately 2 min 58 s, which is a time scale likely to be acceptable to clinicians.

Last but not least, recent technological developments and the progress that has been made over the last few years especially in the field of materials, has paved the road in order for infrared microscopy to be used in endoscopes. IR-fiber-optic sensors can be inserted into the biopsy needle, catheter or endoscope allowing measurements to be carried out on-line and in real time. The greatest progress however, has been in the field of materials. New silver halide optic fibers guide the infrared light in the tissues and although, the research is in early stages and further work has to be made the results so far have been very promising [37].

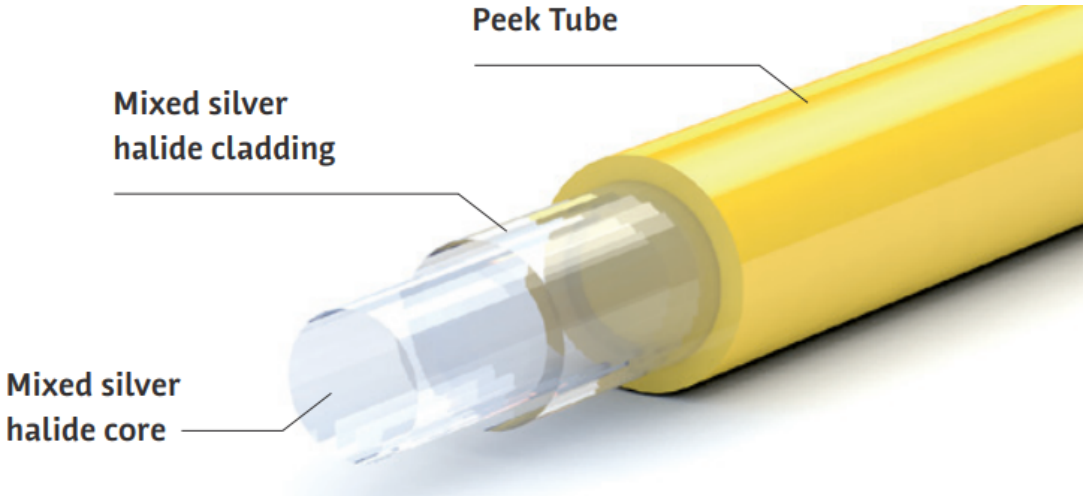

Figure 8.6: *Silver halide optic fiber*

The main drawbacks that researchers must overcome, in order to create efficient infrared endoscopes, are the fact that silver halides are photosensitive crystals that darken irreversibly if they are exposed to radiation. Fibers must be stored in a dry, dark environment (e.g. in a loose, black polymer tube). Furthermore, water and humidity are also factors that can damage the optic fiber; molecules inside the fiber material alter the structure and will also change the spectral transmission. The fiber must be cleaned after the measurement has been completed, after which an immediate change can be determined in the baseline spectrum. Moreover, researchers have

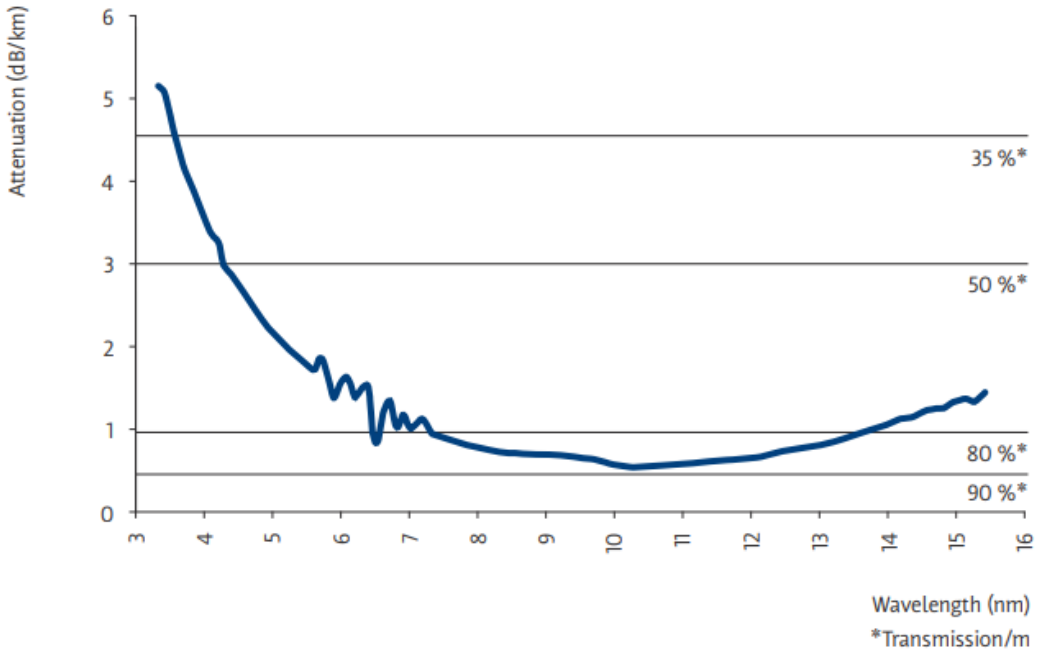

Figure 8.7: *Infrared transparent optic fiber spectrum*

to overcome issues that emerge from the interaction of an optic fiber with the tissue inside the human body. Water from the interstitial space and/or the tissue surface, results in a change in intensity was observed from the amide absorption bands to the lipid absorption bands, reduces the quality of the images, because it absorbs infrared radiation. Chemical reactions with bio-organic sulphur-containing compounds will take place. This leads to an immediate worsening of the fiber transmission properties.

Additional IR-spectroscopic investigations are in progress for more detailed analysis. Nevertheless, it is possible that fibre-optic mapping, if carried out on tissue via minimal invasive procedures and in vivo, would make it possible to distinguish between healthy and cancerous tissues. The commercialization of quantum cascade lasers and the fact that these devices when used as the basis of an infrared microscope provide more stable light source with higher intensity than the FTIR based light sources, ensures that in the next years IR technology will be established for practical use in medicine.

These are only a few potential applications where infrared spectroscopy can be applied. We have only scratched the surface of the benefits that this method has to offer. The process of extracting relevant biomarkers using infrared radiation is on the rise and as we better understand the nature of such derived spectra and the underlying physical phenomena that may modify their structure, our processing of them and as such the information we extract from them will undoubtedly evolve. Also the constant growth that the fields of artificial intelligence, machine learning and neural networks have experienced over the last few years resulted in many new methods and techniques that can detect criteria in the form of spectral signatures and assist

in classification. In the next few years infrared microscopy is expected to boom as a field of research and attract the interest of the scientific community.

Bibliography

[1] I. Gkouzionis. *"Spectral Cube Reconstruction From Multiplexed Spatial and Spectral Data"*, 2017.

[2] D. A. Boas, C. Pitris, and N. Ramanujam. *"Handbook of Biomedical Optics"*,Taylor and Francis, 2011.

[3] T. Vo-Dinh. *"Biomedical Photonics Handbookn"*, Taylor and Francis, 2010.

[4] C. Balas, K. Rapantzikos. *"Hyperspectral imaging: potential in non-destructive analysis of palimpsests"*, IEEE-International Conference on Image Processing (ICIP), pg 11-14, September 2005.

[5] H. Kalluri, S. Prasad, and L. M. Bruce. *"Fusion of Spectral Reflectance and Derivative Information for Robust Hyperspectral Land Cover Classification"*, IEEE Workshop on Hyperspectral Image and Signal Processing: Evolution in Remote Sensing, 2009.

[6] D. Manolakis, D. Marden, and G. Shaw. *"Hyperspectral Image Processing for Automatic Target Detection Applications"*, Lincoln Laboratory Journal, 14(1), 2009.

[7] W. Li, S. Prasad, J. E. Fowler, and L. M. Bruce. *"Locality-Preserving Dimensionality Reduction and Classification for Hyperspectral Image Analysis"*, IEEE Transactions on Geoscience and Remote Sensing, vol. 50, no. 4, pp 1185 - 1198, April 2012.

[8] C. Dames. *"Resistance Temperature Detectors"*, Encyclopedia of Microfluidics and Nanofluidics, January 2015.

[9] J. Janata. *"Principles of Chemical Sensors"*, Springer US, pg 5162, 2009.

[10] V. V. Tuchin. *"Handbook of Coherent-Domain Optical Methods"*, Springer-Verlag GmbH, 2013.

[11] J. Hernandez-Andres, J. Romero, J. L. Nieves, R. L. Lee. *"Color and Spectral Analysis of Daylight in Southern Europe"*, Journal of the Optical Society of America. A. Vol. 18, Issue 6, pg 1325-1335, 2001.

[12] M. R. Derrick, D. Stulik, J. M. Landry. *"Infrared Spectroscopy in Conservation Science"*, J. Paul Getty Trust, pg 1825, 1999.

[13] W. Zeller, L.Naehle, P. Fuchs, F. Gerschueltz, L. Hildebrandt, J. Koeth. *"DFB Lasers Between 760 nm and 16 m for Sensing Applications"*, Sensors, pg 10, 2010 .

[14] J. Faist. *"Quantum Cascade Laser"*, Science, Vol. 264, No. 5158, pg. 553, 22 Apr 1994.

[15] R. F. Kazarinov, R. A. Suris. *"Possibility of Amplification of Electromagnetic Waves in a Semiconductor with a Superlattice"*, Fizika i Tekhnika Poluprovodnikov. 5 (4): pg. 797800, April 1971.

[16] A. Y. Cho. *"Advances in Molecular Beam Epitaxy (MBE)"*, Journal of Crystal Growth Vol. 111 1, 1991.

[17] K. Furuya, Y. Miyamoto. *"GaInAsP/InP Organometallic Vapor Phase Epitaxy for Research and Fabrication of Devices"*, Int. J. Hi. Spe. Ele. Syst. 01, 347, 1990.

[18] R. E. Nahory, M. A. Pollack, W. D. Johnson Jr., R. L. Barns. *"Band gap versus composition and demonstration of Vegards law for InGaAsP lattice matched to InP"*, Appl. Phys., Lett. 33 , pg 659, 1978.

[19] Louise Jumpertz *"Nonlinear Photonics in Mid-infrared Quantum Cascade Lasers"* pg. 63 64, August 31 2017.

[20] D. T. D. Childs, R. A. Hogg, D. G. Revin, I. Ur Rehman, J. W. Cockburn, S. J. Matcher. *"Sensitivity Advantage of QCL Tunable-Laser Mid-Infrared Spectroscopy Over FTIR Spectroscopy"*, Applied Spectroscopy Reviews, pg. 822 - 839, 2015.

[21] C. J. Hirschmugl, K. M. Gough. *"Fourier Transform Infrared Spectrochemical Imaging: Review of Design and Applications with a Focal Plane Array and Multiple Beam Synchrotron Radiation Source"*, Applied Spectroscopy pg. 475 491, 2012.

[22] S. Dupont, C. Petersen, J. Thogersen, C. Agger, O. Bang, S. R. Keiding. *"IR Microscopy Utilizing Intense Supercontinuum Light Source"* Opt. Express, pg. 4887 4892, 2012.

[23] K. Yeh, S. Kenkel, J. N. Liu, R. Bhargava. *"Fast Iinfrared Chemical Imaging with a Quantum Cascade Laser"*, Anal.Chem., pg. 485 493, 2015.

[24] P. Bassan, M. J. Weida, J. Rowlette, P. Gardner. *"Large Scale Infrared Imaging of Tissue Micro Arrays (TMAs) Using a Tunable Quantum Cascade Laser (QCL) Based Microscope"*, Analyst, pg. 3856 3859, 2014.

[25] S. Nudelman. *"The detectivity of infrared photodetectors"*, Appl. Opt., 1(5), pg. 627635, 1962.

[26] P. R. Griffiths, J. A. de Haseth. *"Fourier Transform Infrared Spectrometry"*, John Wiley and Sons Publications, 2nd ed., pg. 172, 2007.

[27] P.Kotidis. *"Quantum Cascade Lasers: QCLs Enable Applications in IR Spectroscopy"* LaserFocusWorld Volume 49, 2013.

[28] L. Hanssen, S. Kaplan, R. Datla. *"Infrared Optical Properties of Materials"*, National Institute of Standards and Technology Special Publication 250 94, February 2015.

[29] J. W. Goodman. *"Some Fundamental Properties of Speckle"*, J. Opt. Soc. Am. 66 (11), pg. 1145, 1976.

[30] J. C. Dainty. *"Laser Speckle and Related Phenomena"* Springer Berlin , 1975.

[31] M. R. Kole, R. K. Reddy, M. V. Schulmerich, M. K. Gelber, R. Bhargava. *"Discrete Frequency Infrared Microspectroscopy and Imaging with a Tunable Quantum Cascade Laser"*, Analytical Chemistry, 2012.

[32] S.E. Taylor, K.T. Cheung, I.I. Patel, J. Trevisan, H.F. Stringfellow, K.M. Ashton, N.J. Wood, P.J. Kaeting, P.L. Martin-Hirsch, F.L. Martin. *"Infrared Spectroscopy with Multivariate Analysis to Interrogate Endometrial Tissue: a Novel and Objective Diagnostic Approach"*, Brit. J. Cancer 104, 2011.

[33] W.H. Nelson. *"Modern Techniques for Rapid Microbiological Analysis"*, VCH, New York, 1991.

[34] P.R. Murray, E.J. Baron, M.A. Pfaller, F.C. Tenover, R.H. Yolken (eds.). *"Manual of Clinical Microbiology"*, Washington, D.C. : ASM Press, 2003.

[35] K.P. Norris. *"Infrared Spectroscopy and its Application to Microbiology"*, Journal of Hygiene, 57, pg. 326345, 1959.

[36] D. Naumann. *"Infrared Spectroscopy in Microbiology"*, Encyclopedia of Analytical Chemistry, 2000.

[37] U. Bindig and G. Muller. *"Fiber-optic laser-assisted infrared tumor diagnostics (FLAIR)"*, Journal of Applied Physics, Volume 38, 22 July 2005.

[38] M. J. Pilling, A. Henderson, P. Gardner. *"Quantum Cascade Laser Spectral Histopathology: Breast Cancer Diagnostics Using High Throughput Chemical Imaging"*, Analytical Chemistry, 89, 7348-7355, 2017.

[39] D. Gupta et.al. *"Polystyrene Films for Calibrating the Wavelength Scale of Infrared Spectrophotometers SRM 1921"*, NIST Special Publication 260-122, 1995.

[40] M. G. Littman and H. J. Metcalf. *"Spectrally narrow pulsed dye laser without beam expander (ET)"*, Appl. Opt. 17, 2224, 1978.